Norwegian University
of Life Sciences

Master's Thesis 2021 60 ECTS
Faculty of Veterinary Medicine

Effects of *Providencia alcalifaciens* and its cytolethal distending toxin on canine intestinal epithelial cells

Hilde Nygård
Biotechnology

1.0 Introduction

1.1 Outbreak of acute hemorrhagic diarrhea syndrome in dogs

On the 4th of September 2019, a chain of private veterinary clinics in Oslo notified the Norwegian Food Safety Authority (NFSA) that they had treated an unusual high number of dogs with acute hemorrhagic diarrhea syndrome (AHDS) in the preceding weeks (Jørgensen et al., unpublished).

AHDS in dogs is characterized by acute onset of hemorrhagic diarrhea, vomiting progressing to hematemesis, severe loss of weight and lethargy. The syndrome used to be called hemorrhagic gastroenteritis (HGE) until a study showed that it is the intestines, not the stomach that is involved in the disease process (Unterer et al., 2014). Dogs are commonly presented with acute diarrhea, and there are numerous potentially causative agent(s). An AHDS diagnosis is made by excluding other causes of acute hemorrhagic diarrhea. When no underlying cause is found, a diagnosis of idiopathic AHDS is made. Acute hemorrhagic diarrhea can be a life-threatening disease due to severe dehydration, and early supportive care and aggressive fluid therapy is vital (Mortier et al., 2015).

The clinical picture of the treated dogs reported by the veterinaries in Oslo included a rapid onset of thin, watery diarrhea that could promptly progress to severe AHDS. Despite intensive care, several dogs died within 1-2 days after first occurrence of symptoms. None of the clinics were able to detect any relevant infectious- or toxic agents in the sick dogs. The NFSA requested support from the Norwegian Veterinary Institute (NVI) to document the extent of a possible outbreak, find the cause, rule out any zoonotic potential and prevent further spread. Epidemiological data were collected through a survey to veterinarians and in-depth interviews of dog owners. A survey was distributed to owners of affected dogs to generate a hypothesis of a common exposure, data from veterinarians treating the dogs were systematically registered, fecal samples from both healthy dogs and dogs with hemorrhagic diarrhea were collected and autopsies on 18 dogs that had died or been euthanized due to AHDS were performed. The Norwegian University of Life Science (NULS) collaborated in treating sick dogs, collecting data and fecal samples (Jørgensen et al., unpublished).

In total, 511 reported cases met the case definition "Dog in Norway presenting with acute hemorrhagic diarrhea with an onset 1st August 2019 or later, reported to NVI or NFSA by a veterinarian". Cases were reported from all counties of Norway, but mainly from Oslo and southeast of Norway. The response to the survey was inconclusive in regard of identifying a common exposure. 73% of households with >1 dog had only one sick dog with relevant symptoms at the time of reporting and there was mainly only one reported case per postal code, leading to the conclusion that the disease was not likely to be transmissible between dogs (Jørgensen et al., unpublished).

The major findings from the autopsies of the dogs were dramatic changes of the intestinal mucosa. The small intestine mucosa was brown or dark red to violet, smooth and glossy, with diffuse loss of surface epithelium and loss of architecture with collapse of the villi lamina propria. In some of the dogs, necrosis of intestinal epithelial cells was observed, and multifocal hemorrhages were seen in the deep lamina propria and submucosa. Gram-stained sections showed rich amounts of small Gram-negative rods, located as single bacteria or thick layers close to the surface or as large clusters deeper in the collapsed lamina propria. The same findings were observed in the large intestine, with the same types of bacteria on the surface and in the lamina propria (Jørgensen et al., unpublished).

Bacteria from intestinal content was cultured, and the result from the first three autopsied dogs were noteworthy. The bacteria *Providencia alcalifaciens* was cultured in almost pure culture and analyses confirmed the small Gram-negative rods found in the Gram-stained sections from the small and large intestine to be *P. alcalifaciens*. Among the 18 autopsied dogs, 16 were positive for *P. alcalifaciens*. Furthermore, *P. alcalifaciens* was detected in 42% of the fecal samples from dogs with hemorrhagic diarrhea in contrast to 11% of fecal samples from healthy dogs, indicating a pathological role of *P. alcalifaciens*. However, the bacteria *Clostridium perfringens* was also cultured from 43% of the received fecal samples from dogs with AHDS and could not be ruled out as a causative agent of the outbreak, although this is a common finding in dogs with diarrhea (Jørgensen et al., unpublished). No difference in severity of clinical signs or outcome between *C. perfringens*- positive dogs and -negative dogs with AHDS have been detected (Busch et al., 2015).

1.2 *Providencia alcalifaciens*

Providencia alcalifaciens is a Gram-negative, rod-shaped bacteria, belonging to the family Enterobacteriaceae (Shah et al., 2019). It is a facultative anaerobe bacterium and motile by peritrichous flagella (Manos & Belas, 2006). The bacteria are found in soil, polluted water and sewage, and has been isolated from a broad range of organisms including chickens, pigs, and sharks (Aibinu et al., 2011; Interaminense et al., 2010; Lauková, 2000).

P. alcalifaciens is not a well-documented enteric pathogen in dogs. It has been reported as the presumptive cause of diarrhea in a four-month-old golden retriever that recovered after antibiotic treatment, and as the causative agent of hemorrhagic diarrhea in three thirteen-days-old puppies that died the day after first occurrence of symptoms (Król et al., 2007; Möhr et al., 2002). In 2006, A Norwegian bachelor thesis identified genetic relationship between isolated strains from six different dogs suffering from diarrhea and investigated their invasiveness on Vero- and HeLa cells. It was concluded through pulsed-field gel electrophoresis (PFGE) that four of the strains showed highly genetic similarities. The same strains were the most invasive into the cells, which supported the hypothesis that *P. alcalifaciens* were the primarily causative agent of diarrhea in the dogs (Fauske & Hirsch, 2006).

Among humans, several incidents of diarrhea caused by *P. alcalifaciens* are reported. Three outbreaks of foodborne infection caused by *P. alcalifaciens* have been reported from Japan, Turkey and Kenya. The spectrum of disease severity was found to vary depending on age groups. The attack rate has been found higher among younger children than high school students and adults, and severe illness has been observed among children compared to adults who required no hospitalization (Chlibek et al., 2002; Murata et al., 2001; Shah et al., 2015). *P. alcalifaciens* has also been implicated as a causative agent of traveler's diarrhea. The bacteria were isolated 7-8 times more frequently among the returning British traveler´s with diarrhea than among patients who had diarrhea but did not have a history of recent travel (Haynes & Hawkey, 1989). This was supported by a similar study in which the pathogen was isolated from traveler´s returning to Japan (Yoh et al., 2005).

A study from 2013 demonstrated that *P. alcalifaciens* is not only limited to intestinal infections. A conventional pig farm located in China experienced an outbreak of a respiratory disease among suckling piglets. The piglets suffered from serious dyspnea and hemorrhagic

pneumonia with high mortality. More than 70% of the piglets died from the disease and typical lung lesions yielded a bacterial isolate identified as *P. alcalifaciens* based on the 16S ribosomal DNA sequence analyses. The lungs of infected piglets were friable, swollen and dark brown in color caused by serious hemorrhage (Wang et al., 2013).

The first reported study of *P. alcalifaciens* strains isolated from human diarrheal stools in 1992 suggested cell invasion as the main virulence factor (Albert et al., 1992). Since then, several cultured mammalian cell lines have been used to study *P. alcalifaciens* invasiveness and the ability to invade cell monolayers has been a well-established mode of pathogenesis in *P. alcalifaciens* (Shah et al., 2019). Twenty years later, a PCR-restriction fragment length polymorphism (RFLP) assay was developed to shed light on the relevance of certain toxin-producing *Escherichia coli* strains in patients with diarrhea. Stool samples from children with diarrhea in Japan were examined, and untypeable toxin genes were detected directly from two of the samples. The bacteria harboring these genes were isolated and identified as *P. alcalifaciens.* The gene cluster encoding a cytolethal distending toxin (CDT) was sequenced including its flanking regions, where genes partly homologous to transposase elements and the IS elements were found. No plasmid was found, and data suggested that the gene cluster most likely is located at the chromosome, acquired by horizontal gene transfer events as a possible virulence factor to facilitate certain strains of *P. alcalifaciens* invasiveness (Shima et al., 2012).

1.2.1 Cytolethal distending toxin

Some of the most potent toxins produced by bacteria and plants are members of a large family known as the AB toxin. In this arrangement, the A chain or subunit typically function as an enzyme that disrupts a specific cell process or pathway, and the B chain or subunit, in monomeric or polymeric form, promotes binding of the holotoxin to the target cell surface (DiRienzo, 2014).

The newest member of the AB toxin superfamily, discovered by Johnson and Lior in 1987, is the cytolethal distending toxin (DiRienzo, 2014). It was then identified as a novel heat-labile toxin in culture filtrates obtained from *Campylobacter* spp., *Escherichia coli* and *Shigella dysenteriae* which caused distinctive and progressive cytoplasmic and nuclear enlargement of cultured mammalian cells (Jinadasa et al., 2011).

Later discoveries showed that CDT is a heterotrimeric AB_2 genotoxin produced by several clinically important Gram-negative mucocutaneous bacterial pathogens belonging to the γ and ε classes of Proteobacteria (Jinadasa et al., 2011). These CDT producing bacteria are responsible for chronic infection and inflammatory disease in both human and animals, and their niches range from the intestinal mucosa, the urogenital mucosa, external genitalia, the respiratory tract, the upper respiratory mucosa, periodontal pockets, dental plaque, the liver and the blood (Jinadasa et al., 2011; Scuron et al., 2016).

CDT is organized into a single operon encoding three polypeptides: CdtA, CdtB and CdtC (Guerra et al., 2011). When the three polypeptides are combined, they interact with one another to form an active holotoxin that exhibits full cellular toxicity (Lara-Tejero & Galán, 2001). The CdtA and CdtC subunits are lectin-type molecules, sharing generally less than 30% structural homology with the B-chain repeats of the plant toxin ricin. However, several conserved structural features are conserved, suggesting that these two subunits are required for binding the holotoxin to the plasma membrane of the target cells, thus forming the B subunit of the AB toxin. Binding of CDT requires intact cholesterol-rich domains on the target cell surface (Guerra et al., 2011). Greater heterogeneity in the composition and structure of the B subunit is most likely because this component of the holotoxin has evolved to recognize a broad range of target cells (DiRienzo, 2014). The CdtB subunit is the most conserved component of the holotoxin amongst all CDT producing bacteria and represent the active A subunit of the AB toxin, which can translocate to the nucleus and induce lesions (Guerra et al., 2011). The catalytic domain of the cdtB subunit belongs to the Exonuclease-Endonuclease-Phosphatase (EEP) domain superfamily which includes DNase-1 (NCBI).

To this date, CDT is the only member of the bacterial AB toxins that display DNase activity and, irrespective of the bacterial species of origin, exerts genotoxic damage by causing double strand breaks (DSBs) in the DNA leading to irreversible cell cycle arrest in the G2/M phase and apoptosis in a broad range of mammalian cell lineages (Jinadasa et al., 2011).

1.3 The anatomy and function of the small and large intestine

The basic structure of the intestine can be considered as a hollow tubular structure with epithelial cells lining the lumen, with circular and longitudinal layers of smooth muscle in the intestinal wall, and with endocrine and neural elements. Together, these elements either

remove fluid and electrolytes from the lumen (i.e., absorption) or add these substances to the lumen (i.e., secretion) in an inferior direction (Boron & Boulpaep, 2009).

The different layers of the intestinal wall, starting from the lumen and moving towards the blood is composed of a mucosal layer, a submucosal layer, two layers of smooth muscle and two plexuses that contain the intestinal nervous system (Figure 1). The mucosal layer consists of a layer of epithelial cells, a lamina propria and a muscularis mucosae. The epithelial cells are specialized to carry out absorptive and secretory functions. The lamina propria consists primarily of connective tissue, but it also includes blood and lymph vessels. The muscularis mucosae consists of smooth muscle cells which regulates the shape and surface area of the epithelial cell layer. Beneath the mucosal layer is a submucosal layer, which consists of collagen, elastin, glands and the blood vessels of the intestines. The motility of the intestines is provided by two layers of smooth muscle, circular- and longitudinal muscles. The circular muscle layer is thick and tightly supplied with nerve fibers while the longitudinal muscle layer is thin and contains few nerve fibers. The longitudinal muscle layer is the outermost layer of the intestine wall, facing the serosa which separates the intestines from the abdominal cavity (Costanzo, 2013). In between the submucosa, the circular- and the longitudinal muscle layer, the submucosal plexus and the myenteric plexus are found. It is generally thought that the submucosal plexus controls secretion and blood flow whereas the myenteric plexus controls motility. A correlation between secretion/blood flow and motility has been shown, indicating communication between the two plexuses (Monro et al., 2008).

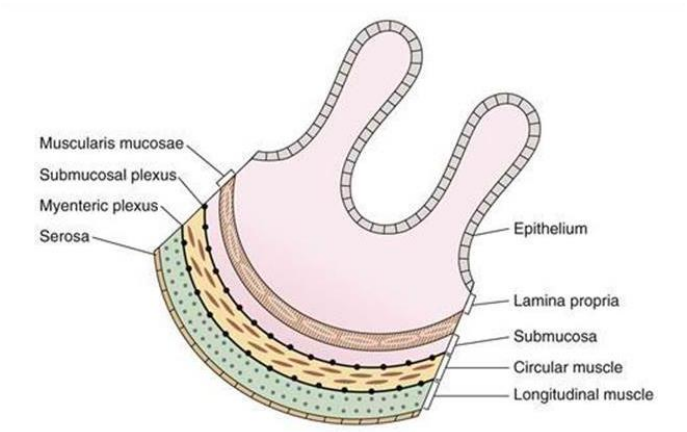

Figure 1: Section of the intestinal wall showing the different type of structural layers (Costanzo, 2013)**.**

In mammals, nutrients are only absorbed in the small intestine, and finger-like projections called villi are exclusive to the small intestine (Figure 2.A). The structure increases the surface area that is available for absorption. The villi are surrounded by the openings of

intestinal glands named crypts of Lieberkühn (from now on called crypts) (Figure 2.A). The large intestine does not have villi (Figure 2.B), but crypts that are similar in structure and function to the small intestine crypts and that increases the surface area of the large intestine. The cells lining the villi in the small intestine and the cells lining the surface of the large intestine are the primary cells responsible for absorption, whereas the crypt cells primarily participate in secretion (Table 1) (Boron & Boulpaep, 2009).

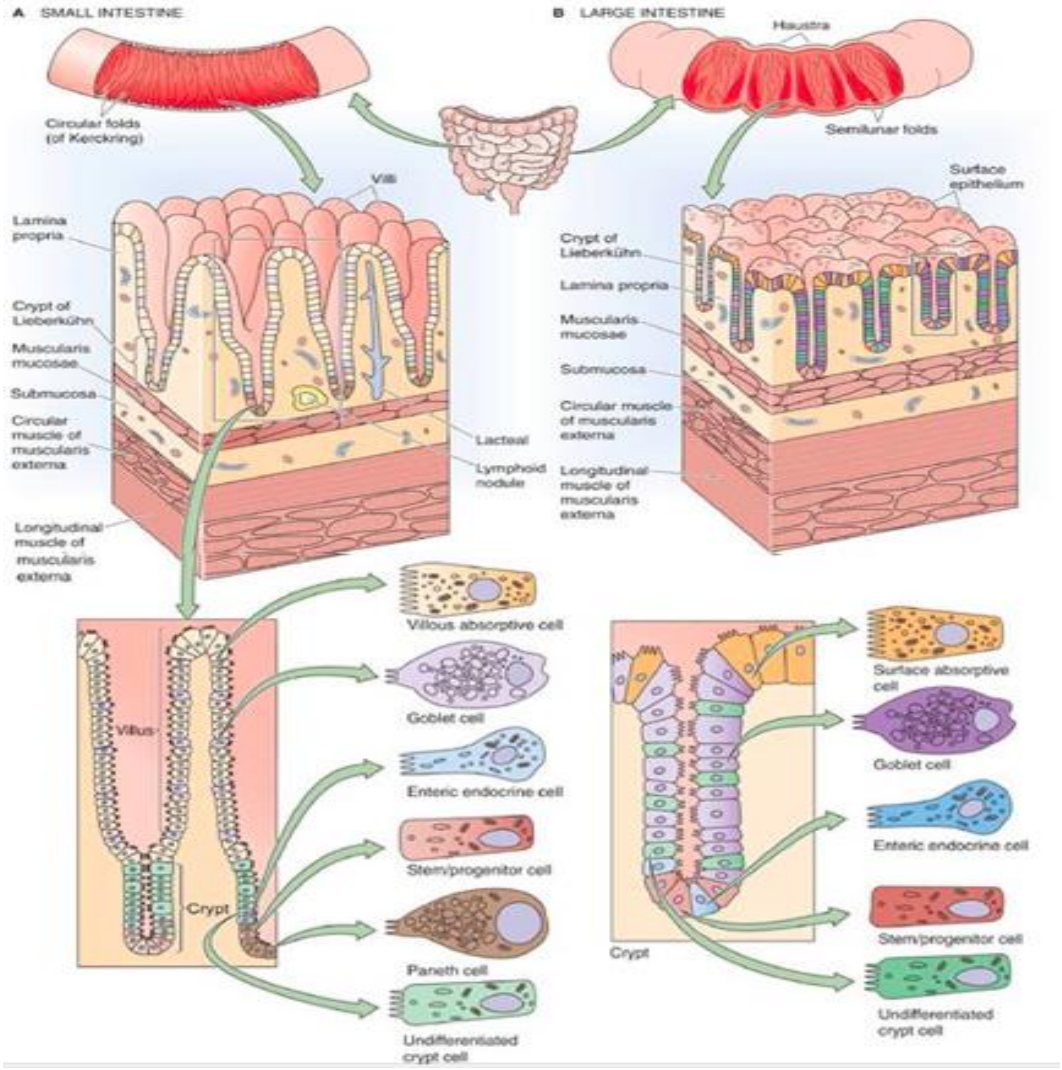

Figure 2: The anatomy and the subset of epithelial cells in the (A) small and (B) large intestine (Boron & Boulpaep, 2009).

The zone of cell proliferation is at the base of the crypt in both the small and large intestine (Boron & Boulpaep, 2009). The progenitor cell is a stem cell that reside at the base of the crypts (Figure 2.A.B) producing daughter cells. As the progeny cells migrate toward the luminal surface, they lose their proliferative capacity and differentiate into specialized cells.

Cells at the luminal surface eventually undergo programmed cell death (apoptosis) and are shed into the lumen (Capaldo et al., 2017). Under optimal functioning, it is estimated that the cells of an entire crypt is replaced every 4-5 days.

The various differentiated cell types found within the gut epithelium, carries out unique and specialized functions (Table 1). In general, the majority of cell types located in the small intestine are also found in the large intestine (Allaire et al., 2018).

Table 1: Intestinal epithelial cell (IEC) subtypes, their localization and their role in the intestines (Allaire et al., 2018).

IEC subtype	Localization	Role
Enterocyte (Villous absorptive cell/Surface absorptive cell)	Small intestine Large intestine	Physical barrier Nutrient/water absorption Epithelial shedding Secrete antimicrobials
Goblet cell	Small intestine Large intestine	Mucin secretion Secret antimicrobials Facilitate luminal antigen transfer to dendritic cells via goblet cell-associated antigen passages
Enteric endocrine cell	Small intestine Large intestine	Secrete hormones
Paneth cell	Small intestine	Secrete antimicrobials factors to protect nearby stem cells at the base of small intestinal crypts
M cell (not shown in figure 1)	Small intestine	Antigen uptake and passage to underlying immune cells

1.3.1 The intestinal mucosa

Intestinal fluid secretion is a vitally important function of the intestinal epithelium used by the intestinal tract to protect itself from bacteria and bacterial toxins (Boron & Boulpaep, 2009). The intestinal tract is inhabited by a high number of microorganisms that live in a mutualistic relationship with the host. To prevent translocation of commensal and pathogenic microorganisms into underlying tissue, a defense mechanism has been developed that includes the formation of an organized glycoprotein network composed of mucin. These proteins are highly O-glycosylated, and hydration leads to swelling of the mucus forming a gel-like structure (Schroeder, 2019). There are two groups of mucins, transmembrane mucins

(MUC1, MUC3A, MUC3B, MUC4, MUC12-18, MUC20 and MUC21) and secreted mucins (MUC2, MUC5AC, MUC5B, MUC6-8 and MUC19) (Apostolopoulos et al., 2015). The major secreted mucus protein in the intestine is MUC2 and is constitutively produced by goblet cells.

In the small intestine, a looser mucin network may be necessary for the uptake of nutrients across the epithelial border. To prevent opportunistic bacteria escaping from their luminal environment, small intestinal mucus is charged with antibacterial proteins and peptides such as Paneth-cell-produced defensins and lysozymes killing microorganisms that reach proximity to the epithelium. The immune system also induce aggregation of bacteria by immunoglobulin A (IgA) to prevent bacteria from crossing the mucosal barrier by size exclusion (Schroeder, 2019). Lymphatic tissue called Peyer´s patches in the lamina propria and submucosa of the small intestine is overlayed by M cells that sample luminal contents and transport intact antigens to dendritic cells for antigen processing and presentation, thereby initiating an immune response or tolerance. The follicle-associated epithelium overlaying Peyer´s patches produce lower levels of antimicrobial peptides, secreted IgA and mucus to access luminal antigens. Small-intestinal goblet cells also appears to deliver antigens to dendritic cells via goblet cell associated passages (Allaire et al., 2018).

In the large intestine, mucus is organized into three distinct layers. The distinct inner layer is nearly sterile and consists of membrane-anchored mucins associated with the large intestine epithelial cells forming the glycocalyx. The glycocalyx gives precedence to a second tightly crosslinked inner layer, primarily composed of the mucin protein MUC2. A less defined outer layer is generated by proteolysis of the inner layer and is a mix of mucus, gut bacteria and dietary material. Bacteria in the large intestine produces metabolites like vitamins and short-chain fatty acids that is absorbed by the epithelium and the bacteria needs to be maintained in a sufficient distance from the absorptive cells. Consequently, the large intestine epithelium produces fewer antimicrobial peptides that stick to the mucus, but rather secretes peptides that bind and aggregate bacteria, inhibiting bacteria crossing the barrier by size-exclusion and inhibiting motility (Capaldo et al., 2017; Schroeder, 2019).

1.3.2 Enterocytes

The absorptive cells are the main cells present in the intestinal epithelium. Enterocytes account for 80-90% of all the small intestine epithelial cells and 60-70% of all the large

intestine epithelial cells (Massey-Harroche, 2000). They form a tight epithelial monolayer along the crypt-villus axis of the intestine, serving as a permeability barrier between luminal contents and the blood supply. Enterocytes show a polarized pattern of arrangement with the formation of functionally and structurally distinct plasma membrane domains, termed apical and basolateral (Figure 3). The apical surface faces the lumen and in a fully differentiated state, each enterocyte is characterized by an apical structure that consist of thousands of microvilli. The structural core of a microvillus is actin filaments that extend from the cell surface into the lumen, making the surface area available for absorption even greater. The microvilli- covered surface is named the brush border and houses digestive enzymes, transporters and channel proteins. The microvilli also secrete antimicrobials compounds (McConnell et al., 2011).

1.3.3 Tight junctions

The intestinal epithelium function as a barrier that separates the internal milieu from the luminal environment. An intact intestinal barrier protects the organism against invasion of microorganisms and toxins, while the barrier must be permeable to absorb essential fluids and nutrients (Bischoff et al., 2014). The intestinal epithelium mediates selective permeability through transepithelial/transcellular and paracellular pathways (Figure 3). Transcellular permeability is generally associated with solute transport through the cell and are predominantly regulated by selective transporters of amino acids, electrolytes, short-chain fatty acids, and sugars. Paracellular permeability refers to the transport of substances through the intercellular space between epithelial cells and is regulated by intercellular multiprotein complexes located at the apical-lateral membrane junction and along the lateral membrane (Figure 3). The tight junctions (TJs) regulate the paracellular barrier which facilitates the passage of ions and solutes through the intercellular space while preventing the translocation of luminal antigens, microorganisms and their toxins into the lamina propria. TJ complexes are also important in the regulation of cellular proliferation, polarization and differentiation (Groschwitz & Hogan, 2009).

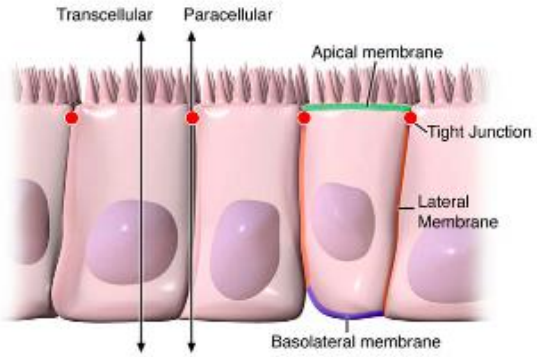

Figure 3: The different pathways of epithelial permeability. Transcellular permeability is regulated by selective transporters across the membrane. Paracellular permeability is regulated by TJs located at the junction of the apical-lateral membranes (Groschwitz & Hogan, 2009).

1.3.4 Tight junction proteins

TJs consist of integral transmembrane proteins and peripheral membrane proteins. Integral transmembrane proteins include occludin, claudin, junctional adhesion molecule (JAM) and tricellulin that form a network between adjacent cell membranes (Figure 4). Peripheral membrane proteins include zonula occludens-1 (ZO-1), ZO-2 and ZO-3. Peripheral membrane proteins connect the integral transmembrane proteins to the actin cytoskeleton and to signaling proteins. The interaction of occludin to adjacent cells and to ZO-1 is regulated by phosphorylation of occludin and is essential for TJ stability and permeability, but not for normal TJ structure (Lee et al., 2018). The two extracellular loops of claudin participate in cis- and trans- interaction between claudins in adjacent cells, forming the backbone of TJ strands. Based on their barrier properties, claudins can be divided into two functionally distinct groups determined by their first extracellular loop. Barrier forming claudins tightens the paracellular pathway completely while pore forming claudins increases permeability to a certain group of ions (Günzel, 2017).

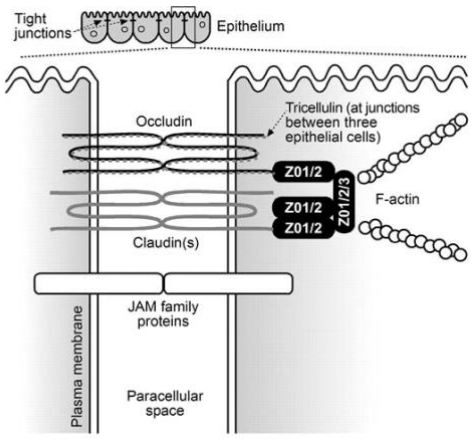

Figure 4: Integral transmembrane proteins seal the paracellular space between adjacent epithelial cells. Peripheral membrane proteins connect integral transmembrane proteins to actin cytoskeleton (Ulluwishewa et al., 2011).

1.4 Cellular model system

1.4.1 Dog intestinal epithelial cell line

The dog epithelial cell line, SCBN, was originally established as a human small intestinal epithelial cell line derived from a human patient, BN. It was first reported as one of the first human small intestinal epithelial cell line growing as monolayers *in vitro*, showing morphological and functional characteristics typical of crypt- like intestinal epithelial cells. However, it was also reported that the cell line showed abnormal karyotype with modal chromosomal number 76 (Pang et al., 1996). Experimental difficulties were later encountered during PCR-based experiments with the cells. It was only possible to amplify DNA sequences from SCBN cells using primers common to vertebrates and specific for dog genes. By sequencing 9 different genes from SCBN cells it was concluded that SCBN cells are of dog, not human genotype, and that these observations hold true for one of the early cell stocks obtained directly from the laboratory where the cell line was first isolated (Buret & Lin, 2008).

SCBN cells are comparable in morphology and function to dog small intestinal epithelial cells and have been used extensively to study epithelial pathophysiology and epithelial barrier function (Lamb-Rosteski et al., 2008). The cells have been shown to form polarized monolayers that express TJ proteins and brush border enzyme activity, as well as microvilli (Pang et al., 1996). The monolayers have a high transepithelial electrical resistance (Lamb-

Rosteski et al., 2008; Teoh et al., 2000). For this reason, SCBN cell line serves as a good *in vitro* model for studying toxic effects on dog intestinal epithelial cells.

A common method for *in-vitro* experiments with barrier forming cells is to cultivate the cells on removeable, hanging cell culture transwell inserts for a standard well plate (Figure 5). Cell inserts contain a porous membrane, simulating the physiological conditions where the cell monolayer act as a selective barrier between the apical and basolateral sides. The removeable insert allow access to both sides. Methods for accessing the barrier permeability are, among others, immunofluorescent staining of proteins related to TJs and measurement of the electrical resistance (Linz et al., 2020).

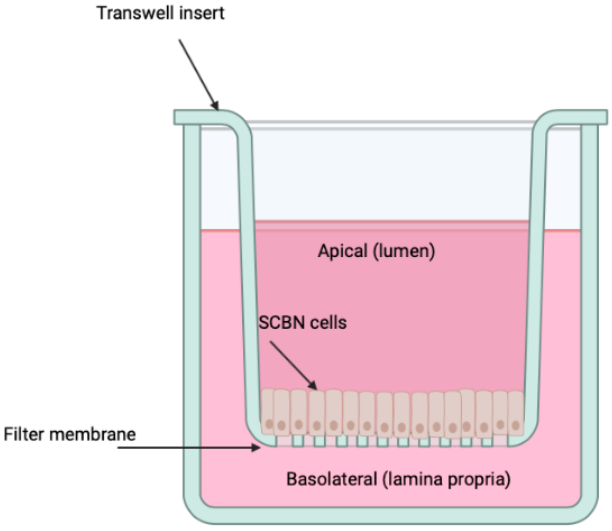

Figure 5: The SCBN cells are seeded onto transwell inserts where they form polarized monolayer. The apical side represent the lumen, whereas the basolateral side represent the lamina propria. Created with Biorender.com.

1.5 Aims of the study

The hypothesis: CDT from *P. alcalifaciens* induce toxicity in the dog intestinal epithelial cell line SCBN.

To test this hypothesis several aims were generated:

- Characterize SCBN cells grown on membrane with focus on barrier function (TJ, TEER, mucin production).

- Characterize the effect of exposure to CDT from *E. coli* on SCBN cells (TEER, cytotoxicity).

- Optimize culture conditions of *P. alcafaciens* for increased CDT production.

- Characterize the effects of cultures of CDT-producing *P. alcafaciens* on SCBN cells (cytotoxicity).

- Study cytotoxicity of genetic variants of subunit cdtB by cloning and transfection in SCBN cells

2.0 Materials and methods

2.1 Cell culturing and treatments

2.1.1 Cell culturing

The dog epithelial cell line, SCBN, was a gift from Dr. André Buret (University of Calgary, Canada). All cells were grown in T75 cm^2 culture flasks, with Dulbecco´s Modified Eagle´s Medium high glucose with L-Glutamine (DMEM) supplemented with 5% heat-inactivated Fetal Bovine Serum (FBS) and 1% penicillin/streptomycin (from now on referred to as DMEM complete). The cells were stored in a humidified incubator at 37ºC with 5% CO_2. The cell line was adherent.

Passaging or splitting of the cells is a way of reducing cell density and to stimulate further cell proliferation. Splitting of the cells was done when the cells had reach approximately 80% confluence as a fully confluent monolayer may alter the properties of the cells, leading to problems of experimental reproducibility (Natoli et al., 2011; Puliafito et al., 2012).
The cells were detached from culture flask by using trypsin-EDTA (2.5 g/l). EDTA binds divalent cations and weakens the cell-cell/cell-matrix Ca^2 dependent adhesion mechanism (Attili et al., 2019). The cleavage ability of the proteolytic enzyme trypsin is enhanced by EDTA and the trypsin-EDTA solution is a commonly used mixture for detachment of adherent cells in culture.

The cells were washed with PBS to remove residual cell medium before incubated with trypsin-EDTA (2.5 g/l), 2 ml per 75 cm^2 for 10 min at 37ºC. Re-suspension was done in 8-13 ml DMEM complete that inactivates the trypsinization process. The cells were split every Monday and Wednesday 1:10, on Fridays 1:15. After each trypsinization, the cells were given a new passage number. The use of similar and identified passage number throughout a project will better ensure reproducible results as the number of times the cell line has been passaged may have an impact on the cells (Hughes et al., 2007). The passage number for the SCBN cell line was kept between 22-62.

2.1.2 Cell seeding

The cells were trypsinized as described in section 2.1.2 and the number of cells per milliliter were counted using a Moxi™ Z Mini Automated Cell Counter by ORFLO Technologies. Various cell densities were seeded out either onto tissue culture treated, nonpyrogenic polystyrene, sterile cell culture lidded 96 well plates or hanging cell culture transwell inserts (Millicell® cell culture inserts, 0.4 µm polyethylene terephthalate).

2.1.3 Cryopreserving

Dimethyl sulfoxide (DMSO) is commonly utilized for cell cryopreservation. It induces transient pore formation that involves modulation or disruption of ion/water transport across a cell membrane and prevents cellular damage caused by formation of ice crystals during the freezing process (Gurtovenko & Anwar, 2007). The cells were stored in media containing 0.1% > DMSO in liquid nitrogen (-196°C). High concentrations of DMSO may disrupt the lipid bilayer of the cells, therefore the thawing of the cells was done quickly in a water bath at 37°C followed by centrifugation and re-suspension in fresh medium (Gurtovenko & Anwar, 2007). Cells were transferred to a T75 cm^2 culture flask and medium was refreshed 24 hours after thawing.

2.2 Characterization of the dog intestinal epithelial cells

2.2.1 Transepithelial electrical resistance

Transepithelial electrical resistance (TEER) is the measurement of electrical resistance across a monolayer in the unit ohms (Ω). A continuous current pass through the cells in both transcellular and paracellular pathways. The epithelial resistance is mainly influenced by specific TJs proteins (Chen et al., 2015). TEER can be measured manually with a chopstick-like electrode connected to a Millicell® ERS Voltmeter, or automatically by a cellZscope® instrument. By inserting one electrode in the basolateral compartment and one in the apical compartment of cells seeded onto a hanging cell culture transwell, the potential between the two sides can be measured. Monolayer resistance can be obtained by subtracting the resistance of a transwell insert without cells containing only DMEM complete (R_{blank}) from the resistance of cells seeded onto transwell insert with DMEM complete (R_{total}) giving R_{Ω} (equation 1).

1. $R_{\Omega} = R_{total} - R_{blank}$

Multiplication of R_{Ω} by the effective area of the membrane (equation 2) gives the final unit area resistance, TEER (Srinivasan et al., 2015).

2. $TEER = R_{\Omega} \text{ x } Area\ (cm^2)$

2.2.2 Immunofluorescent staining

Immunofluorescent (IF) staining was done to visualize ZO-1 and MUC1. IF is a technique that permits visualization of a wide variety of different components in cells. Specific antibodies tagged with fluorophores binds to a molecular target, called an epitope, in the protein or other cellular components of interest. The antibodies can either be monoclonal in that they are identical and target only one epitope, or polyclonal meaning that they are not identical and can bind to several epitopes in the target molecule (Saper, 2009). Here, a primary polyclonal antibody binds to the molecule of interest. A secondary polyclonal antibody coupled to a fluorophore then attach to the primary antibody. IF can be used in combination with other, non-antibody methods of fluorescent staining, such as DAPI (4´,6-diamidino-2-phenylindole) DAPI is a fluorescent, synthetic dye that binds to minor groove at the AT-rich regions of DNA as well as intercalating at CG rich regions (Reis & Rocha, 2017).

The cells were grown on permeable transwell inserts. At different timepoints, the cells were washed and fixated as described in section 2.2.2. For the detection of intercellular molecules, different permeabilization/blocking methods were used for staining ZO-1 and MUC1. For MUC1, the cells were permeabilized with ice-cold 100% MeOH and incubated at -20ºC followed by blocking in PBS/5% normal goat serum/0.3% Triton X-100 to eliminate unspecific binding. For ZO-1, the cells were permeabilized with 0.05% saponin/PBS and blocked with 1% BSA/PBS.

The membranes were cut out of the transwell inserts by using a scalpel, split in two, and stained with the primary antibodies MUC1 (mouse; 1:200) diluted in antibody dilution buffer (PBS/1% BSA/0,3% Triton X-100) or ZO-1 (Cat. No 61-7300) (rabbit; 1:1000) diluted in blocking buffer (1% BSA/PBS), and incubated overnight at 4ºC. The cells were washed 3 x

PBS for 5 min each to remove unbound antibody. The fluorophore-conjugated secondary antibodies used were goat-anti-mouse IgG (H+L)-Alexa 488 (Cat. No. A-11029) for MUC1 (1:500 dilution in antibody dilution buffer) or goat-anti-rabbit IgG (H+L)-Alexa Fluor Plus 488 (Cat. No. A32731) for ZO-1 (1:500 dilution in blocking buffer). The secondary antibody was incubated for 2 hours, room temperature, dark, and rinsed 2 x PBS. DAPI (Cat.no. D1306) was added for the visualization of nuclei. The membranes were mounted as described in 2.2.2. The slides were then analyzed by Zeiss AXIO observer A1, invert fluorescence microscope.

2.2.3 Alcian Blue staining of mucins

Alcian blue contain cationic dye molecules in solution at a specific pH. All acidic mucin, whether carboxylated or sulfated will ionize at a pH of 2,5 to produce anionic groups and stain with Alcian blue. The Alcian blue staining solution contained 1% Alcian Blue in 3% acetic acid.

Cells (3 x 10^4 cells/cm^2) were seeded on permeable transwell insert and allowed to grow/differentiate for 21 days. The culture medium was removed gently not to disturb the mucus layer, and the cells fixed with 4% PFA for 1 hour at room temperature. The cells were washed 2 x PBS. Incubation with Alcian Blue staining solution (Merck KGaA) was done for 15 min, at room temperature. The staining solution was decanted, and the cells were rewashed once with 3% acetic acid followed by 4 x washes with PBS to remove excessive staining. A transwell insert containing TH29-MTX cells were stained as a positive control (Esch et al., 2014). The glycoproteins stained by Alcian Blue were visualized with a Leica DM2000 LED microscope with a DeltaPix HDMI16MDPX camera (color camera).

2.2.4 Intestinal Alkaline Phosphatase staining

Intestinal alkaline phosphatase (IAP) is a brush border enzyme produced by enterocytes of the small intestine. The enzyme exerts anti-inflammatory properties that detoxifies a variety of bacterially derived proinflammatory factors such as lipopolysaccharide and flagellin. IAP also displays other physiological roles, including the regulation of intestinal surface pH, the control of gut microbiota composition and function, and the ability to regulate the levels of key tight junction proteins and their cellular localization (Lallès, 2019).

The Fast Red Substrate Kit (Cat. No. ab64254) was used to detect IAP. In the presence of the enzyme, Fast Red produces a red reaction that can be seen using either brightfield or fluorescence microscopy.

Cells (3 x 10^4 cells/cm^2) were seeded on permeable transwell insert and allowed to grow/differentiate for 21 days. The cell culture medium was removed carefully, and the cells washed 1 x PBS. Fast Red (1:75, diluted in Liquid Fast Red Substrate) was added to the insert and incubated for 20 min, at room temperature. One drop of the solution was added to a glass slide before the cells were washed 2 x PBS. The membrane was cut of the transwell insert and transferred to the slide with the cell side facing down. A transwell insert containing Caco-2 cells were stained as a positive control (Basson et al., 1996). The IAP stained by Fast Red was visualized with a Leica DM2000 LED microscope with a DeltaPix HDMI16MDPX camera (color camera).

2.2.5 Phalloidin staining of actin

Phalloidin is derived from a toxic mushroom and binds with high specificity to F-actin in the cytoskeleton. Direct conjugation of fluorophores to phalloidin makes it a convenient tool for visualization of actin filaments in the cell (Mazloom-Farsibaf et al., 2021).

Cells were grown on permeable transwell inserts. At different timepoints the cell culture medium was removed carefully, and the cells washed 1 x PBS. The cells were fixed with 4% Paraformaldehyde for 15 min, room temperature, and washed 3 x PBS, 5 min each. PFA forms methylene bridges with proteins in the cells, preserving the structure by immobilization (Huang & Yeung, 2015). The cells were permeabilized in 0,05% saponin/PBS and incubated for 10 min, room temperature, followed by blocking the cells in 1% BSA/PBS.

The membranes were split in two and stained with phalloidin AF555 (Cat.no. A34055) (1:300 diluted in blocking buffer). The cells were incubated for 1 hour and membrane washed twice in PBS. For visualization of the nucleus, the cells were stained with DAPI (1:1000 dilution in PBS), 5 minutes, room temperature, dark. The membrane was transferred to the slide with the cell side facing up. 15 µl mowiol mounting medium was added on top of the membrane and mounted by a coverslip. The slides were stored flat and protected from light for 24 hours. The slides were then analyzed by Zeiss AXIO observer A1, invert fluorescence microscope.

2.3 Toxin production *in vitro* and gene expression measurement

2.3.1 Toxin production *in vitro*

For characterizing the effect of cultures of CDT-producing *P. alcalifaciens* on SCBN cells, different isolates were chosen for toxin production. The *P. alcalifaciens* isolates were categorized by NVI and NULS in regard of the clinical picture of the dogs when sampling.

2.3.2 *Providencia alcalifaciens* strains and culture conditions

All isolates were sampled from dogs in which the owner had consulted a veterinarian due to diarrhea.

- Strain 29292 was isolated from a dog that presented good general condition but suffered from diarrhea without blood and the CDT sequence was identical to that of strain 27799
- Strain 27799 is related to pathology and the CDT sequence was identical to that of strain 1723
- Strain 1723 was isolated from a dog that died the day after sampling and suffered from thin, watery, hemorrhagic diarrhea
- Strain 1722 was isolated from a dog that presented good general condition but suffered from diarrhea without blood
- Strain 3283 was isolated from a dog that presented good general condition but suffered from diarrhea without blood

In addition, *E. coli* strain v27 (CDT-II positive) was cultivated for use as a positive control.

Three different media for bacterial growth were applied;
Brain Heart Infusion (BHI) broth consists of beef heart (5 g/l), calf brain (12,5 g/l), disodium hydrogen phosphate (2,5 g/l) and D (+)-glucose (2,5 g/l). BHI is recommended for the cultivation of fastidious pathogenic microorganisms (Merck KGaA).

Evan´s toxin medium consists of 20 g Casamino Acids, 6 g yeast extract, 2,5 g NaCl, 8,71 g K_2HPO_4 (0,05 M), 1 ml of trace salts. Added to distilled water in that order, adjusted to pH 8,5 with 0,1 N NaOH (4 g/liter). The trace salt mixture consisted of 5% $MgSO_4$, 0,5% $MnCl_2$, and 0,5% $FeCl_3$ dissolved in 0,001 N H_2SO_4.
Evan´s toxin medium has been applied in a study to cultivate a CDT producing *E. coli* strain (Johnson & Lior, 1988).

Blood agar plates consists of heart extracts and peptones (20 g/l), sodium chloride (5 g/l), agar (15 g/l), and blood (50-80 ml). The culture medium represents a rich nutrient base, which provides optimal growth conditions for all relevant microorganisms (Merck KGaA).

Three different conditions were applied:

- aerobic at 120 rpm
- "microaerophilic" (without shaking) with 5% CO_2
- anaerobic milieu

All conditions were applied at 37°C. For growth under aerobic conditions, bacterial cultures were incubated with shaking by 120 rpm. For growth under "microaerophilic" conditions, bacterial cultures were incubated without shaking, at 5% CO_2. For creating an anaerobic milieu, cultures and blood agar plates were stored in a sealed box containing an Anaerocult® A sachet (Merck). Anaerocult® A contains components which chemically bind oxygen completely, creating an oxygen-free milieu and a CO_2-rich atmosphere (Merck).

Three different experimental designs for toxin production were performed (Figure 6-8).

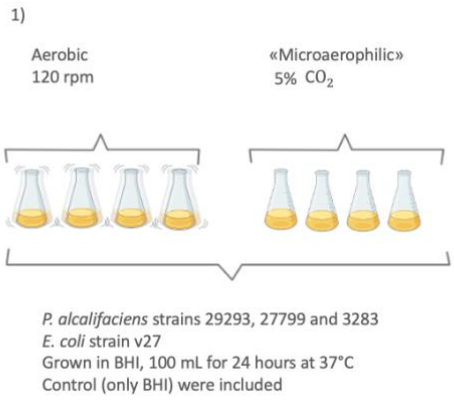

Figure 6: The first experimental design for toxin production *in vitro. P. alcalifaciens* strains 29292, 27799 and 3283 plus *E. coli* strain v27 were grown aerobically and microaerophilic in 100 ml BHI medium for 24 hours. Figure created with Biorender.com.

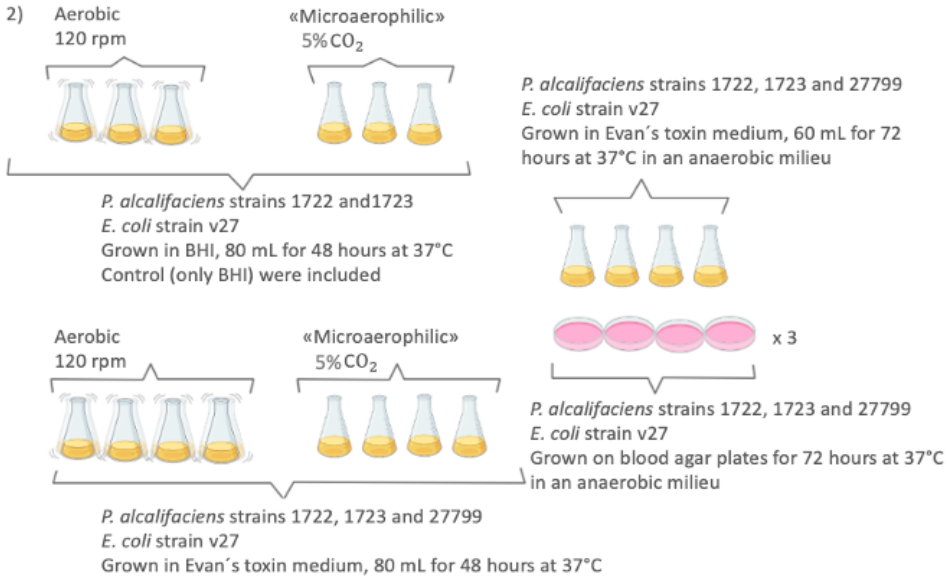

Figure 7: The second experimental design for toxin production *in vitro. P. alcalifaciens* strains 1722, 1723 and *E. coli* strain v27 were grown aerobically and microaerophilic in 80 ml BHI/Evan´s toxin medium for 48 hours. The bacteria were also cultivated in 60 ml Evan´s toxin medium and on blood agar plates in a CO_2-rich atmosphere for 72 hours at 37°C. *P. alcalifaciens* strain 27799 were included under all conditions described, except from BHI medium. Figure created with Biorender.com.

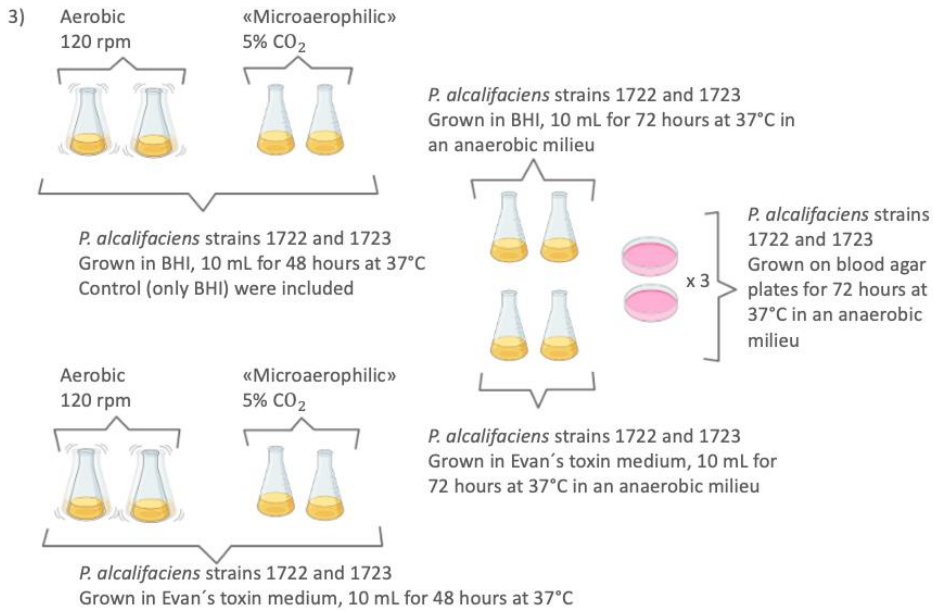

Figure 8: The third experimental design for toxin production *in vitro. P. alcalifaciens* strains 1722 and 1723 were grown aerobically and microaerophilic in 10 ml BHI/Evan´s toxin medium for 48 hours. The bacteria were also cultivated in 10 ml BHI/Evan´s toxin medium and on blood agar plates in a CO_2-rich atmosphere for 72 hours at 37°C. Figure created with Biorender.com.

For all three types of experimental designs, cryopreserved culture of bacterial strains was streaked out on blood agar plates and incubated overnight at 37°C with 5% CO_2. The next day, colonies were selected, transferred into Erlenmeyer flasks with BHI medium and incubated overnight at 37°C, 120 rpm. A 1:500 dilution of the mother culture was then prepared into the appropriate medium in Erlenmeyer flask the next day according to the experimental design. In experimental design number 2 and 3, each mother culture was also streaked out on three blood agar plates per strain using a sterile inoculation loop. For the harvesting of CDT into filter-sterilized samples, slightly different methods were applied for the three different types of experimental designs:

Experimental design 1: After 24 hours, 50 ml of bacterial cultures and negative control were transferred to a Sarstedt Inc Screw Cap tube and centrifugated at 4600 x g, 4°C for 15 min. Supernatant was filtrated through a sterile syringe 0,22 µm filter, pellet washed once in 5 ml Dulbecco´s PBS to remove residual cell culture medium. Resuspended pellet was centrifuged at 4600 x g, 4°C for 5 min. Supernatant was then carefully decanted and pellet resuspended in 10 ml PBS. Bacterial cells were lysed by ultrasonication, 3 bursts for 30 sec, the samples were cooled down between each burst to prevent protein degradation. The cell lysate was

centrifuged at 4600 x g, 4°C for 15 min. Supernatant was then filtrated through a sterile syringe 0,22 μm filter.

Experimental design 2: As Evan´s toxin medium contains yeast extract not compatible with the SCBN cells, supernatants from cultures grown in Evan´s toxin medium were discarded. The pellets were washed once in BHI, 25 μM HEPES. Resuspended pellet was centrifuged at 4600 x g, 4°C for 5 min. Supernatant was then carefully decanted and pellet resuspended in 4 ml BHI, 25 μM HEPES. Bacterial cells were lysed, centrifuged and filtrated as described above. After 72 hours, bacterial cultures in BHI and Evan´s toxin medium plus negative control were treated as described above. From the three blood agar plates per strain, bacteria were collected with an inoculation loop and resuspended in BHI, 25 μM HEPES, then treated as a pellet described above.

The modification step of experimental design number 1, with the change of resuspension buffer was applied in design 2 because the use of Ca^2-free PBS onto the SCBN cells may alter cell-cell/cell-matrix adhesion as described in section 2.1.2. BHI medium is compatible with the SCBN cells and 25 μM HEPES was applied as it is commonly used in cell culture media as a buffer that ensure stable pH values (Depping & Seeger, 2019).

Experimental design 3: Sonicated cells and cell culture medium was obtained in one fraction (applies for BHI only). Tubes containing Evan´s toxin medium were treated as described above.

The modification of experimental design number 1 and 2, with sonicated cells and cell culture medium in one fraction was applied in design 3 to possible enhance toxin concentration in the sample.

All filter- sterilized samples were streaked out on blood agar plates and incubated for 24 hours at 37°C to ensure the absence of bacteria. The samples were stored at -20°C until use.

2.3.3 Measurement of optical density at 620 nm during bacterial growth

The different growth phases of bacteria are dependent on several parameters such as nutritional conditions, aeration and the bacterial species (Navarro Llorens et al., 2010). It was

decided to measure OD_{620} by sampling cultivated bacteria at different timepoints to see how the bacteria grew in the various conditions in experimental design 2, described in section 2.3.2.

ELISA plate reader was used to determine scattered light and measured absorbance values from each sample. A volume of 100 µl from each Erlenmeyer flask were sampled in duplicates and applied to a 96 well plate in a 1:2 dilution with the appropriate medium, at seven different timepoints from 0 to 48 hours. Triplicates of BHI/Evan´s toxin medium only were applied as blank samples. From the Erlenmeyer flask incubated without shaking, the samples were taken carefully to avoid aeration into the medium. Bacterial cultures grown for 72 hours were sampled at 72 hours only. Growth curves was constructed as a graphical representation of the bacterial density at the different timepoints.

2.3.4 Isolation of nucleic acid

2.3.4.1 Sampling for ribonucleic acid extraction

For investigating under which conditions and bacterial growth phase the transcription rate of CDT genes in *P. alcalifaciens* and *E. coli* were at its highest, sampling for RNA extraction at multiple timepoints were done for later use in reverse-transcription quantitative polymerase chain reaction (RT-qPCR) assay.

From each Erlenmeyer flask in experimental design 2 (section 2.3.2), a 1:6 dilution in RNAlater® Solution (Ambion®) were added in triplicates in 1.5 ml Eppendorf safe-lock tubes, inverted by hand and incubated at room temperature for 1 hour before storage at -20°C. For bacterial cultures cultivated for 48 hours, this was applied after 3, 6, 24 and 48 hours of growth. For bacterial cultures cultivated for 72 hours, this was applied after 72 hours of growth only.

RNAlater® Solution is a commonly used RNA preservative as it stabilizes cellular RNA and preserves intact RNA by precipitating RNases into an aqueous sulfate salt solution (Salehi & Najafi, 2014).

2.3.4.2 Extraction and purification of total ribonucleic acid from bacteria

Difficulties were encountered during the process of RNA extraction and purification. Therefore, two different methods were applied. In the first method, the RNeasy® Mini Kit (Qiagen) was used. This column-based RNA extraction was performed as described in the manufacturer`s protocol. Samples in RNAlater® Solution were centrifuged at 5000 x g, 4°C for 5 min. Briefly, bacterial pellets were suspended in lysis buffer RLT, supplemented with 0.1% β-mercaptoethanol (β-ME), 350 µl buffer per sample. Intracellular RNases are released during the lysis step, and β-ME is a reducing agent that irreversibly denature RNases by reducing disulfide bonds and destroying the native conformation required for enzyme functionality (Sánchez et al., 2016). Recommended method of mechanical disruption was followed by disrupting cells in Tissuelyser II (Qiagen) for 5 minutes at maximum speed. Buffer RLT contains a high concentration of guanidine isothiocyanate which separates RNA from DNA and proteins in acidic solution. RNA binds to the positively charged RNeasy silica-membrane in the presence of 70% ethanol. Washing buffers were then added to the column for the removal of carbohydrates, proteins, fatty acids and traces of salts that are unspecific bound to the silica membrane and (Ding et al., 2008; Tan & Yiap, 2009) Finally, RNA was eluted by adding 30 µl RNase-free water directly to the spin column membrane.

The second method applied for RNA extraction was an optimized version of the conventional solution-based phenol-chloroform RNA extraction method. The protocol is customized by an additional chloroform extraction step to avoid protein and phenol contamination, and two extra ethanol washes for removal of residual salts and phenol contamination (Toni et al., 2018). QIAzol (Qiagen) were applied for lysis of the bacterial cells followed by the use of chloroform (VWR Chemicals BDH®) for RNA extraction. RNA-containing aqueous phase were transferred to isopropanol for RNA precipitation. After centrifugation, the pellet was washed with 75% ethanol, the RNA was solubilized by adding 30 µl RNase-free water followed by heating of the samples at 65°C for 3 min.

RNA concentration and purity were assessed by Nanodrop spectrophotometer before storing the samples at -80°C.

2.3.4.3 Isolation of bacterial deoxyribonucleic acid

DNA from strain 1722 and 1723 grown on blood agar plates was isolated and used as template for cloning. The QIAmp DNA Mini Kit was used for isolation of DNA,

manufacturer´s protocol for DNA Purification from Tissues was followed. Briefly, five colonies of each strain were dissolved in an Eppendorf tube containing 10 mM Tris, pH 7.4. The suspensions were centrifuged at 13,4 rpm for 5 min, supernatant decanted and tissue lysis buffer ATL, 180 µl added. Proteinase K was added to tubes for digestion of protein contaminants, tubes were incubated at 56°C on a rocking platform for 1 hour. Bacterial suspension was added 4 µl RNase and pulse-vortexed for 15 sec before adding lysis buffer AL. Ethanol 100% was then added for DNA precipitation and binding to the QIAamp Mini spin column. Washing buffers were added and recommended step followed by an extra centrifuge step of the column before eluting DNA with 100 µl Buffer AE.

DNA concentration was determined by Nanodrop spectrophotometer before storing the samples at -20°C.

2.3.5 Quality and concentration analysis

2.3.5.1 Quality and concentration measurement by Nanodrop

Quantification and quality assessment of DNA and RNA can be done by pipetting a microvolume of the sample on the lower optical pedestal of a NanoDrop® 2000 Spectrophotometer. Nucleic acid has its absorption maximum at 260 nm and the calculation of the concentration (ng/µl) is based on the A260 reading. Sources of contaminants commonly associated with nucleic acid isolation techniques include TriZol/Phenol/QIAzol, residual guanidine and proteins. To assess nucleic acid quality, 260/280 and 260/230 ratios can be analyzed as the contaminants will absorb at 230 or 280, or less (Figure 9). Pure nucleic acid typically yields a 260/280 ratio of ~1.8 and ~2.0, for DNA and RNA, respectively. This ratio is dependent on pH and the ionic strength of the buffer, and it is important to use exactly the same buffer as a diluent and as the blank. Also, an acidic solution will under-represent the ratio by 0.2-0.3, while a basic solution will over-represent the ratio by 0.2-0.3. The 260/230 ratio is a second indicator of how pure the nucleic acid is, and should be very close to 2.0 (Desjardins & Conklin, 2010).

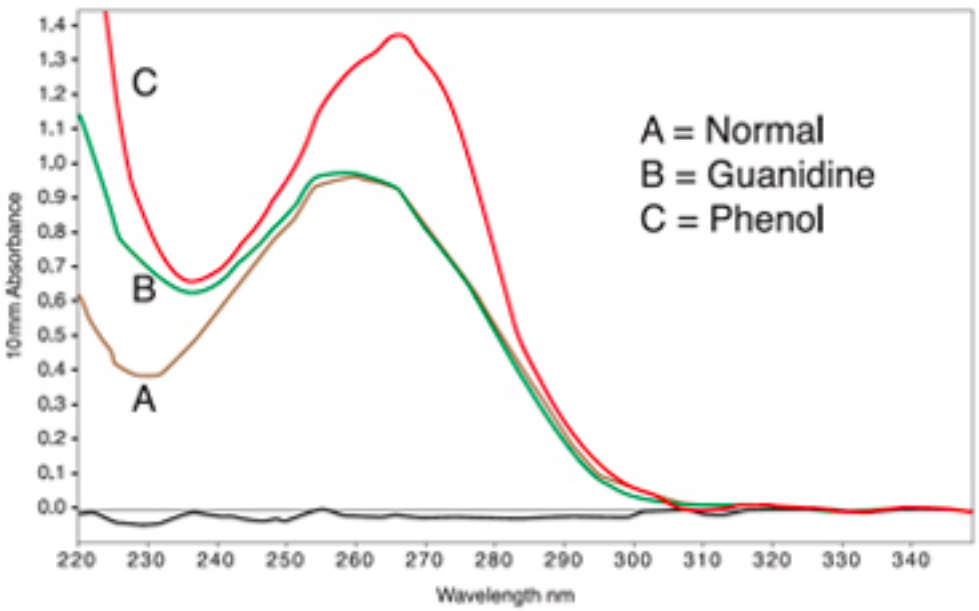

Figure 9: Comparison of absorbance in samples with or without 2 common contaminants (Desjardins & Conklin, 2010).

2.3.5.2 Quality analysis of primer pairs by Bioanalyzer

In gene expression analysis, it is essential that the correct gene has been amplified during PCR. The amplicon length of the RT-qPCR products (ds-cDNA) was evaluated by the use of 2100 Bioanalyzer (Agilent Technologies) in conjunction with the DNA 1000 Lab-Chip kit for detection of DNA fragments with a maximum size of 1000 bp (Gottwald et al., 2001). The manufacturer´s protocol was followed.

The Lab-Chip consists of microchannels that separates nucleic acid fragments by capillary electrophoresis (Nachamkin et al., 2001). In capillary electrophoresis, unlike conventional electrophoresis (described in section 2.6.2), the use of a supportive, solid medium such as agarose is not necessary. Analysis can be carried out in free aqueous solution (Camilleri, 1997). Each chip contains 16 wells, 3 of them for loading the gel-dye mixture, 1 for a molecular size ladder, and 12 for experimental samples. The gel-dye mixture consists of linear polymers and a fluorescent, intercalating dye. An electric field is introduced to the Lab-Chip when inserted into the Bioanalyzer. The polymers in the gel mix allows negative charged ds-cDNA fragments to move through the microchannels, separating the fragments electrophoretically by size as smaller fragments migrates faster than the large ones (Panaro et al., 2000). Laser-induced fluorescence (LIF) detection technique translate the result into gel-

like images using the loaded ladder as a reference when sizing the fragments (Pan et al., 2018).

2.3.6 Gene expression measurement

2.3.6.1 Primer design for reverse transcriptase quantitative polymerase chain reaction

The appropriate choice of reference genes is critical for accurate normalization of gene expression data. The ideal reference gene should have constant expression regardless of the physiological state and with minor variations during experimental conditions (Gomes et al., 2018). In two reported studies, the expression of CDT genes was analyzed in *Campylobacter* by RT-qPCR. The target genes were then normalized using *16S rRNA* and *rpoA* genes as reference genes (Johansson et al., 2019; Oliveira et al., 2019). *16S rRNA* and *rpoA* genes are constant expressed genes, encoding the 16S ribosomal RNA and DNA-directed RNA polymerase, α subunit (Carrillo-Casas et al., 2008; Naser et al., 2005). In another study, bacterial genes that have been most commonly selected and validated as reference genes in gene expression studies by RT-qPCR were identified. *16S rRNA* and *rpoA* genes were found to be among the top five most tested and validated reference genes in the analyzed studies (Rocha et al., 2015). For this reason, the same genes were selected as reference genes in this study and included in the primer design.

All primer pairs were designed in primer-BLAST (Ye et al., 2012). Target- and reference gene sequences of isolated *P. alcalifaciens* strains were obtained by NULS. The exact sequence of *E. coli* strain v27 was unknown. Therefore, the target- and reference gene sequences of *E. coli* were obtained from NCBI nucleotide database search, and by alignment of different *E. coli* strains the most conserved domains were used as PCR template. Each genomic sequence was input as target sequence with the following parameters:

PCR product size: from 75 to 200 bp
Primer melting temperature: from 58 to 62°C, with temperature optimum at 60°C

Primers with a product length of 80-160 bp, GC content of 50-55% and low self-complementarity were selected (Table 2). A nucleotide-BLAST (NCBI) search was performed for each primer pair to ensure their target specificity in that they were unable to bind to other parts of the bacterial genomes or to other organisms.

Table 2: Designed primers for RT-qPCR

RT-qPCR primers		
Strain	Target	Sequence
P. alcalifaciens 1722	*cdtB*	F:5´-CAACGCTTCGATTTCCAGCC-3´ R:5´-GGGGCAACGCTCCATTGTTA-3´
P. alcalifaciens 1723 + 27799	*cdtB*	F:5´- GCGAGCCGATGAAGTGTTTG-3´ R:5´- TGCATCATTGTTTCGCGTCG-3´
E. coli V27	*cdtB*	F:5´- CCGCACCCGCAGTATCTTTA-3´ R:5´- TCGTATTTGGCCTGGTTCCG-3´
E. coli V27	*cdtB*	F:5´-CCGGCTCTTGTTGAGGAAGT-3´ R:5´-CCAGTTAAGCGCCTGGTGTA-3´
P. alcalifaciens 1722, 1723 + 27799	*rpoA*	F:5´- TCTAAAACCGCGCCTGGTAG-3´ R:5´- CACAACCCGGCATAGACGAA-3´
E. coli V27	*rpoA*	F:5´- ACGACGAATCGCCTCTTCAG-3´ R:5´- TTGAAGCAGCGCGTGTAGAA-3´
P. alcalifaciens 1722, 1723 + 27799	*16S*	F:5´- AAAGCAGGGGAACTTCGGTC-3´ R:5´- GCCTTGGTGAGCCATTACCT-3´
E. coli V27	*16S*	F:5´-CGCAGGCGGTTTGTTAAGTC-3´ R:5´-CGAGACTCAAGCTTGCCAGT-3´

Additionally, two published primer pairs targeting the V3-V4 region of the bacterial *16S rRNA* gene (Lazarevic et al., 2016) and the *rpoA* gene (Kendall et al., 2012) in *E. coli* were ordered from Sigma-Aldrich® (Table 3).

Table 3: Published primer pairs targeting reference genes in *E. coli*.

Primers		
Strain	Target	Sequence
E. coli V27	*16S rRNA*	F:5´-ACTCCTACGGGAGGCAGCAGT-3´ R:5´-ATTACCGCGGCTGCTGGC-3´
E. coli V27	*rpoA*	F:5´-GCGCTCATCTTCTTCCGAAT-3´ R:5´-CGCGGTCGTGGTTATGTG-5´

2.3.6.2 DNase treatment of extracted ribonucleic acid and complementary deoxynucleic acid synthesis

Genomic DNA (gDNA) can act as a template during RT-qPCR, thus the removal of gDNA in the RNA sample is essential for obtaining valid results in gene expression analyzes. Difficulties were encountered in the process of the removal of gDNA. Therefore, two different treatments in two different experiments were applied for this purpose. In the first treatment, the gDNA wipeout Buffer, 7x from the QuantiTect Reverse Transcription Kit (Qiagen) were added according to manufacturer's protocol. In the second treatment, the TURBO DNase™Enzyme (Thermofisher) was applied. The TURBO DNase is a recombinant version of wild type DNase I, engineered for enhancing catalytic efficiency and affinity for DNA, making it effective in removing trace quantities of DNA contamination (ThermoFisher, 2018). DNase treatment with TURBO DNase™ was performed according to manufacturer's protocol. After the removal of gDNA, the RNA sample is ready for reverse transcription. In this step, the synthesis of complementary DNA (cDNA) from a single-stranded RNA template takes place. Reverse transcriptase enzymes are derived from RNA-containing retroviruses which transcribe its own RNA into DNA and thereafter replicates as a part of the host cell´s DNA. Reverse transcription *in vitro* utilizes this mechanism to transcribe RNA to DNA (Figure 10). RNA-dependent DNA polymerase transcribes cDNA after the hybridization of primers to the RNA sequence, while RNase H activity degrades the RNA in RNA:DNA hybrids, leaving the sample free from RNA and ready for use in RT-qPCR (Qiagen, 2009).

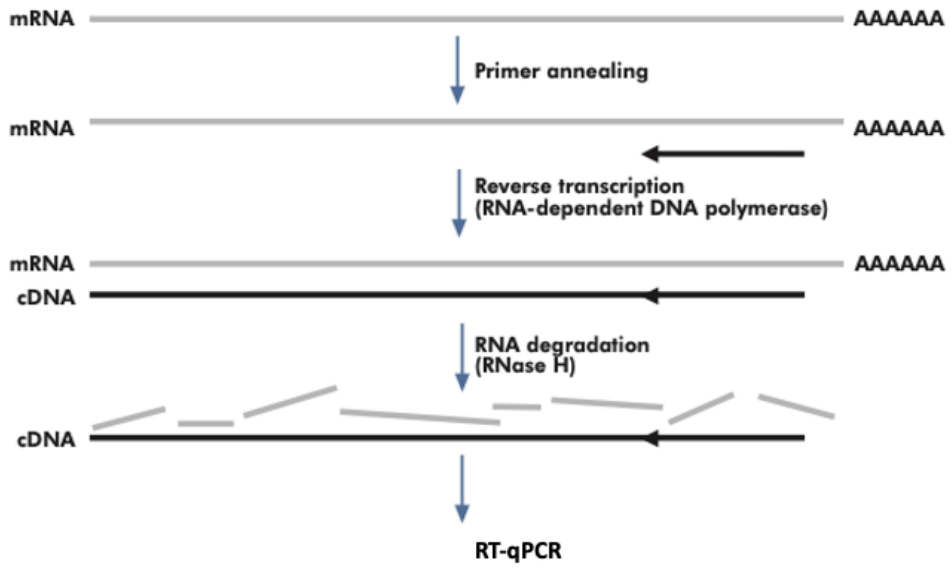

Figure 10: The synthesis of cDNA from a single-stranded RNA template (Qiagen, 2009).

Reverse-transcription master mix was prepared by adding Quantiscript Reverse Transcriptase, Quantiscript RT Buffer and RT primer mix to a total volume of 20 µl with the input of up to 1000 ng RNA. To activate the reverse transcription, the samples were incubated at 42°C for 15 min followed by inactivation of the reaction at 95°C for 3 min. No-reverse transcriptase (no-RT) samples were made by substituting reverse transcriptase enzyme with nuclease-free water in the reaction for the use as a control of gDNA contamination in the RT-qPCR.

All samples were diluted 1:10 in aliquots of 20 µl and stored at -20°C.

2.3.6.3 Reverse transcriptase quantitative polymerase chain reaction

RT-qPCR is a combination of three steps. The first step is the reverse transcriptase (RT)-dependent conversion of RNA into cDNA as described in section 2.3.6. The second step is the amplification of the cDNA in the PCR (Nolan et al., 2006).

The PCR method is based on the *in vitro* replication of the target- DNA or cDNA, through repetitive cycles of reactions. The cycles are divided into three steps:

1. Denaturing: The double stranded (dsDNA) is denatured into single stranded DNA (ssDNA) by high temperature (94- 98°C) that breaks the hydrogen bonds holding the strands together.
2. Annealing: The temperature is lowered according to the optimal temperature for the primers (55-65°C). The primers hybridize to the complementary sequence in the template ssDNA.
3. Elongation: The temperature increases to 72°C which is the optimal temperature for the heat stable DNA polymerase that elongates the DNA strand from the primers.

The cycles are typically repeated 25-40 times. All previously synthesized products serve as template in the next cycle, leading to an exponential amplification of new DNA products (Siqueira & Rôças, 2003).

The third step is the detection and quantification of amplicons in real time.

The application of fluorescence techniques to the PCR allows for the quantification of the target- DNA or cDNA. There are two frequently used qPCR techniques. In probe-based chemistry qPCR, the TaqMan probe is designed with a fluorophore attached to its 5´end. A quencher molecule in the 3´end blocks the fluorescent signal of the fluorophore. When the TaqMan probe binds to its target sequence, the nuclease activity of DNA polymerase cleaves off the probe. The fluorophore is then released, and the fluorescence is detected by a thermocycler. In DNA binding dye qPCR, the SYBR® Green dye is nonspecific as the dye immediately binds to any dsDNA present. When bound, it emits a fluorescent signal that is up to 1000 fold greater than unbound SYBR® Green dye which is then detected by a thermocycler (Thornton & Basu, 2011). The SYBR® Green qPCR were the method of choice because of the ease in designing the assays and its relatively low running costs (Cao & Shockey, 2012). Individual reactions are characterized by the PCR cycle at which fluorescence first rises above a threshold background fluorescence. This parameter is known as the threshold cycle (C_t)(Figure 11).

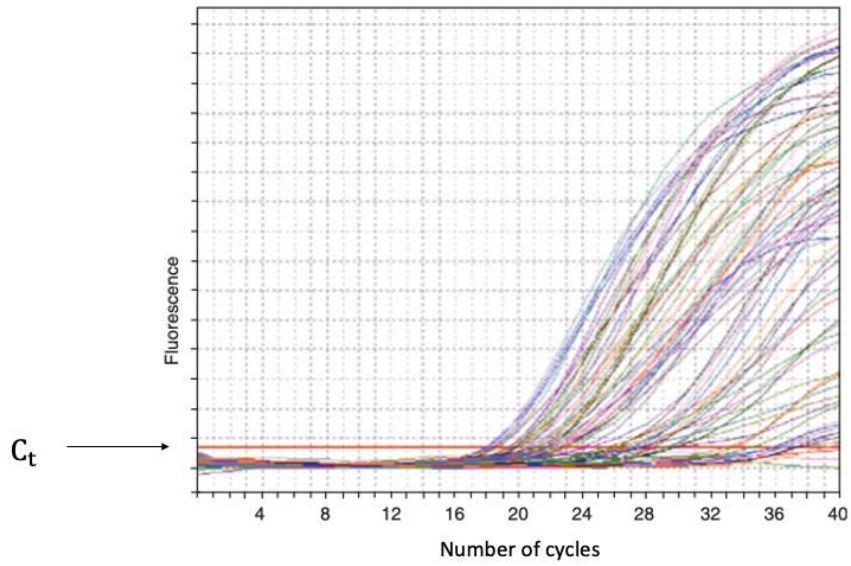

Figure 11: Individual reactions with C_t values ranging from ~18 to 40 (Nolan et al., 2006).

The more target DNA there is in the starting material, the lower C_t values are obtained. This correlation between fluorescence and amount of amplicons permits the quantification of gene transcripts in RT-qPCR (Nolan et al., 2006).

2.3.6.4 Reverse transcriptase quantitative polymerase chain reaction setup

Master mix for SYBR® Green assay (Bio Rad) was prepared according to table 4.

Table 4: The composition of master mix for SYBR® Green assay.

Master Mix, volume for	1 reaction (µl)	2,5
Mastermix (2X)	5	12,5
Primer F (10 uM)	0,5	1,25
Primer R (10 um)	0,5	1,25
dH2O	2	5
In total	8	20
Additionally		
cDNA	2	5

Each Master mix with the appropriate primer pair and cDNA sample were pipetted in duplicates in a PCR 384-well plate (Bio-Rad laboratories). To ensure enough reagents and sample material when pipetting, the volume was multiplied by 2.5. A 1:2 serial dilution with 5-points in duplicates was created from a cDNA sample for each primer pair to obtain a standard curve. From the standard curve the primer efficiency can be calculated. The primer efficiency is later applied for calculating the relative gene expression. In addition, two negative controls were applied for each primer pairs:

1: no-template
2: no-RT

After pipetting samples with master mix, the plate was sealed and centrifuged. The plate was then analyzed in a CFX384 Touch Real-Time PCR Detection System (Bio Rad laboratories) with the software CFX Manager, 3.1. The following PCR program was used:

95℃: 30 sec
95℃: 15 sec - denaturing (x 39 cycles)
60℃: 30 sec - hybridization and polymerization (x 39 cycles)

Sometimes the annealing and extension step are combined into one, and performed at a temperature of 60°C. The transition time between temperatures should be as short as possible to avoid non-specific PCR products and to reduce the thermal stress on the polymerase (Neuzil et al., 2006).

After the last cycle, the temperature was gradually increased to 95℃ for the detection of potentially unspecific PCR products. Optimally, the size of all amplicons should be close in length. As shorter sequences separate faster than longer sequences, the fluorescence will decrease faster during dissociation (Thornton & Basu, 2011). This information gives a melting curve, showing the melting point for each sample in the analysis. The melting curve makes it possible to evaluate if several products have been amplified in the same sample, and if the correct target sequence has been analyzed.

The levels of expressed genes may be measured by an “absolute” quantification or by a “relative” RT-qPCR. In the absolute quantification approach, a standard curve for each gene of interest (GOI) is made, based on a dilution series of known template concentration and its related C_t values. The unknown mRNA copy number of your GOI is then quantified by interpolation on the standard curve. The standard curve can be derived from diluted PCR products, recombinant DNA or RNA, and linearized plasmids. This method assumes that the amplification efficiency (*E*) of the native mRNA target is the same as *E* of the standard. As the absolute quantification is shown relative to the standard curve, the quantification accuracy may be affected. Factors such as the DNA source applied for the standard curve, exact concentration determination, dilution preparation, and stability during storage all introduce uncertainty to the standard curve. Relative quantification does not require a standard curve, mRNA copy numbers are instead correlated to biological parameters such as constant expressed reference genes. The relative quantification approach is ideal where the goal is to measure the regulation of a gene in response to a particular treatment. The normalization of gene expression data by the use of reference genes can be calculated on the basis of $\Delta\Delta_{C_t}$ values. The $\Delta\Delta_{C_t}$ method assumes similar primer efficiencies between the GOI and the reference genes, while the Pfaffl method accounts for efficiency differences. The Pfaffl

method requires primer efficiencies for your GOI and reference genes, as well as C_t values for your samples. The relative expression ratio is relative to a selected sample (calibrator), either a sample with the highest GOI C_t value or the lowest. ΔCt is obtained by subtracting sample C_t value from the calibrator C_t value. The equation for calculating the relative gene expression is displayed below.

$$\textit{Relative expression ratio} = \frac{(E_{GOI})^{\Delta CtGOI}}{GeoMean[(E_{Ref})^{\Delta CtRef}]}$$

The *E* in the equation refers to the base of exponential amplification. For example, for a primer efficiency of 97%, the *E* value is 1.97. The ΔCt is the index of the *E* value. Finally, when there is more than one reference gene, the geometric mean of the $(E_{Ref})^{\Delta CtRef}$ from each reference gene has to be calculated (Pfaffl, 2007; Sivaganesan et al., 2010).

2.4 Effect of CDT

2.4.1 Exposure to recombinant CDT from *E. coli*

Lyophilized recombinant CDT from *E. coli* was obtained by MyBioSource, Inc (San Diego, USA). All three subunits were reconstituted in deionized sterile water (diH_2O) with 50% glycerol. Mao and DiRenzio (2002) studied the effect of recombinant CDT originating from *A. Actinomycetecomitans*. CDT was cloned in *E. coli*, purified and exposed to Chinese hamster ovary (CHO) cells in culture. A ratio of 15 μg cdtA: 3 μg cdtB: 15 μg cdtC per 240 cells reduced the survival of CFU in culture by 70% after 6 days of growth (Mao & DiRienzo, 2002). The same concentration of the obtained subunits was prepared for exposure in a volume of 150 μl. Subunits cdtA and cdtC were reconstituted to a final concentration of 0,676 mg/ml, subunit cdtB were reconstituted to a final concentration of 0,135 mg/ml. A toxin solution of equal volumes of the three subunits were then prepared ready for use in cytotoxicity assays.

Cells (340 cells/cm^2) were seeded onto a 96-well plate in a volume of 150 μl per well. The cells were allowed to adhere as described in section 2.4.1. After 3 hours, the cells were

exposed to cdtAC, 2,25 µg/µl and cdtB, 0,45 µg/µl and cdtAC, 1,125 µg/µl and cdtB, 0,225 µg/µl. Ctrl were added diH_2O with 50% glycerol, 10 µl. The length of exposure was 72 hours.

Cells (3 x 10^4 cells/cm^2) were seeded onto transwell inserts in a volume of 150 µl and allowed to grow/differentiate for 6 days before exposure of cdtAC, 2,25 µg/µl and cdtB, 0,45 µg/µl and cdtAC, 1,125 µg/µl and cdtB, 0,225 µg/µl. Ctrl were added diH_2O with 50% glycerol, 10 µl. The length of exposure was 72 hours.

2.4.2 Exposure to samples from toxin production

A volume of 100 µl cell suspension was seeded onto a 96-well plate. The cells were allowed to adhere by incubation at 37ºC with 5% CO_2 for 3 hours. After 3 hours, cells were exposed to sample from toxin production, 100 µl. Control cells (ctrl) were added the appropriate negative control, 100 µl. The length of exposure was 72 hours.

2.5 Toxicity test

2.5.1 CellTox™ Green

CellTox™ Green contains a non-permeable cyanine dye which binds to the minor groove to stain DNA of dead cells (Riss et al., 2019). When the dye binds to DNA, the fluorescent properties are enhanced and will be proportional to induced cytotoxicity (Promega Corporation 2020). The CellTox™ Green dye was added to cells seeded onto plastic plates in a 1:1000 dilution with the cell culture medium and incubated for 30 min. Cytotoxicity was quantified with the Spectramax® i3x plate reader (510 ± 9 nm_{ex}/535 ± 15 nm_{em}; 200 points read/well).

2.6 Cloning and transfection

The isolated *P. alcalifaciens* strains from the sick dogs were categorized in regard to the clinical picture of the dogs when sampling, as described in section 2.3.2. Some of the strains caused more severe disease course than others. Mutations in the *cdtB* gene have been associated with increased CDT activity as a result of different evolutionary forces acting on the variable region of virulence genes (Bandhaya et al., 2012; Torres-Morquecho et al., 2010). Sequence analysis of the cdtB subunit revealed a frameshift mutation due to the insertion of one nucleotide in strains related to a severe disease course. The frameshift mutation results in

two open reading frames (ORFs), each of them with catalytic domains belonging to the Exonuclease-Endonuclease-Phosphatase (EEP) domain superfamily. It was therefore decided to clone the different genetic variants of cdtB and transfect the SCBN cells.

Transfection is the procedure of introducing foreign nucleic acid into the host genome, in this case making the cells express *cdtB* intracellularly. The introduced genetic material exists in the cell either stably or transient. For stable transfection, the DNA are integrated into the host genome and will be present even after host cells replicate. For transient transfections, the nucleic acids are not integrated into the genome and are only present and expressed for a limited period of time. Loss is due to degradation and cell division (Kim & Eberwine, 2010). Integration of DNA into the host genome is most efficient when linear DNA is introduced (Abdel-Banat et al., 2010). Circular plasmids with *cdtB* inserts were introduced into the SCBN cells for transient transfection. By removing signal peptides and adding epitope tags on the different constructs it would be possible to detect the proteins after transfection in addition to screen for differences in cytotoxicity.

Strain 1723 had a frameshift mutation in the cdtB sequence, resulting in two catalytic domains instead of one. An ORF of 184 aa were found in the N-terminus of the protein, a second ORF of 83 aa in the C-terminus. The two catalytic domains are from now on referred to as cdtBn and cdtBx, respectively. Strain 1722 had the full-length version of cdtB with one ORF and one EEP domain. These two strains, having genetic variations causing different pathogenesis in the dogs, were selected as templates for four different DNA constructs used for transfection.

A summary of the main experimental steps performed for cloning and transfection is visualized in figure 12.

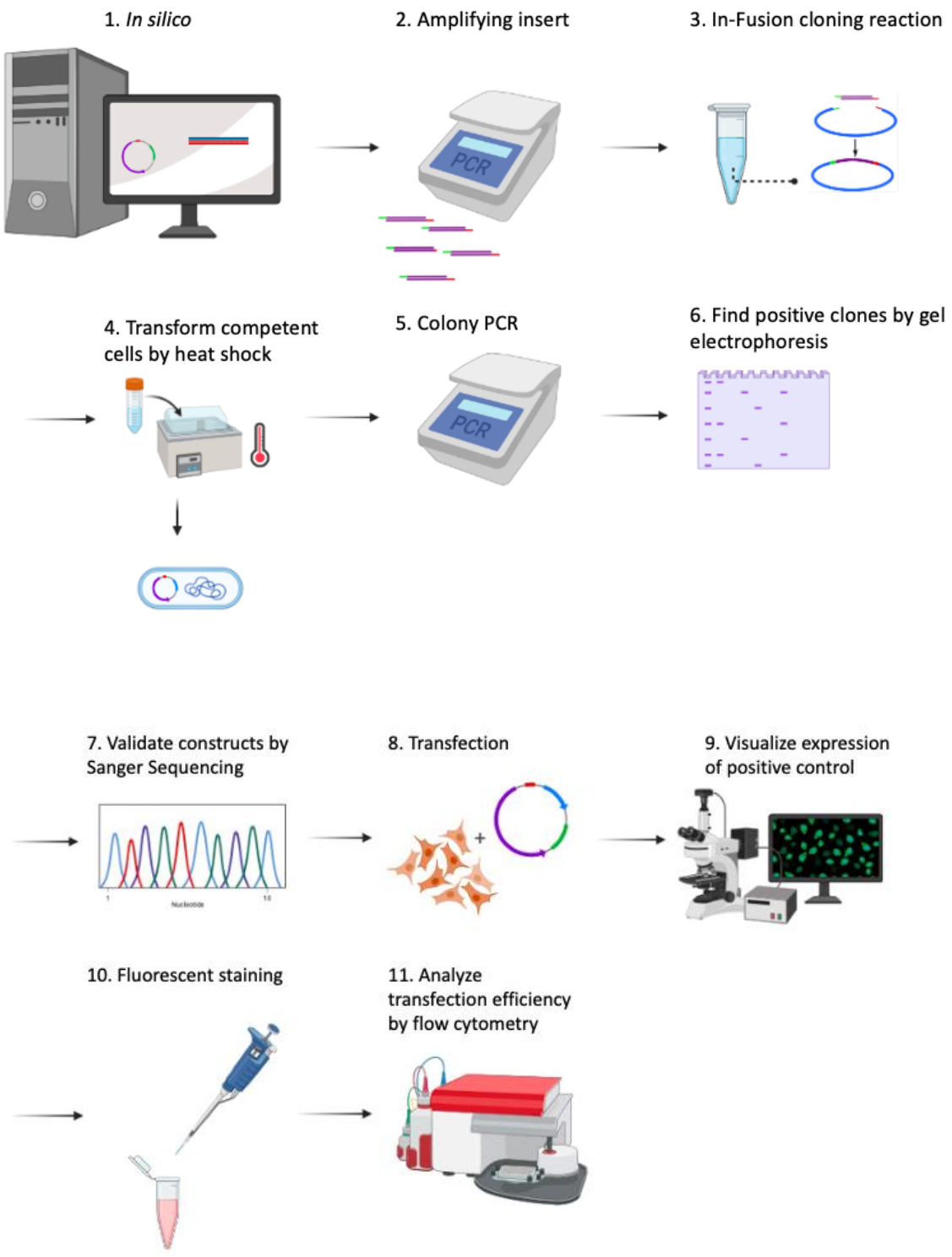

Figure 12: A summary of the main experimental steps performed for cloning and transfection.
1: Preparation of cloning by analyzing gene sequences, vector, and designing primers. 2: Amplify inserts by PCR. 3: Insertion of construct into pcDNA3.1 vector 4: Transform competent cells by heat shock. 5: Amplify inserted construct in transformed cells. 6: Confirm correct insert by gel electrophorese and grow correct bacterial clones for miniprep. 7: Sequence the selected clones to verify correct insert into pcDNA3.1 vector. 8: Transfect cells. 9: Visualize and examine the cells by fluorescence microscopy. 10:

Fluorescent staining of the cells to visualize inserted construct. 11: Analyze transfection data by flow cytometry. Figure created with Biorender.com.

2.6.1 Bioinformatic analysis and primer design

2.6.1.1 Online bioinformatic tools, databases and sequence analysis

The cdtB sequences were analyzed *in silico* to predict functional properties. ORF finder (https://www.ncbi.nlm.nih.gov/orffinder/) was used to search for protein encoding segments. The program returns protein translation of the ORF, and proteins were verified by blastp (NCBI). Conserved domain search (https://www.ncbi.nlm.nih.gov/Structure/cdd/wrpsb.cgi) returns hits of conserved domain families related to functional properties and their related nucleotide sequence interval. As the proteins are secreted to the extracellular milieu *in vivo*, signal peptides had to be predicted and removed prior to cloning for observing cytotoxic effect without subunit A and C (Hall et al., 1990). Predication of signal peptides was done with the SignalP online tool (http://www.cbs.dtu.dk/services/SignalP/). The software program CLC Main Workbench (Qiagen) was used to view and analyze sequence data, to align multiple sequences and *in silico* translation. The software was also used for primer design, preparation and planning of cloning, and to analyze Sanger sequencing data.

The pcDNA™3.1 (+) vector (Invitrogen) was chosen to ferry cdtB sequences into the SCBN cells. The vector is a 5.4 kilobases (kb) plasmid designed for high-level, constitutive expression in a variety of mammalian cell lines. The features of the vector are summarized in figure 13. The cytomegalovirus (CMV) immediate-early (IE) genes promoter, together with enhancer, is the most widely used promoter for expression of target genes in mammalian cells (Kim et al., 2011). With a strong promoter, a strong transcription terminator should be used to ensure that RNA polymerase does not continue to transcribe downstream genes (Rai & Padh, 2001).The Bovine Growth Hormone (BGH) polyadenylation sequence is an efficient transcription terminator in addition to form stable mRNA ready for translation. Plasmids vary widely in their copy numbers within the bacterial cell depending on their origin of replication (ori), as well as the plasmid size and the size of insert. The pUC ori region in the vector

allows replication of the vector in a high copy number (500-700 per cell) (ANINDYAJATI et al., 2016).

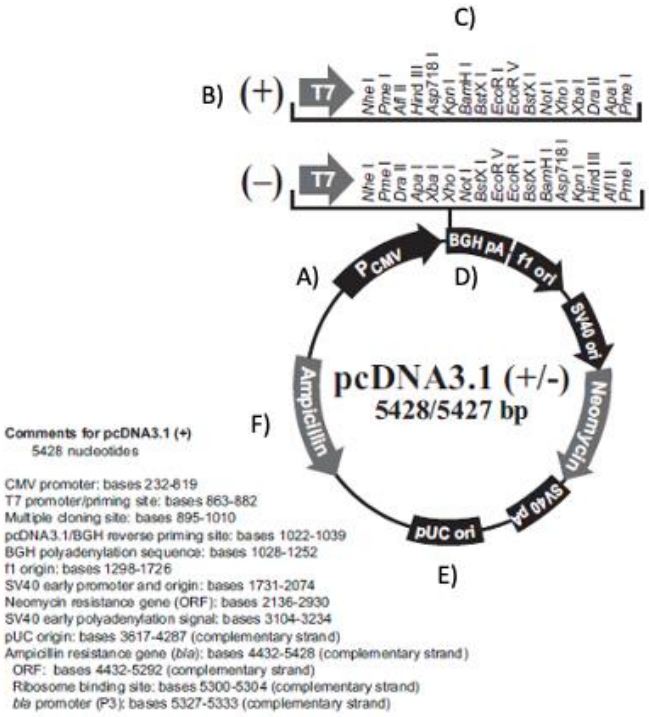

Figure 13: Vector map of the plasmid pcDNA™3.1 (+). Letters in the figure indicate relevant features of the vector. A: Promoter derived from human CMV, where the host DNA dependent RNA polymerase binds and initiates transcription. B: T7 promoter allows for *in vitro* transcription in prokaryotes. C: Multiple cloning site (MCS) allows insertion of the gene of interest and facilitates cloning. D: BGH polyadenylation signal provides efficient transcription termination and polyadenylation of mRNA. E: The pUC origin ensures high-copy number replication. F: Ampicillin resistance gene allows for selection of positive clones (Invitrogen).

2.6.1.2 Primer design

The CLC Main Workbench and In-Fusion cloning primer design tool (Takara Bio, Inc) were used for designing primers for cloning. The pcDNA3.1 was linearized at HindIII cloning site, cdtB sequences inserted *in silico* and the In-Fusion cloning primer tool returned primers that contain 15 nucleotide extensions homologous to the end of the linearized vector.

Epitope tags are peptide sequences that are widely used to facilitate the detection of recombinant proteins. The peptide sequence is fused to the target protein by the insertion of the sequence either onto the N- or C terminus of the open reading frame in the target protein. The expressed recombinant protein can then be detected by immunofluorescence staining

with specific antibodies (Zhao et al., 2013). For the detection of cdtB variants, two different epitope tags were added in the reverse primers. The FLAG tag sequence (5´-GACTACAAAGACGATGACGACAAG-3´) was inserted in the reverse primer between the stop codon and the encoding sequence of 1723 cdtB, 1723 cdtBx and 1722 cdtB. The c-Myc tag sequence (5´-GAACAAAAACTCATCTCAGAAGAGGATCTG-3´) was inserted in the reverse primer between the stop codon and the encoding sequence of 1723 cdtBn. Both Flag-tag and c-Myc tag are small-size tags, and should not impact the structure or biological activity of the fusion partner protein. By adding a different tag on cdtBn, it would be possible to detect potential co-localization of cdtBx and cdtBn (Zhao et al., 2013). Designed primers are shown in table 5.

Table 5: Designed primers with Flag/c-Myc epitope tag in C-terminus.

Primers		
Name	**Tag**	**Sequence (5'-3')**
1723 *cdtB* F	None	GTTTAAACTTAAGCTATGTCTCTGATAGTGTTTTTATCGTTTT
1723 *cdtB* Flag R	Flag-Tag at C-terminus	GCTCGGTACCAAGCTTTACTTGTCGTCATCGTCTTTGTAGTCTCTTCTGAATACACCTACAGGG
1723 *cdtBn* F	None	GTTTAAACTTAAGCTATGTCTCTGATAGTGTTTTTATCGTTTT
1723 *cdtBn* c-Myc R	Myc-Tag at C-terminus	GCTCGGTACCAAGCTTTAGTCTAGGAGAAGACTCTACTCAAAAACAAGCAGGGCTAAGAACAAACACTT
1723 *cdtBn* c-Myc R	Myc-Tag at C-terminus	GCTCGGTACCAAGCTTTACAGATCCTCTTCTGAGATGAGTTTTTGTTCCAGGGCTAAGAACAAACACTT
1723 *cdtBx* F	None	GTTTAAACTTAAGCTATGATTATTGGTGATTTCAACCGTG
1723 *cdtBx* Flag R	Flag-Tag at C-terminus	GCTCGGTACCAAGCTTTACTTGTCGTCATCGTCTTTGTAGTCTCTTCTGAATACACCTACAGGG
1722 *cdtB* F	None	GTTTAAACTTAAGCTATGTCTCTGATAGTGTTTTTATCGTTTT
1722 *cdtB* Flag R	Flag-Tag at C-terminus	GCTCGGTACCAAGCTTTACTTGTCGTCATCGTCTTTGTAGTCTCTTCTGAATACACCTACAGGG

Vector
Flag tag
c-Myc tag
gene sequence

2.6.2 Agarose gel electrophoresis

Agarose is a natural linear polymer extracted from seaweed. When heated in a buffer and allowed to cool, the linear polymer forms a gel-matrix by hydrogen bonding. A 1% concentration of agarose is used for resolving linear DNA fragments 500-5000 bp of length. The buffer maintains the pH within the gel-matrix, which makes the separation of the nucleic acids possible. The salt content of the buffer contributes to electrical conductance and affects the electrophoretic mobility of the DNA (Barril & Nates, 2012).

Agarose gel electrophoresis was used to run plasmids and PCR products. A protocol from the electronic database at NVI was followed. A 50 mL gel was prepared with 0,5 g agarose and 50 mL 1x Tris-Borate-EDTA (TBE) buffer. After heating, GelRed™ DNA stain from Biotium, 5 µl was added to the gel-mix and the gel was allowed to cool down in a gel tray, with a gel comb for creating wells. When cooled down, the gel was transferred to an electrophoresis chamber filled with 1x TBE buffer. Loading dye 6X (Thermofisher) were added to PCR products, in a 1:6 solution. Ladder, 1 µl peqGOLD 1 kb, and samples were pipetted into their respective wells before running the gel at 100 V. The loading dye contains glycerol to increase the density of the DNA solutions, ensuring that the DNA forms a layer in the bottom of the well. The dye indicates the progress of electrophoresis as the dye molecules migrate quickly through the gel (Barril & Nates, 2012). The electric current was stopped when the dye had migrated approximately 2/3 of the length of the gel. GelRed™ DNA stain is a red fluorescent nucleic acid dye. The stained PCR products were imaged by the ChemiDoc XRS+ Gel Imaging System (BioRad).

2.6.3 Cloning

Cloning gene sequences into a vector requires several steps including fragment preparation, vector linearization, insertion, transformation of bacteria for plasmid amplification and confirmation of successful cloning by PCR and sequencing.

2.6.3.1 Polymerase chain reaction for amplification of gene sequences

The CloneAmp™ HiFi PCR Premix Protocol from Takara Bio was followed. Isolated DNA from section 2.3.3.3 was used as template in four reactions. In addition, negative controls for

each primer pair were prepared without template. Reagents in table 7 were added to their respective well in a PCR strip and mixed briefly in a short spin.

Table 7: Reaction mix for the CloneAmp™ HiFi PCR.

CloneAmp™ HiFi PCR		
Reagent	*Volume (µl)*	*Final Conc.*
HiFi Premix	12,5	1X
F-primer	1,0	0,2-0,3 µM
R-primer	1,0	0,2-0,3 µM
Template	5,5	<100 ng
Nuclease-Free water	5,0	
Total	25,0	

The following PCR program was used:
98°C: 10 sec - denaturing (x 35 cycles)
55°C: 5 sec - hybridization and polymerization (x 35 cycles)
72°C: 5 sec – elongation (x 35 cycles)

After electrophoresis of PCR products on agarose gel, the PCR products with estimated correct sizes were treated with Cloning Enhancer. Cloning Enhancer, 2 µl was applied to 5 µl PCR product and incubated in a thermocycler at 37°C for 15 min, then at 80 °C for 15 min.

2.6.3.2 Vector linearization

The vector pcDNA™3.1 (+) was linearized *in vitro* using the Anza™ Restriction Enzyme Cloning System (Thermofisher). HindIII is a type II restriction enzyme that recognize a specific sequence and cuts DNA at its restriction site (Figure 14) (Vincze et al., 2003).

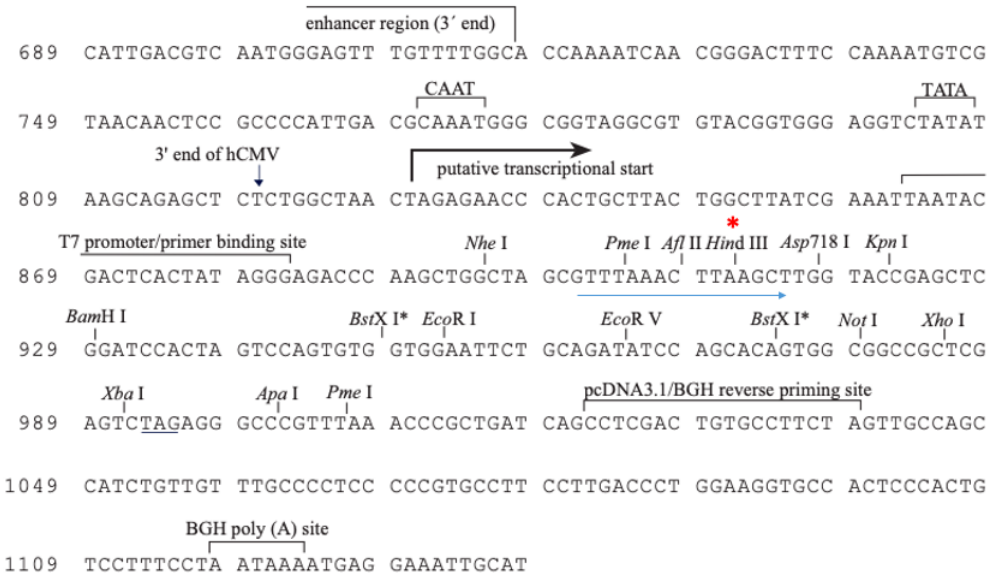

Figure 14: DNA sequence of the MCS in the pcDNA™3.1 (+) vector. The red dot indicates the recognition site of the HindIII enzyme. The blue arrow lines the 15 nucleotides that are homologous to the designed forward primers (Invitrogen).

Reagents were added in the same order as indicated in Table 6 and incubated at 37°C for 15 min. The concentration of pcDNA3.1 vector added to the reaction was 1 µg. Gel electrophoresis was performed as described in section 2.6.2 to confirm linearization of the vector. Circular pcDNA.3.1 vector was also included in the electrophoresis as a control to confirm linearization. A linearized vector will migrate slower in the gel than the supercoiled circular vector. The uncut vector should generate two distinct bands due to a mix of supercoiled and relaxed DNA. The supercoiled plasmid is the smallest fragment and will migrate faster than the relaxed form.

Table 6: Vector linearization reaction mix.

Restriction digestion protocol	
Reagent	*Volume (µl)*
Nuclease-Free water	15
Anza™ 10X buffer	2
pcDNA3.1 vector	2
HindIII	1
Final volume	20

2.6.3.3 In-fusion Cloning Reaction

The In-Fusion® HD cloning kit (Takara Bio USA, Inc.) was used to perform the cloning. The In-Fusion™ enzyme reaction can join any two pieces of DNA that have 15 bp of identity at their ends. Amplified target gene sequences and vector were combined with an In-Fusion enzyme mix. The enzyme mix displays the same unique properties of the 3´-5´ exonuclease activity of poxvirus DNA polymerase. The 3´-5´ proofreading activity of poxvirus DNA polymerase removes nucleotides from the 3´end (Figure 15). The exposure of complementary regions on substrate DNAs makes the DNA spontaneously anneal through base pairing. Introduction of the annealed vector into *E. coli* repairs any single-stranded gaps (Zhu et al., 2007).

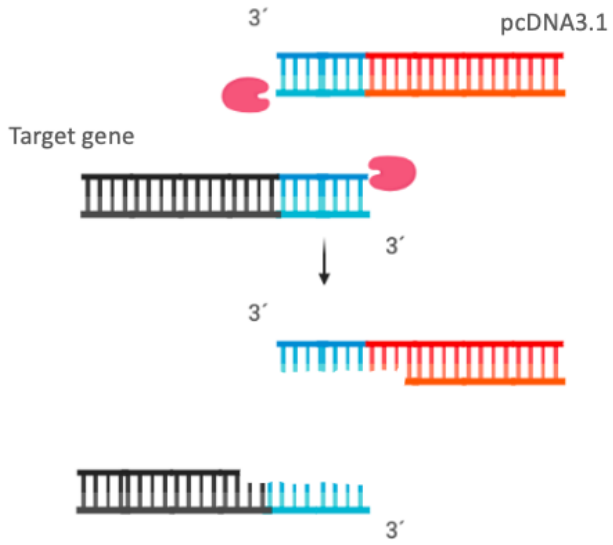

Figure 15: The mechanism of the In-Fusion™ enzyme reaction. Figure created with Biorender.com.

The Takara Bio lab-manual was followed. Reagents in table 8 was incubated at 50°C for 15 min and then put on ice.

Table 8: Reaction mix for In-Fusion cloning.

In-Fusion cloning reaction

Reagent	*Volume (µl)*
5X In-Fusion HD Enzyme Premix	2
Linearized pcDNA3.1	2 (50-100 ng)
Purified PCR fragment	2 (<4)
Nuclease-Free water	4
Total	10

2.6.3.4 Bacterial transformation

Bacterial transformation is the mechanism by which bacteria are competent to acquire naked DNA from the extracellular environment across the cellular envelope and undergo genetic transformation. The In-Fusion® HD cloning kit includes Stellar ™ Competent Cells. The competent cells are *E. coli* strain HST08, treated with calcium chloride. $CaCl_2$ heat shock transformation is a powerful technique used to introduce plasmid into a host cell for plasmid amplification. The exact mechanism is still unknown, but it is hypothesized that the calcium ions act as a cation bridge between the negatively charged plasmid and cell membrane. Membranes absorb calcium readily and it is thought that the temperature imbalance produced by a heat shock enlarges the pore size on the cell membrane, which facilitates DNA entry into the cells. Cells that are successfully transformed are identified by an antibiotic resistance marker (Asif et al., 2017; Chang et al., 2017).

The Takara Bio lab-manual was followed. Stellar ™ Competent Cells were thawed on ice, In-Fusion reaction mixture (from table 7), 2, 5 µl was applied to 50 µl competent cells in a 14-ml round-bottom Falcon® tube. A negative control with 100 ng of linearized vector, and a positive control were included to verify that the system was working properly. The positive control consisted of linearized control vector, 100 ng, control insert, 80 ng, and 5X In-Fusion HD Enzyme Premix, 2 µl. The six tubes were put on ice for 30 min before the cells were heat shocked at 42°C for 45 sec. The tubes were then cooled down on ice for 1-2 min and preheated SOC-medium (37°C) were added to a final volume of 500 µl. After incubation of the cells at 37°C, 170 rpm for 1 hour, three different dilutions of each transformation reaction were prepared:

1: 20/100 = SOC medium, 80 µl, cells, 20 µl

2: 60/100 = SOC medium, 60 µl, cells, 40 µl

3: pellet from each transformation reaction resuspended in 100 µl SOC medium

Each dilution, 100 µl was plated out on separate petri dishes containing Luria-Bertani (LB)-agar and 100 mg/l ampicillin. The plates were incubated overnight at 37°C and screened for positive clones the next day.

2.6.3.5 Colony-PCR

Colony-PCR was performed to confirm that the gene sequences had been inserted into the vector. Sequencing will later be the final verification. Ten colonies from each of the transformation reactions were collected and each colony were resuspended in SOC medium, 200 µl on a 96-well plate. The resuspended bacteria were incubated at 37°C, 130 rpm for 3 hours. Bacterial suspension, 1 µl was used directly in the PCR setup (Table 9). The primers applied for colony-PCR bind to the T7 promoter- and BGH polyadenylation sequences in the vector (Primer sequences are found in appendix). These sequences are located close to each end of the insert and the PCR products will include the gene sequence, if inserted.

Table 9: Reaction mix for the colony-PCR

Colony-PCR		
Reagent	*Volume (µl)*	*Final concentration*
Phusion Master Mix	10	2X
F-primer (T7)	1	0,5 µM
R-primer (BGH)	1	0,5 µM
Template	1	
Nuclease-Free water	7	
Total	20	

The following PCR program was used:

94°C: 3 min - preheating

94°C: 45 sec – denaturing (x 34 cycles)

55°C: 30 sec - hybridization and polymerization (x 34 cycles)

72°C: 3 min - elongation (x 34 cycles)

72°C: 10 min - elongation

If the PCR products had the correct size estimated by agarose gel electrophoresis, bacterial suspension, 10 µl was added to a Sarstedt Inc Screw Cap tube with LB medium, 3 ml containing ampicillin, 50 µg/ml and incubated overnight at 37°C, 130 rpm. Three wells for each construct with correct size were chosen. The next day plasmids were purified by miniprep.

2.6.3.6 Mini- and midiprep of plasmid

The PureLink™ Quick Plasmid Miniprep kit (Thermofisher) was used to purify plasmids from transformed bacteria. Manufacturer's protocol was followed. The column-based kit is designed for rapid isolation of sequencing-grade plasmid DNA from *E. coli* and resembles conventional DNA isolation methods described in section 2.3.3.3. Miniprep yields up to 40 µg purified plasmid. The miniprepped clones were sequenced by Sanger sequencing technique to verify correct insert of construct. It was then possible to determine which bacterial suspensions from the colony-PCR plate to apply for midiprep.

The Purelink™ HiPure Plasmid Midiprep kit (Thermofisher) was used to purify plasmids from transformed bacteria. Bacterial suspension, 50 µl with correct insert of construct from the colony-PCR plate was added to a Sarstedt Inc Screw Cap tube with LB medium, 50 ml containing ampicillin, 50 µg/ml and incubated overnight at 37°C, 130 rpm. Manufacturer´s protocol for high copy number was followed. The column-based kit is designed to isolate transfection-grade plasmid DNA from *E. coli.* The purification system does not use organic solvents, ethidium bromide, or cesium chloride, all of which can be difficult to dispose of. Instead, an anion-exchange resin is used (Thermofisher). The highly charge density of resin separates various nucleic acids forms over a broader range of salt concentration so that overlapping elution peaks of protein, RNA and DNA are prevented (Budelier & Schorr, 1998). Typically, after plasmid midiprep the DNA will have a 260/280 ratio of > 1.8 which is pure enough for mammalian cell transfection. Midiprep typically yields 100-350 µg plasmid DNA from 15-25 ml bacterial culture (Thermofisher). The midiprepped clones were stored in aliquots of 10 µl at -20°C.

2.6.3.7 Sanger sequencing

The Sanger technique is based on a standard PCR setup, with specific primers that hybridize to the complementary sequence in the template ssDNA. The primers applied for sequencing the purified plasmids were the same primers applied for colony-PCR, that bind to the T7 promoter- and BGH polyadenylation sequences in the vector. The natural nucleotides, deoxynucleotides (dNTPs), are mixed with a low concentration of the building blocks in a modified form, dideoxy nucleotides (ddNTPs). DNA polymerase cannot use ddNTPs as a substrate when elongating the DNA strand from the primer, so when a ddNTP is incorporated in place of a dNTP, the elongation is terminated. Each of the ddNTPs (C, T, G and A) is attached to a fluorescent dye, four different colors. The PCR product will consist of fragments of different lengths with different fluorescence. When the electrophoresis gel is scanned with a laser, the software will process the data and assembles the different signals to one continuous sequence (Thornley, 1997).

The sequencing was performed in-house at the sequencing facility at NVI.

2.6.4 Transfection

There are several methods of transfection. The ideal method should have high transfection efficiency, low cell toxicity, and minimal effects on normal physiology. This can be cell type dependent, two types of transfection were therefore tested on the cells (Kim & Eberwine, 2010).

2.6.4.1 Lipid-based transfection

The use of cationic lipid for transfection is based on the principle of positively charged chemicals that bind to negatively charged cell membrane. The process of internalization by endocytosis, followed by nucleic acid escape from the endosomes and transport to the nucleus for transcription, involves a number of poorly understood intermediate stages. Some of the advantages of lipid-based transfection is relatively low cytotoxicity and no size limitation on the packaged nucleic acid (Kim & Eberwine, 2010; Koynova & Tenchov, 2011).

The K2® Transfection System (Biontex), METAFECTENE® (Biontex) and Lipofectamine™ 3000 (Thermofisher) kits were used for lipid-based transfection. Manufacturer´s protocol was followed. Plasmid DNA Monster Green ® Fluorescent Protein (phMGFP) was applied as positive control. Briefly, cells in various concentrations, ranging from 850- to 3400/cm^2 were seeded onto a 96-well plate in a volume of 100 µl and allowed to grow for 24 hours. The next

day, various concentrations of each transfection reagent were incubated with positive control for 15 min before applied to the cells. After 72 hours, fluorescence microscopy of the cells was performed to observe if the positive control were expressed.

2.6.4.2 Electroporation

Electroporation is the use of brief electrical pulses to destabilize the cell membrane which transiently induce formation of aqueous pathways or membrane pores that allow nucleic acid entry into the cells. Advantages of electroporation are that it can be applied to a wide variety of cells, it is able to transfect a large number of cells in a short time and the method is easy to perform (Kim & Eberwine, 2010; Kumar et al., 2019).

The Amaxa® Cell Line Optimization Nucleofector® Kit (Lonza) was used for electroporation. Cells (0,5 x 10^6/ml) were applied to Eppendorf tubes (1 ml each) and centrifuged at 90 x g for 10 min. Medium was removed and pellet dissolved in 100 µl RT Nucleofector® Solution V. Positive control, pmaxMGFP, 1 µg was added to the solution before transferred to certified cuvette. The appropriate Nucleofector® Programs were selected and cuvette inserted into the Nucleofector™ 2b Device. Pre-equilibrated DMEM without penicillin/streptomycin, 500 µl was added to the cuvette after transfection, and sample gently transferred into a prepared 12-well plate for adherent cells with pre-equilibrated DMEM. Each sample of transfected cells were split into two wells. After 3-6 hours, medium exchange with DMEM complete was performed. After 72 hours, fluorescence microscopy of the cells was performed to observe if the positive control were expressed.

2.6.5 Flow cytometry

Flow cytometry is a technology that analyzes single cells or particles as they flow past single or multiple lasers. Each particle is analyzed for visible light scatter and fluorescence. Visible light scatter can indicate the relative size and granularity of the cell. Data analysis can be used to exclude dead cells and count cells that fluoresce to obtain transfection efficiency (McKinnon, 2018).

Transfected cells with pcDNA3.1 were fixated by 4% PFA, permeabilized with 0.05% saponin/PBS and blocked with 3% BSA/PBS. After centrifugation at 500 x g, 4 °C, cells were resuspended in 0,05% saponin/0.5% BSA/PBS, 100 µl added anti-FLAG (1:500)

(DYKDDDDK Tag Monoclonal Antibody (FG4R) DyLight 488, cat.: MA1-91878-D488) or anti-MYC (1:500) (AEEQKLISEEDLLRKRREQLKHKLEQLRNS (mouse monoclonal IgG_1) 555 conjugate, cat.: 16-263) and incubated on a rocking platform for 24 hours at 4°C. The cells were analyzed by BD Accuri ™ C6 Plus Flow Cytometer.

3.0 Results

3.1 The dog intestinal epithelial cell model system

TEER values were measured to assess the tightness of the monolayer and to determine the optimal period for exposure to CDT. Cells (1 x $10^5/cm^2$) were seeded onto transwell inserts and allowed to grow for 11-23 days. TEER was measured manually on day 2-23. The medium was changed every 2-3 days. The TEER increased gradually from day 9 and reached a plateau after about 11-14 days (Figure 16A). Next, we compared the manual TEER measurement with the automatic cellZscope® instrument, which allow TEER measurements every hour (Figure 16B). Here we discovered that TEER increased for the first 3 days, then started to decrease. After medium exchange, the TEER started to increase again. Prior medium exchange the pH indicator in the medium indicated low pH, thus the cells did not have optimal culture conditions. The experiment was ended after only 8 days, as optimization of the protocol clearly was needed.

A)

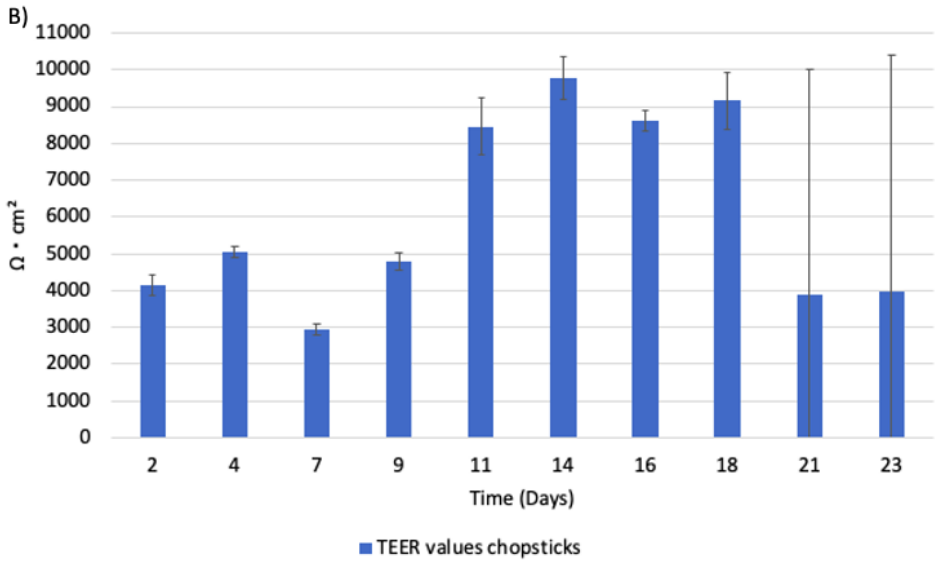

B)

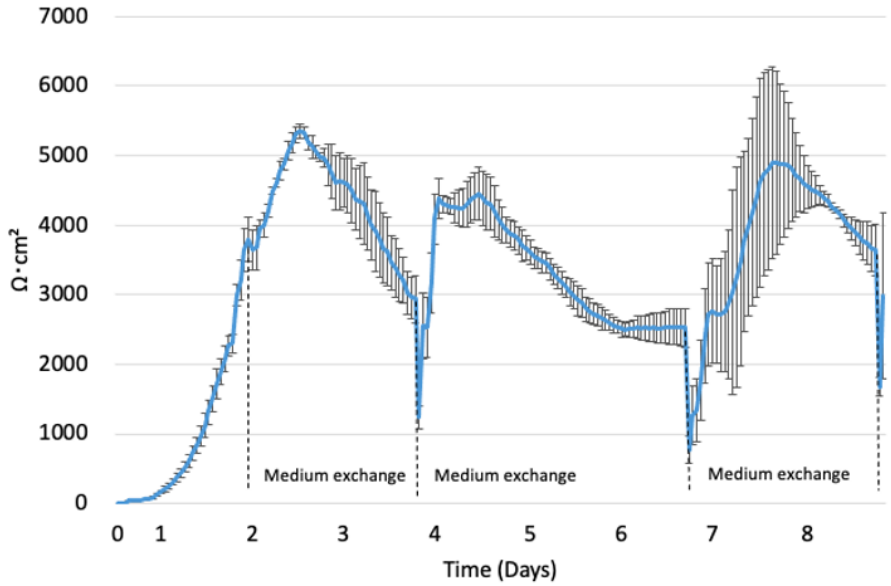

Figure 16: TEER at different timepoints of cells seeded onto transwell inserts. Results represent the mean ± SD from one independent experiment (n = 3). A: TEER was measured on days 2, 4, 7, 9, 11, 14, 16, 18, 21 and 23. B: TEER was measured constant for 8 days.

To optimize the environment for the cells in the transwell inserts, we tested the impact of different seeding densities. To cope with the pH changes in the medium, we also included HEPES (25 µM) in the culture medium. Different cell densities (1,2 x 10^5, 6 x 10^4, and 3 x 10^4 per cm^2) were seeded onto transwell inserts and allowed to grow/differentiate for 21 days. TEER was measured for 21 days with cellZscope® (Figure 17). Timepoints of medium

exchange is not marked in the figure, but the characteristic pattern of drops and peaks of TEER before and after refreshment of medium is found every second or third day of measurement.

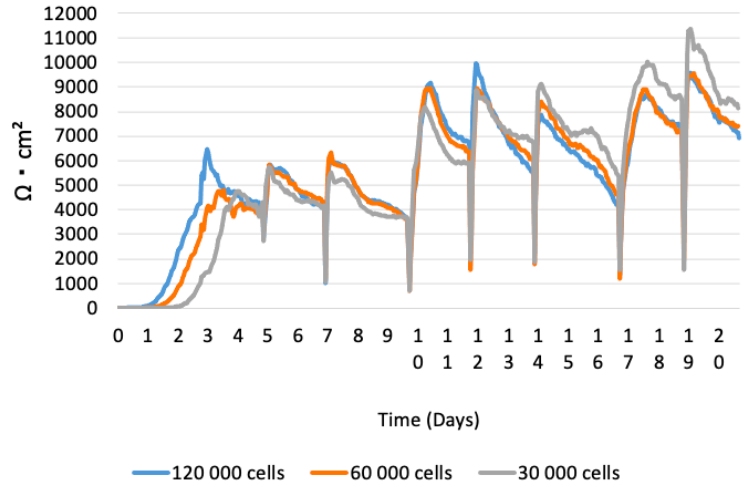

Figure 17: TEER at different timepoints for three different cell densities seeded onto transwell inserts. The figure represents one experiment, mean of 2 parallel inserts each cell density.

Cells seeded with the lowest density of cells (3 x 10^4/cm^2) displayed tight monolayer at the same level as the higher cell densities. The TEER increased gradually and reached a plateau after 10 days. Cell density and the included HEPES in the medium did not seem to affect the drops and peaks of the TEER.

To further characterize the cell barrier, cells seeded onto the transwell inserts were stained for the TJ protein ZO-1 as described in materials and methods. A high level of organization of the TJ protein ZO-1 was seen on day 9 and 16 (Figure 18). This was in correspondence to the observed TEER values, as the monolayer is considered to be confluent when TEER reaches a plateau (Mukherjee et al., 2004).

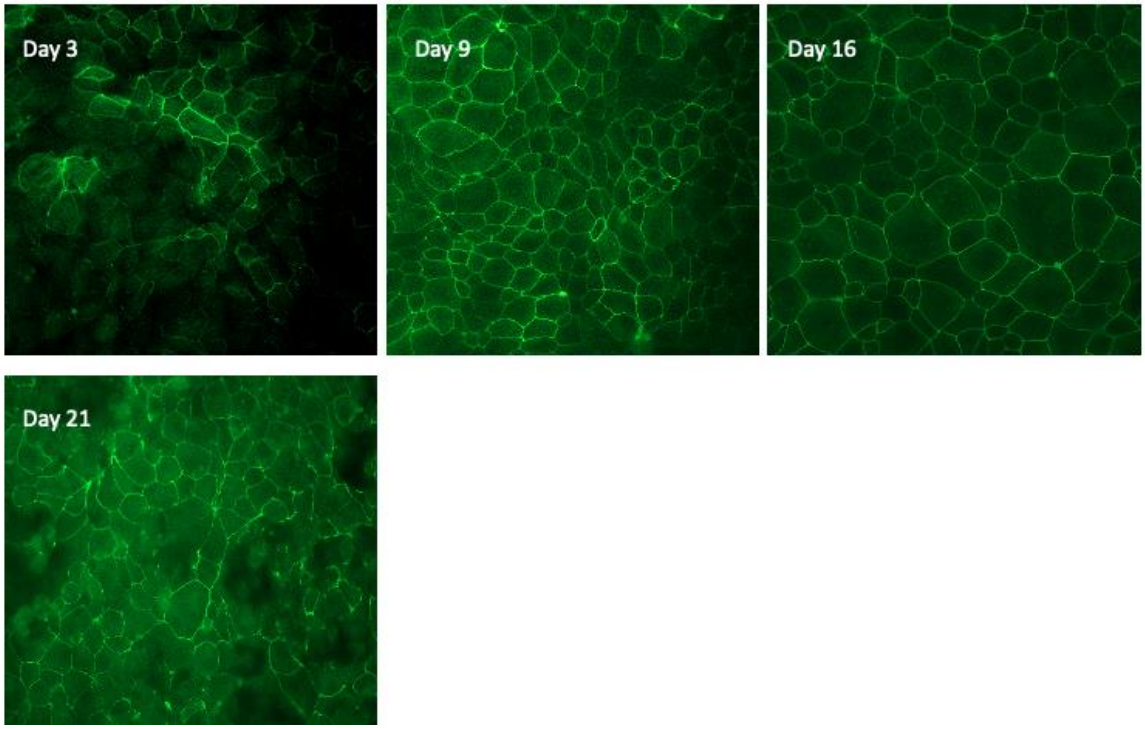

Figure 18: Time-course of ZO-1 expression in cells grown for 21 days. Pictures were taken by Zeiss AXIO observer A1 with 40x magnification on day 3, 9, 16 and 21. The pictures are representative for one experiment.

It was concluded that the cells seeded onto transwell inserts for cytotoxicity assays should be allowed to grow/differentiate until TEER values comparable with approximately 9 days were obtained, before any exposure to CDT.

Based on the TEER measurements (Figure 17) it was concluded that the initial cell seeding density onto transwell inserts for further cytotoxicity assays should be of 3 x $10^4/cm^2$. To characterize the cells further, inserts with this cell density were stained as described in materials and methods to visualize mucins and Alkaline Phosphatase (Figure 19)

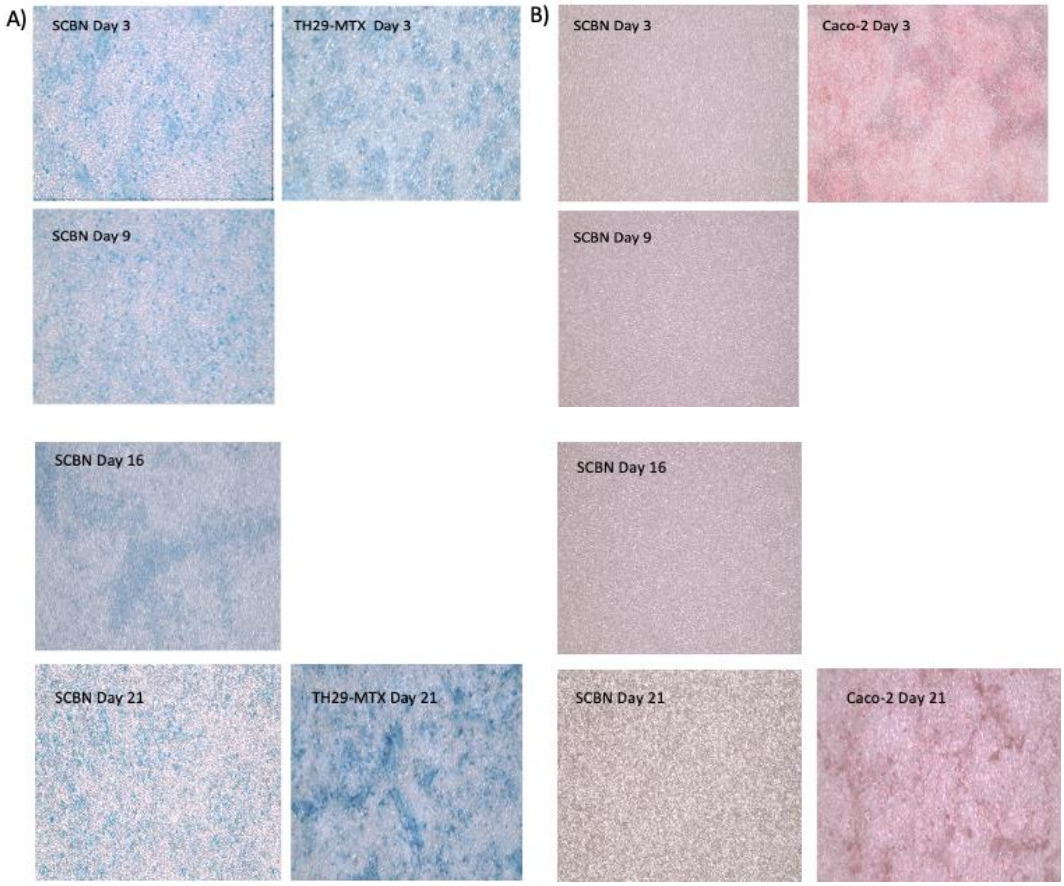

Figure 19: Staining of SCBN cells and ctrls (TH29-MTX and Caco-2) for the visualization of mucins and Alkaline Phosphatase on day 3, 9, 16 and 21 of growth. Pictures were taken with a Leica DM2000 LED microscope. A: Cells were stained with Alcian Blue for the visualization of mucus layer. TH29-MTX cells were included as a positive control on day 3 and 21. B: Cells were stained with Fast Red for the visualization of Alkaline Phosphatase. Caco-2 cells were included as a positive control on day 3 and 21. The experiment was performed one time.

No expression of mucus layer or the differentiation marker alkaline phosphatase were seen in SCBN cells allowed to grow/differentiate for 21 days (Figure 19). THE29-MTX (human intestinal goblet cell line) and Caco-2 (human colorectal enterocyte cell line) were used as a positive control for mucus production and alkali phosphatase, respectively. The cells were cultured and provided by supervisor Dr. A. Solhaug.

To characterize the SCBN cells further, visualization of actin filaments (F-actin) in the cytoskeleton and nuclei were performed with immunostaining after 11 and 23 days of growth (Figure 20). Based on the organization of the F-actin and nuclei, the cell layer appeared to be well organized. Also, when looking at the nuclei morphology; no or very little fragmented nuclei were seen, which may indicate little or no induction of apoptosis.

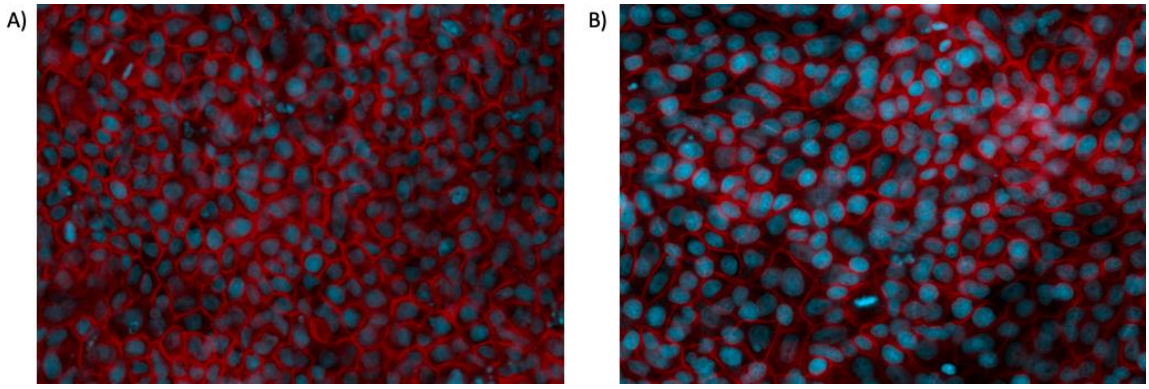

Figure 20: Actin filament expression in the cells at day 11 (A) and 23 (B). Pictures of nuclei stained with DAPI (blue) and F-actin stained with phalloidin Alexa Fluor555 (red) were taken by Zeiss AXIO observer A1 invert fluorescence microscope with 40x magnification.

Further, immunostaining of the mucin MUC1 was performed on cells grown for 11 days. In accordance with the Alamar blue staining (Figure 19), no staining of MUC1 were found (data not shown).

3.1.2 Sensitivity to recombinant CDT

To determine the cytotoxicity of CDT on the SCBN cell line, the cells were seeded onto plastic plates and exposed to recombinant CDT from *E. coli* up to 72 hours. High cytotoxicity in the cells after analyzation by the CellTox™ Green assay were observed after 24 hours of exposure to a concentration of cdtAC, 2,25 μg/μl and cdtB, 0,45 μg/μl (the concentrations are described in section 2.4.1 in materials and methods) (Figure 21A). However, a 50% reduction of the toxin concentration did not seem to have any cytotoxic effect compared to ctrl (0 μg). When examining the cells by light microscopy, less viable cells were seen in samples exposed to high concentration of CDT compared to the other samples (Figure 21B).

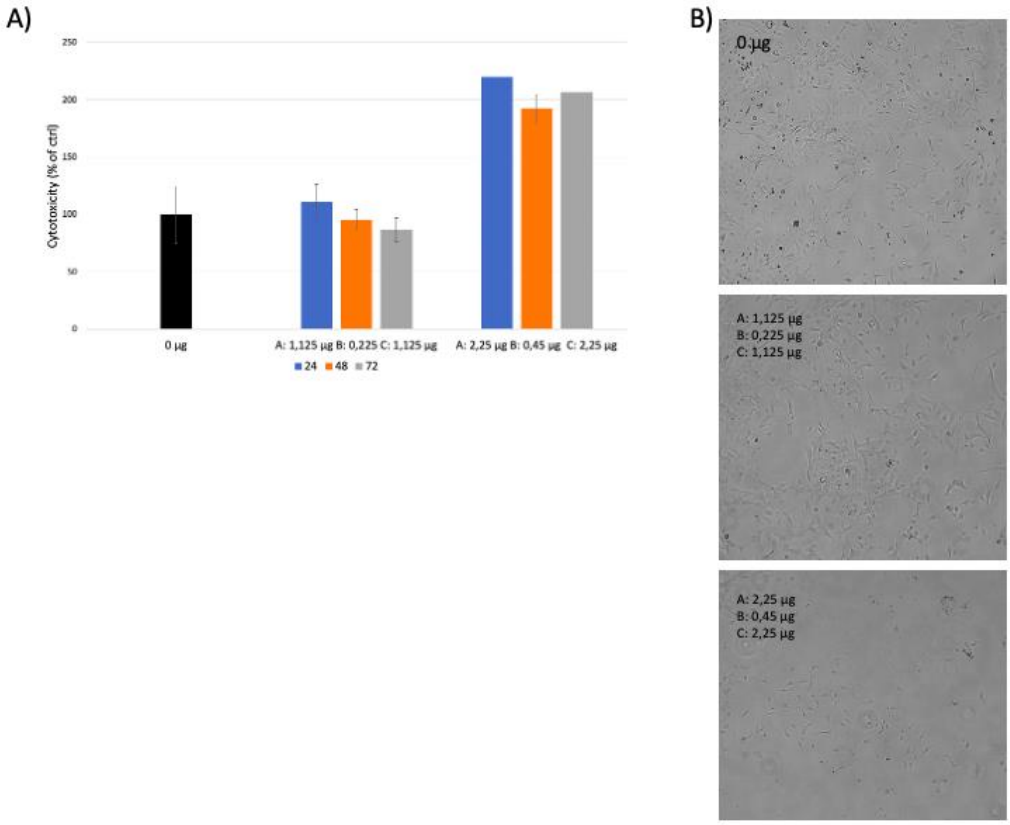

Figure 21: Cell viability in cells after exposure to recombinant CDT from *E. coli*. A: The cytotoxicity in cells treated with CDT was assessed by the Celltox™ Green assay and analyzed with the Spectramax® i3x (200 points) at 24, 48, and 72 hours of exposure. Error bars represent the difference between the mean of two independent experiments. B: Brightfield imaging with Zeiss AXIO observer A1, 5x magnification revealed less viable cells in samples exposed to a concentration of cdtAC, 2,25 µg/µl and cdtB, 0,45 µg/µl compared to a 50% reduction of toxin concentration and ctrl (0 µg). The pictures are representative for two independent experiments.

Further, to determine the effect of CDT on barrier function, cells were seeded onto transwell inserts and allowed to grow/differentiate until TEER values reached approximately 8000 Ω x cm^2. Cells were then exposed to the different concentrations of EcCDT. TEER was measured at time 0 before exposure, then at 4, 8, 12, 24, 36, 48 and 72 hours after exposure (Figure 22).

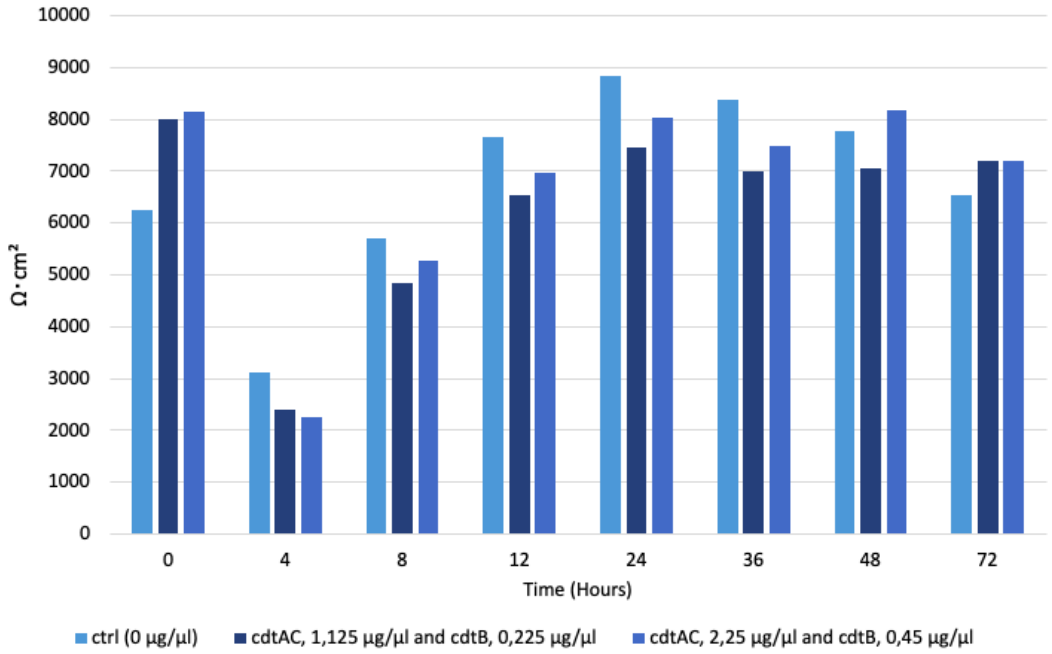

Figure 22: TEER of cells seeded onto transwell inserts before and at different timepoints after exposure to EcCDT (n = 1). The experiment was performed one time.

A decrease of TEER was observed 4 hours after exposure, included ctrl. The TEER increased gradually again and reached TEER values comparable to before exposure to CDT during the next days. Immunofluorescence staining was performed to visualize ZO-1 and phalloidin/DAPI staining was performed to visualize actin filaments and nuclei 72 hours after exposure (Figure 23).

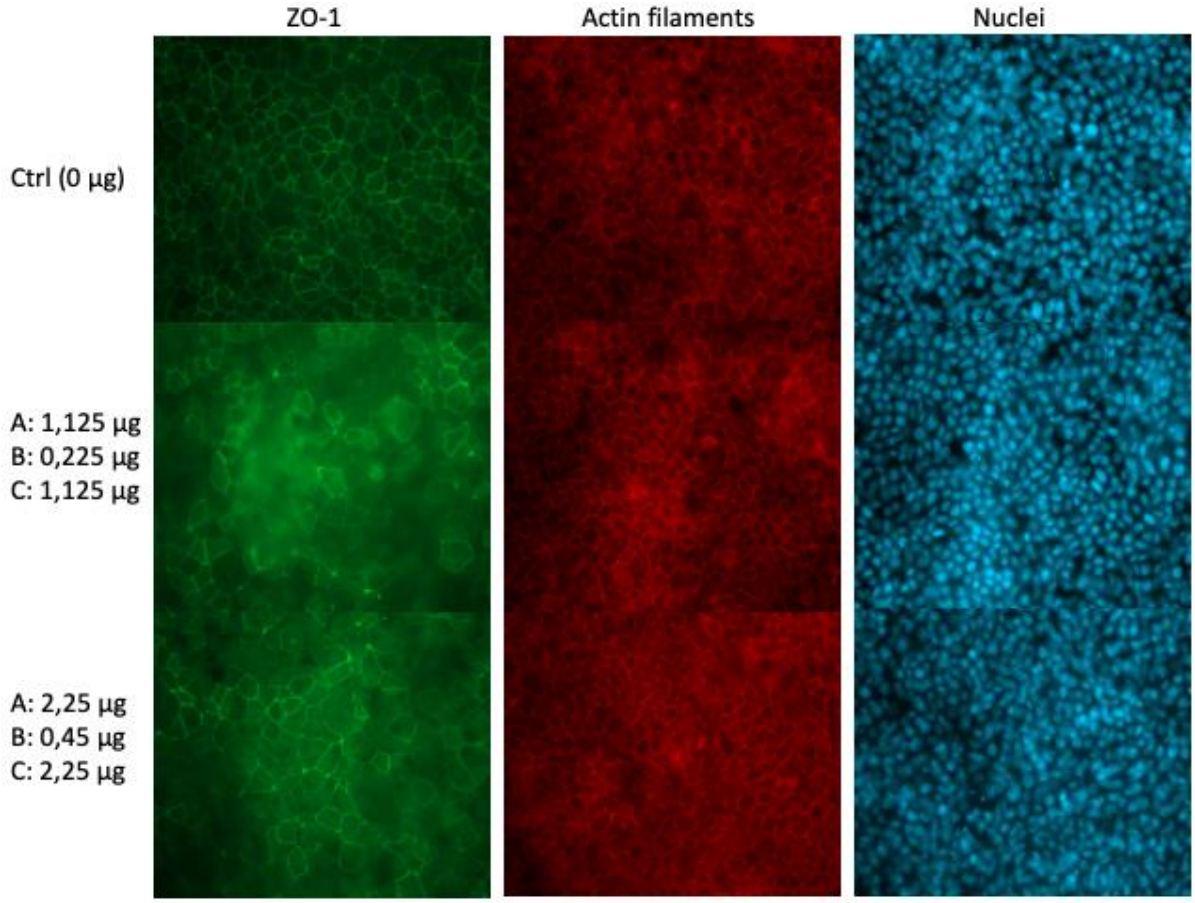

Figure 23: ZO-1, actin filaments and nuclei in cells 72 hours after exposure to EcCDT, plus ctrl. Pictures were taken by Zeiss AXIO observer A1 with 40x magnification. The pictures are representative for one experiment.

The result indicated that cells seeded on transwell inserts were not affected by the exposed concentrations of EcCDT.

3.2 Optimalization of bacterial culture conditions

First, the cells (340 cells/cm^2) were exposed to samples from toxin production *in vitro*, experimental design 1. Analyzation by the CellTox™ Green assay did not detect any cytotoxicity (data not shown), and further microscopy of the cells confirmed the Spectramax® i3x (200 points) plate reader data. We therefore decided to optimize culture conditions for increased CDT production.

3.2.1 Growth curves of bacteria grown under different conditions

OD_{620} measurements at multiple timepoints were performed to assess the bacterial growth under the different culture conditions. Growth curves of *P. alcalifaciens* strains 1722, 1723 and *E. coli* strain v27 are found in figure 24 (Evan´s toxin medium is abbreviated to "Evan´s" in the figure).

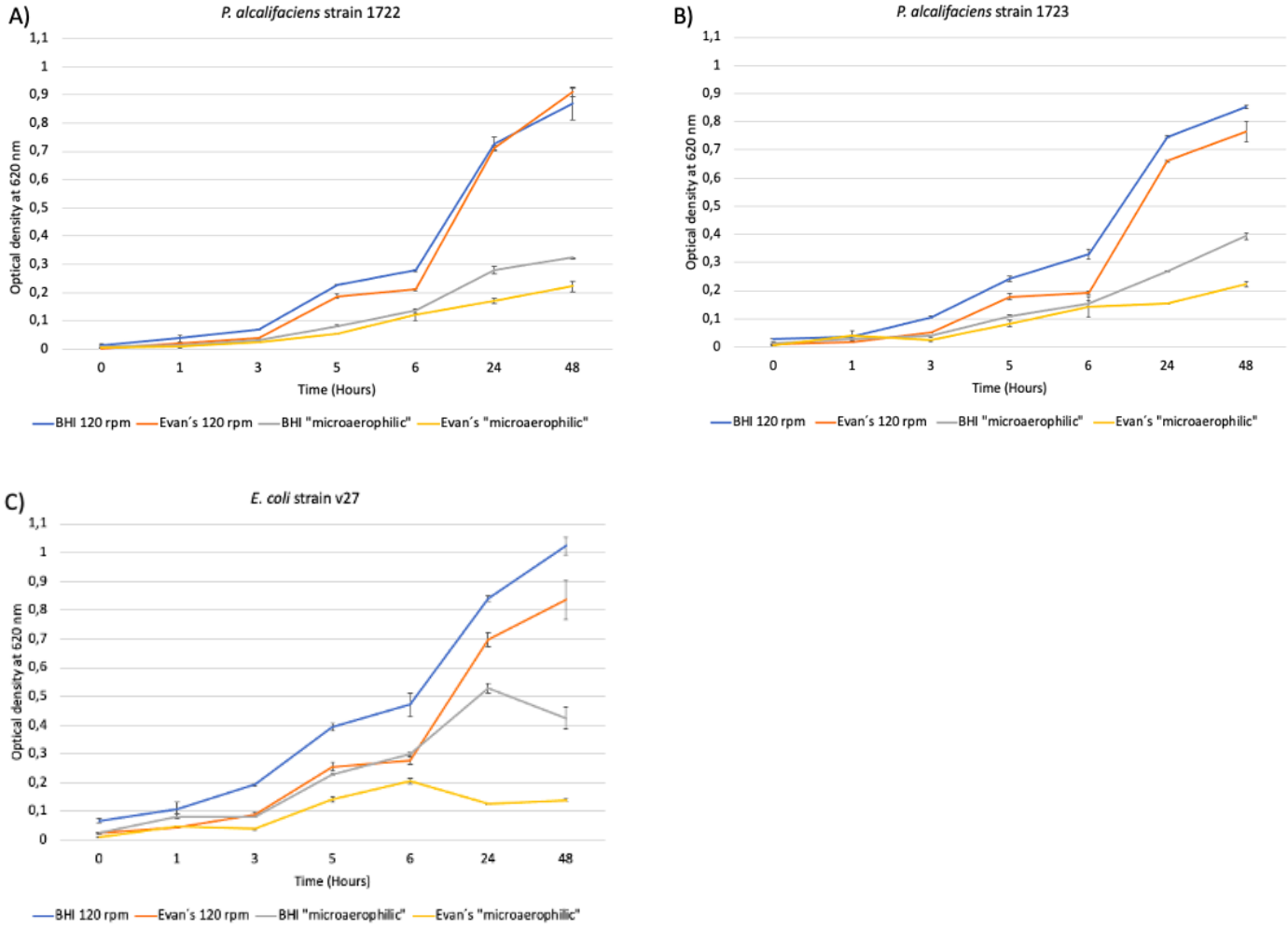

Figure 24: Growth curves of CDT producing bacteria grown under 4 different conditions for 48 hours. Error bars represent the difference between duplicates from one experiment (n = 2). A: *P. alcalifaciens* strain 1722. B: *P. alcalifaciens* strain 1723. C: *E. coli* strain v27.

The results indicated an exponential phase from approximately 3 hours until 48 hours of growth under aerobic conditions for all three strains. The curves start to flatten out after 24 hours of growth, indicating that the cultures enter stationary phase at approximately 48 hours. Some variation between strains were observed for growth under microaerophilic conditions (without shaking), where *E. coli* strain v27 (Figure 24C) seems to have a loss of viable cells

after 6 and 24 hours of growth in Evan´s toxin medium and BHI, respectively. *P. alcalifaciens* strain 1723 (Figure 24B) grown under microaerophilic conditions may have an extended exponential phase, as the curves do not seem to flatten out after 24 hours of growth.

OD_{620} measurement of bacteria grown in an anaerobic milieu had absorbance values below 0,09 after 72 hours of cultivation (data not shown).

Next, sampling for RNA extraction were performed during bacterial growth, and concentration and quality analysis of extracted RNA were assessed by Nanodrop.

3.2.2 Gene expression measurement

3.2.2.1 Concentration and quality analysis of extracted RNA

For both the column- and solution-based RNA extraction methods, various RNA concentrations were obtained. The concentrations were ranging from 268 ng/µl to 0 ng/µl, with most of the RNA sample concentrations measured to <20 ng/µl. The 260/280- and 260/230 ratio assessed by Nanodrop indicated contamination in almost all of the samples, giving a characteristic peak at 230 nm.

The extracted RNA samples were applied for the RT-qPCR assays for investigating under which cultivation conditions the transcription rate of CDT genes was at its highest.

3.2.2.2 Quality analysis of designed primer pairs for RT-qPCR

To evaluate if the amplicon length of the qPCR products matched the expected amplicon length of each primer pairs, the PCR products were analyzed by Bioanalyzer (Figure 25).

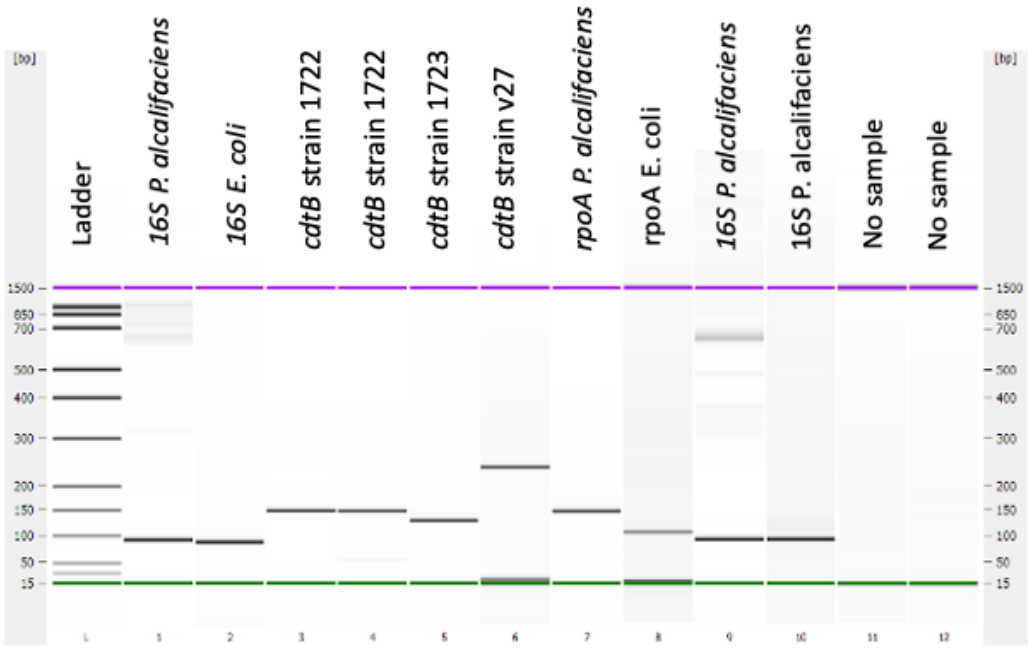

Figure 25: Gel image from Bioanalyzer. The size of PCR products from all primer pairs are shown compared to the ladder.

The expected amplicon length (bp) of each primer pairs are found in table 10. Expected amplicon lengths that differ from PCR products are marked with *.

Table 10: The expected PCR amplicon length (bp).

Strain	**Gene**	**Amplicon length (bp)**
P. alcalifaciens 1722	*cdtB*	146
P. alcalifaciens 1723	*cdtB*	123
E. coli v27	*cdtB*	158 *
P. alcalifaciens	*rpoA*	139
E. coli	*rpoA*	97 *
P. alcalifaciens	*16S*	82
E. coli	*16S*	81

The gel image revealed unspecific PCR products amplified by primer pairs *cdtB* strain v27 and *rpoA* strain v27. A published primer pair targeting E. coli *rpoA* and an additionally designed primer pair targeting *E. coli* v27 were obtained. The designed primer pair are found in table 11.

Table 11: The second designed primer pair targeting *E. coli v27.*

E. coli V27	*cdtB*	F:5´-CCGGCTCTTGTTGAGGAAGT-3´ R:5´-CCAGTTAAGCGCCTGGTGTA-3´

3.2.2.2 Relative gene expression ratios

It was not possible to determine valid relative gene expression ratios. Ct values from No-RT samples were found in the same range as Ct values obtained from the target genes, indicating that the removal of gDNA was incomplete. A difference of Ct values between no-RT samples and target gene samples of five cycles or more ensures that the RT-qPCR results will not be significantly impacted by gDNA contamination (Padhi et al., 2016). Thus, it was not possible to distinguish cDNA from gDNA in the RT-qPCR assay and relative gene expression ratios could not be obtained.

3.3 Exposure to samples from toxin production

Without quantification of the relative changes in mRNA expression levels, we decided to test the different samples from strain 1723, grown under various culture conditions from experimental design 3. Cells (680 cells/cm^2) were seeded onto plastic plates and exposed to samples up to 72 hours. Analyzation by the CellTox™ Green assay did not detect any cytotoxicity (data not shown). However, when examining the cells by microscopy, a change in morphology was observed in cells exposed to two of the samples (Figure 26B and 26C).

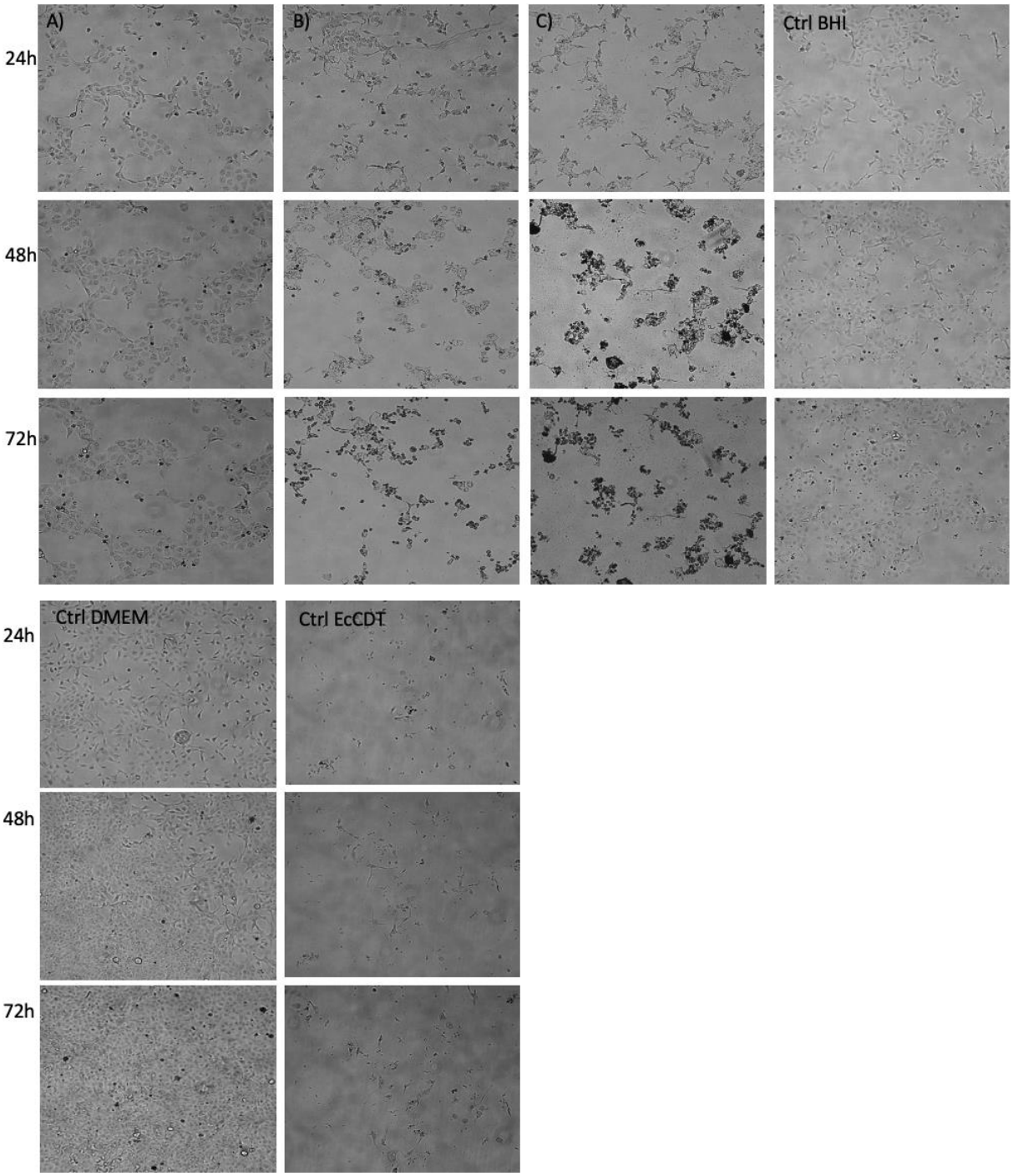

Figure 26: Brightfield imaging with Zeiss AXIO observer A1, 5x magnification of cells exposed to samples from experimental design 3. A: Cells exposed to samples from strain 1723 grown for 72 hours in BHI. B: Cells exposed to samples from strain 1723 grown for 72 hours in Evan´s toxin medium. C: Cells exposed to samples from strain 1723 grown for 72 hours on blood agar plates. The figure is representative for three independent experiments.

All culture conditions were tested, but less viable cells were only observed when exposed to samples included in the figure. The result indicated that growth for 72 hours in an anaerobic

milieu, either on blood agar plates or Evan´s toxin medium, did affect the composition of the bacterial lysate. Whether it was CDT causing the indicated necrosis of the cells is not known.

3.3 Cloning preparation

3.3.1 Confirmation of correct amplicon lengths and linearized pcDNA3.1 vector

The genetic variants of subunit cdtB were amplified by PCR using primers designed with epitope tags. To confirm that the PCR products had the correct amplicon length, samples were applied to gel electrophoresis. Negative controls for each primer pair without template were added to the PCR and applied onto four wells in the gel. Expected amplicon lengths are found in table 11. The result from gel electrophoresis is shown in figure 27. Two different concentrations of peqGOLD ladder 1 kb were applied to the gel, due to uncertainty of which concentration to use.

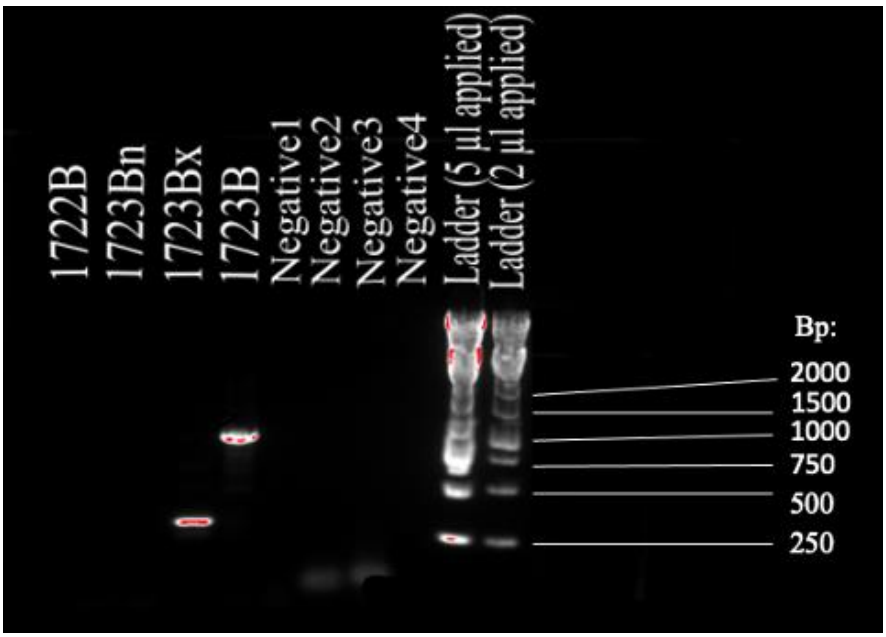

Figure 27: PCR products applied to gel electrophoresis for confirmation of correct amplicon lengths. Gel was imaged by the ChemiDoc XRS+ Gel Imaging System.

Table 11: The expected PCR amplicon length (bp).

Gene	**Expected amplicon length (bp)**
1723 cdtB	851
1723 cdtBn	447
1723 cdtBx	304
1722 cdtB	850

The amplification of 1722 cdtB and 1723 cdtBn was negative. PCR products from 1723 cdtBx and 1722 cdtB had the expected amplicon lengths confirmed by gel electrophoresis. Negative controls did not show any unspecific bands. A new gel electrophoresis was performed. PCR products of 1722 cdtB- and 1723 cdtBn were applied one more time to check whether application to gel went wrong or if the sequences were not amplified during PCR. In addition, linearized vector from restriction digestion reaction plus uncut vector were applied to the gel. The result of gel electrophoresis is found in figure 28.

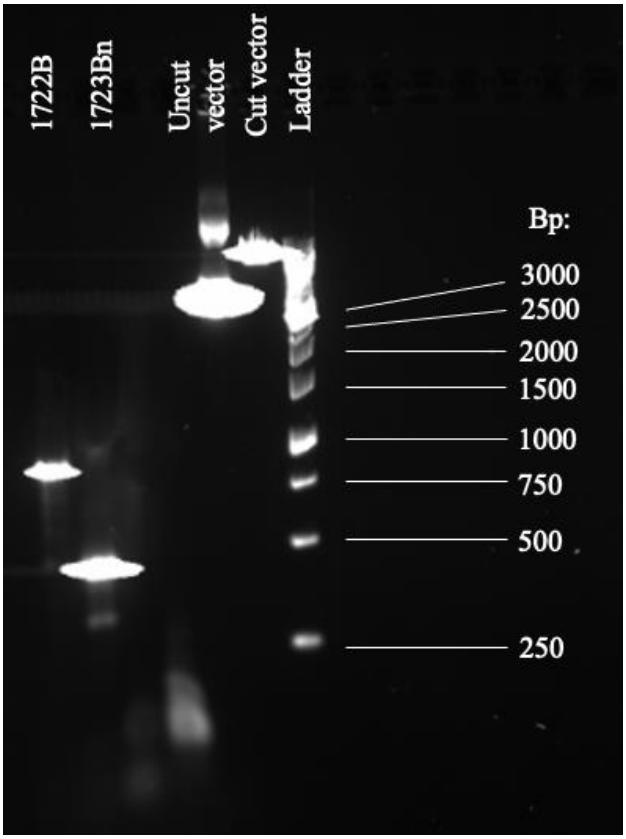

Figure 28: The result of gel electrophoresis with applied samples from vector restriction reaction plus PCR products of 1722 cdtB and 1723 cdtBn. Gel was imaged by the ChemiDoc XRS+ Gel Imaging System.

PCR products of 1722 cdtB and 1723 cdtBn had the expected amplicon lengths confirmed by gel electrophoresis. The uncut vector showed the expected distinct bands, while cut vector migrated slower in the gel than the supercoiled vector and faster than the relaxed vector.

The amplified PCR products were treated by Cloning Enhancer and added to the In-Fusion Cloning reaction. After bacterial transformation, 10 colonies from LB agar, dilution 20/100 were applied for colony PCR. Negative control included in bacterial transformation showed growth of transformed bacteria, indicating that vector linearization was incomplete.

3.4 Cloning confirmation

3.4.1 Colony-PCR

To confirm successful insertion into the vector, a colony-PCR was performed, and the result was examined by gel electrophoresis (Figure 29).

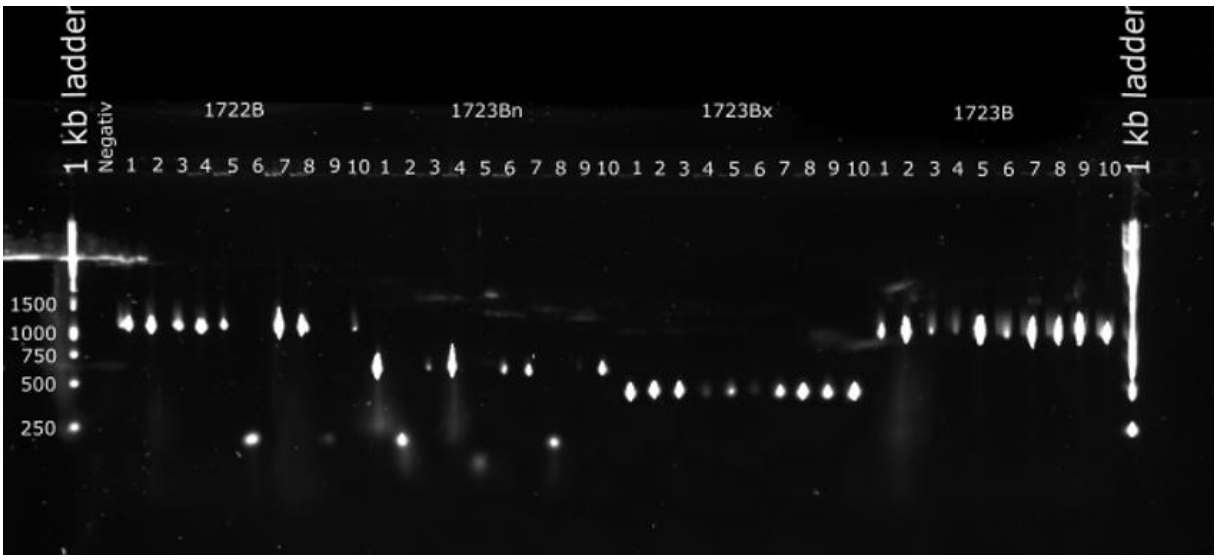

Figure 29: The result of gel electrophoresis with applied samples from colony-PCR. Gel was imaged by the ChemiDoc XRS+ Gel Imaging System.

The concentration of ladder applied were 1 µl. Still the bands from ladder were smeared. It was decided to add half of ladder concentration next gel electrophoresis. It seemed like most

of the colonies had the correct inserts and 3 wells of each clone from the 96-well plate with bacterial suspension was selected for miniprep:

1722B: well 2, 4, and 7
1723Bn: well 1, 4, and 10
1723Bx: well 2, 8, and 10
1723B: well 2, 5, and 9

3.4.2 Sequence verification

The three colonies from each clone were sequenced by Sanger sequencing. The sequencing data were analyzed by CLC Main Workbench. Data obtained from Sanger sequencing were aligned with a reference sequence, where the different constructs were inserted into the pcDNA3.1 vector *in silico*. By analyzing the data, it is possible to verify that the start codon, the target gene, the FLAG/c-MYC-tag, and the stop codon was intact.

When analyzing the Sanger sequence data, it was observed that the c-MYC tag was incorrectly constructed. A new primer was obtained with correct c-MYC sequence, and all steps performed had to be repeated for 1723Bn. On the second attempt, it was verified that the clone had the right sequence. One cultured colony from each cdtB construct were chosen for midiprep. The plasmid DNA concentrations after performed midiprep are found in table 12.

Table 12: Concentration of each construct after midiprep, assessed by NanoDrop.

Construct	**Concentration (μg)**
1722B	130
1723B	60
1723Bn	110
1723Bx	80

3.5 Transfection

First, transfection optimalization was performed by lipid-based transfection and electroporation. After 72 hours, fluorescence microscopy of the cells was performed to observe if the positive control, phMGFP were expressed. The results are found in figure 30 and 31.

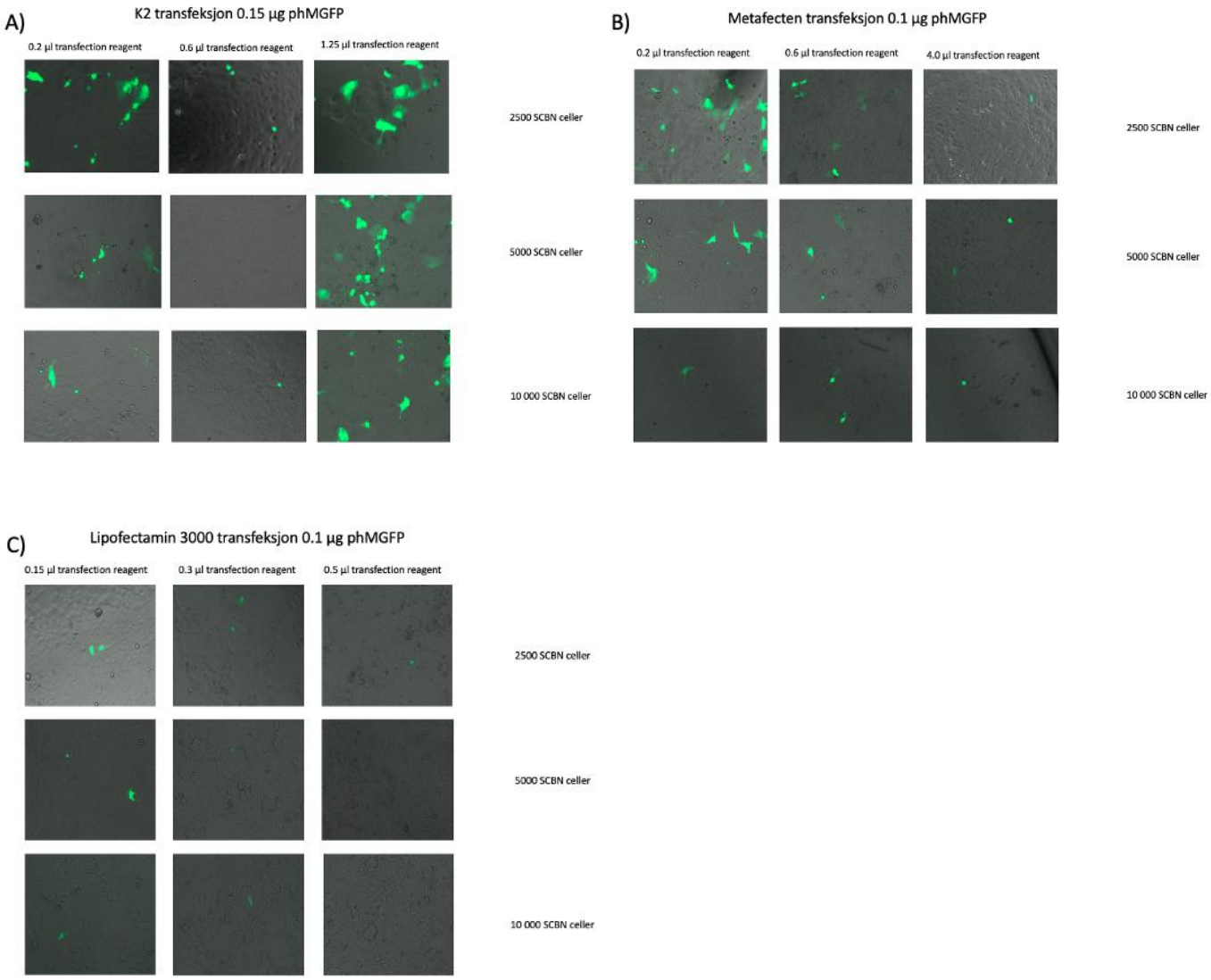

Figure 30: The expression of phMGFP 72 hours after lipid-based transfection. A: K2 transfection. B: Metafecten transfection. C: Lipofectamin transfection. Pictures were taken by Zeiss AXIO observer A1 with 40x magnification. The pictures are representative for one experiment.

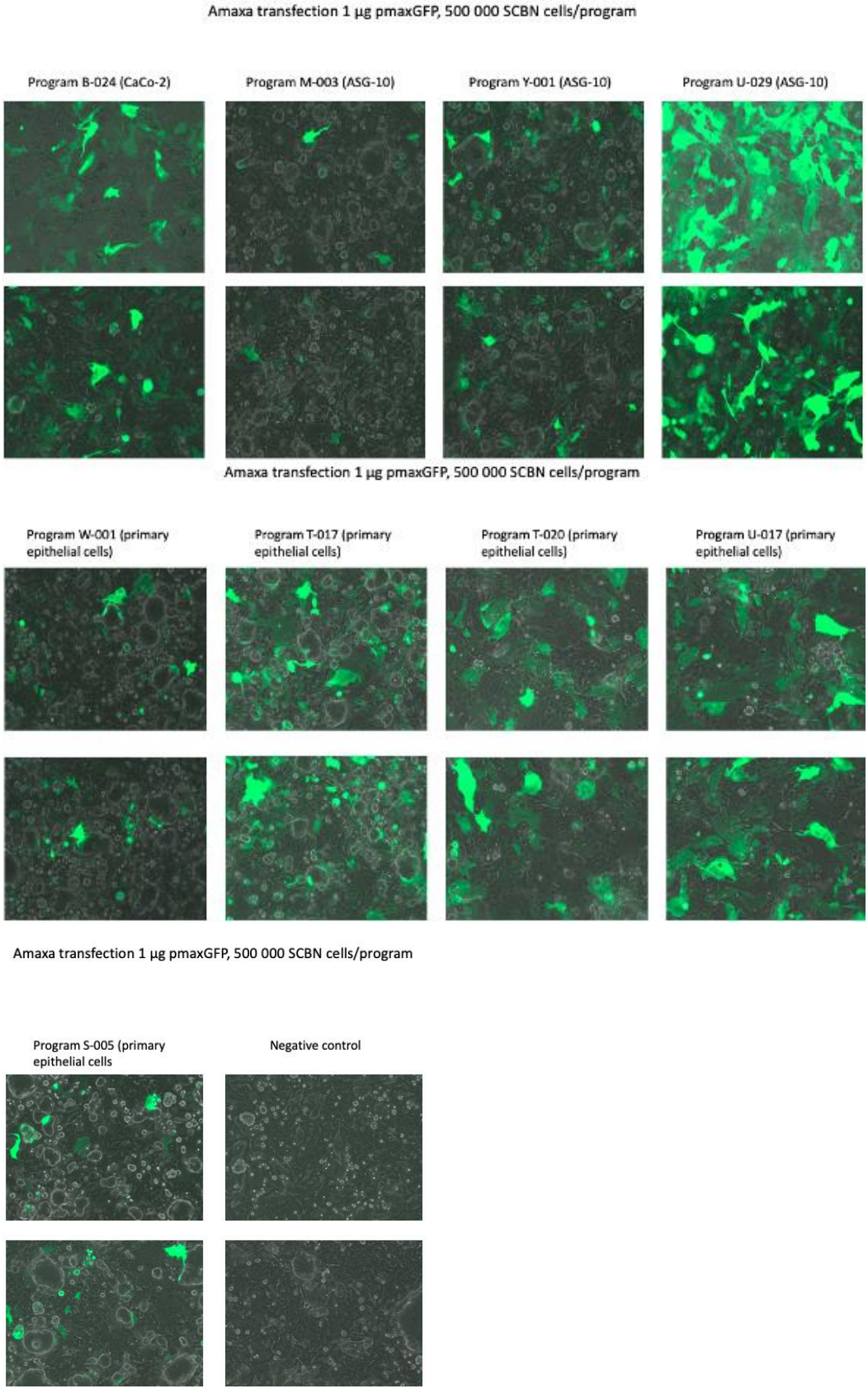

Figure 31: The expression of pmaxGFP 72 hours after electroporation. Nine different Nucleofector® Programs were tested. Pictures were taken by Zeiss AXIO observer A1 with 40x magnification. The pictures are representative for one experiment.

Nucleofector® Programs for different types of epithelial cells were chosen to identify the optimal program for the SCBN cell line; The human colon adenocarcinoma Caco-2 cell line, the Atlantic salmon gill ASG-10 cell line, and primary epithelial cells.

When examining the cells by fluorescence microscopy, it seemed like Amaxa transfection with Nucleofector® Program U-029, designed for Atlantic salmon gill cells was the appropriate transfection method to apply for the SCBN cell line. Supporting data from flow analysis were obtained (Figure 32).

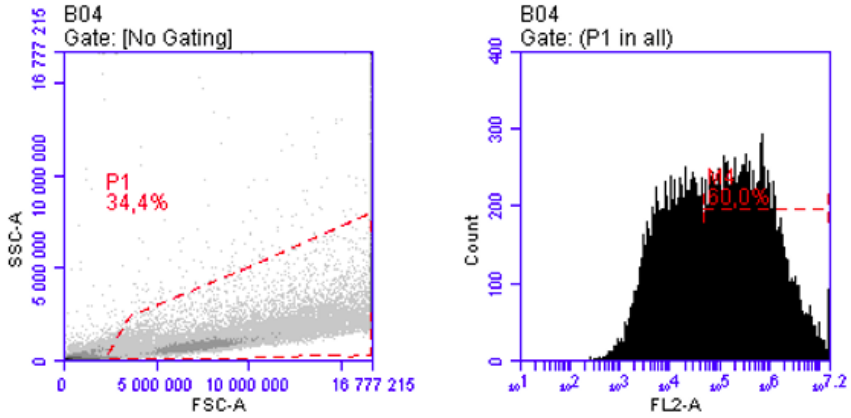

Figure 32: Flow cytometry result from Amaxa transfection with Nucleofector® Program U-029. Data from transfection with pmaxGFP is shown in the figure.

(Det var her jeg gjorde feil med 70%etOH i stedet for PBS da jeg skulle løsne celler fra brett etter lipid transfeksjon før flow. Jeg kan evt. sette opp en tabell med transfeksjons prosent fra Amaxa programmene og skrive at det ikke ble kjørt flow fra lipid transfeksjon)

When excluding necrotic cells (P1), 60% of the cells were transfected, expressing pmaxGFP. Based on the results, we decided to apply Nucleofector® Program U-029 for the transfection of cells with the different cdtB constructs.

The positive control was observed by fluorescence microscopy and started to express pmaxGFP already 6 hours after transfection (data not shown). Picture from 24 hours after transfection is shown in figure 33.

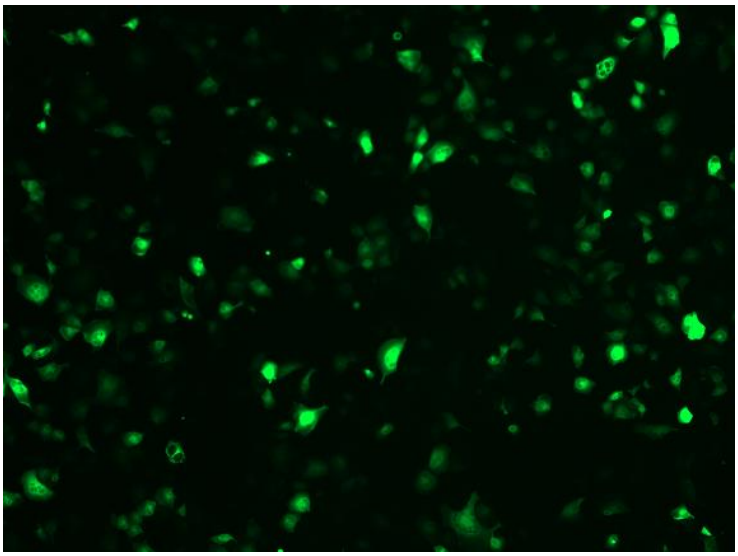

Figure 33: The expression of phMGFP 24 hours after electroporation with Nucleofector® Program U-029. Pictures were taken by Zeiss AXIO observer A1 with 40x magnification. The picture is representative for one experiment.

We decided to stain the cells with anti-FLAG (DyLight®488) and anti-c-MYC (Alexa Fluor® 555). How the different constructs were stained and in which flow cytometry channel the fluorochrome were read are found in table 13.

Table 13: Staining of the different constructs and the flow cytometry channels.

cdtB construct	**Staining**	**Flow cytometry channel**
1722B	anti-FLAG	FL2-A
1723B	anti-FLAG	FL2-A
1723Bn	anti-c-MYC	FL3-A
1723Bx	anti-FLAG	FL2-A
1723BnBx	Anti-c-MYC/anti-FLAG	FL2-A/FL3-A

The overlapping nature of emission spectra may result in detection of a single fluorochrome in two different channels (Jaroszeski & Radcliff, 1999).

Data from flow cytometry are found in figure 34.

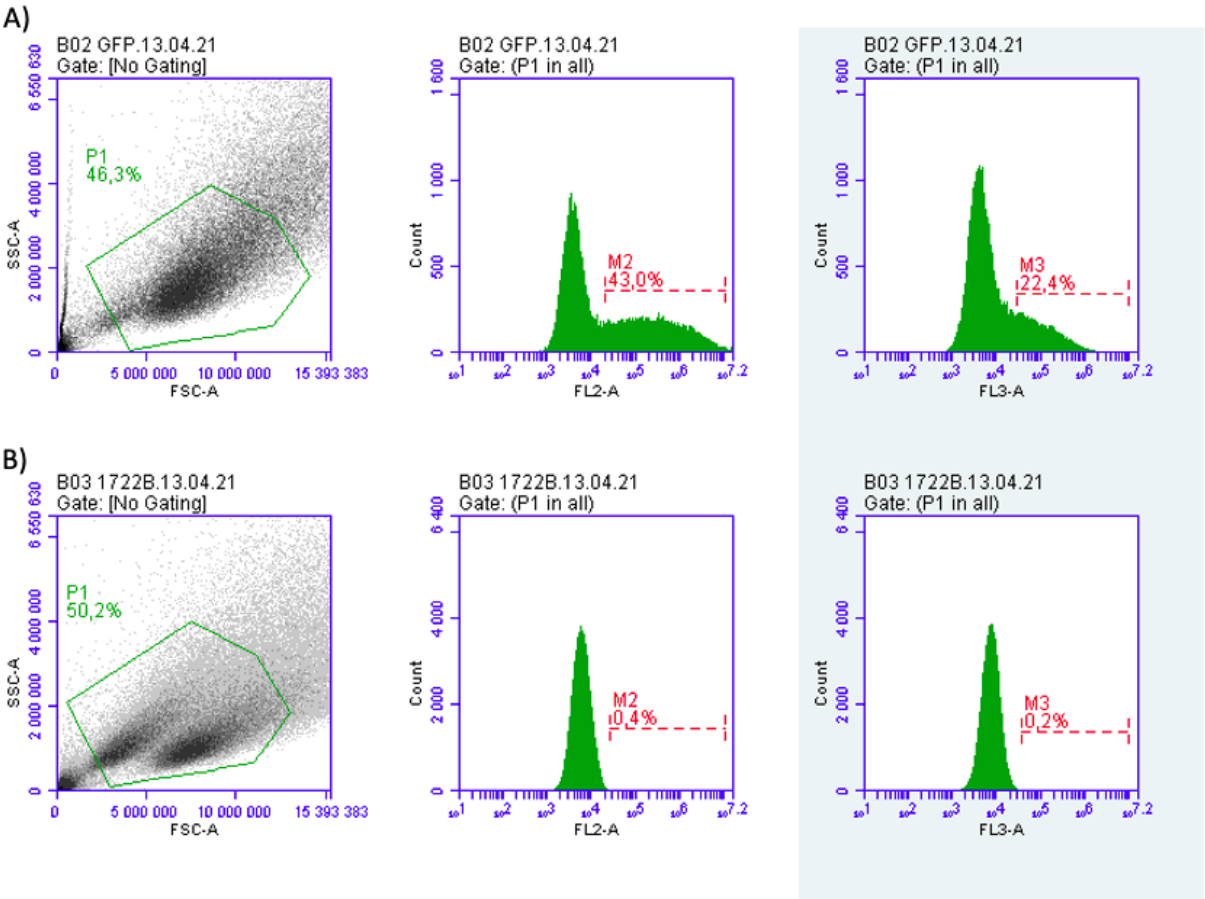

Figure 34: Flow cytometry result from Amaxa transfection with Nucleofector® Program U-029. A: Data from transfection with positive control phMGFP. B: Data from transfection with construct 1722B.

When excluding necrotic cells in figure 34A, 43% of the cells were transfected, expressing pmaxGFP. When excluding necrotic cells in figure 34B, 0,4% of the cells are transfected. The transfection of the other constructs was also analyzed by flow cytometry, with less than 0,4% transfected cells. The results indicated that the cells were not transfected by the cdtB construct, while transfection with positive control were obtained.

2 Discussion

P. alcalifaciens is known for its ability to invade epithelial cells, and its more recently discovered toxin, CDT, is produced by several clinically important Gram-negative bacteria that has been shown to exert toxicity in a broad range of mammalian cell lines. The results from this study did show that recombinant CDT from *E. coli* at specific concentrations induced toxicity in the dog intestinal epithelial cell line, SCBN, after 24 hours of growth onto plastic plates. These findings support the existing theory of CDT´s ability to cause toxicity in intestinal epithelial cells. Furthermore, results indicated that filter-sterilized lysates from *P. alcalifaciens,* grown under certain conditions, induced toxicity in the SCBN cells. It is not known whether the bacterial lysates harbored CTD, but these specific culture conditions have been shown to produce CDT activity in previous studies (Johnson & Lior, 1988; Yamano et al., 2003). Finally, to the best of the author´s knowledge, this is the first study reporting of transfection methods applied for transfection of the SCBN cell line, which may be useful for future studies.

4.1 Model system

The TEER of approximately 8000 Ω x cm^2 when reaching a plateau, indicated monolayer confluency and the behavior of a tight epithelia. The observed high level of organization of the TJ protein ZO-1 confirmed the indications. These findings were in accordance with the previous literature stating the ability of SCBN cells to form polarized monolayers that express TJ proteins. The observed TEER values are higher than previously reported TEER values of the cell line, where confluent monolayers had a TEER>1000 Ω x cm^2 (Buret et al., 2002; Lamb-Rosteski et al., 2008). High starting TEER values permit more detailed studies on changes in barrier function induced by bacterial infections, making the cell line suitable for studying the effect of CDT with focus on barrier function (Schierack et al., 2006). When measuring TEER constant every hour, a pattern of drops and peaks of TEER values were observed. When measuring TEER manually, prior to medium exchange, these peaks were not visible, and the values seemed more stable. Presumably, the variation of TEER values observed by automatic measurement would also have been present if measured manually at the same timepoints and were probably due to the enhanced access of nutrients obtained from fresh medium and variation of pH.

Further, we were unable to detect goblet cells by Alcian blue staining and staining of MUC1 was negative. The absence of the differentiation-associated marker Alkaline Phosphatase indicated no brush border activity after 21 days of growth. Cells with features of mucin secretion and enterocytic differentiation will be closer to intestinal epithelial cells *in vivo* and more resistant to cell invasive substances (Barbat et al., 1998; Schierack et al., 2006). In addition, MUC1 has been shown to bind bacteria in tissue culture, it is constructed to act as a guardian and sensor of the cell surface, and to signal to the interior of the cell if something is wrong. Also, MUC1-negative intestinal cells have been demonstrated *in vivo* to have decreased resistance to CDT produced by *Campylobacter jejuni* (Gendler, 2001; McAuley et al., 2007).

These findings suggest that the effects of CDT on SCBN cells seen *in vitro* cannot accurately predict the effects of CDT on dog intestinal epithelial cells *in vivo*, as they probably will be overestimated. When the cell line first was established, it was reported that the cells expressed brush border enzyme activity as well as microvilli indicating that they were of enterocyte-like cells of the small intestine (Pang et al., 1996). The results of the present study do not support this theory. However, since the origin of the SCBN dog intestinal epithelial cell line is unknown, it is not known from which part of the dog intestine originates from, and the features of enterocytic differentiation may have been lost on the way.

4.2 The effect of exposure to CDT from *E. coli*

The model whereby TEER is applied for the determination of a polarized monolayer to assess the optimal period for exposure to substances causing epithelial injury on SCBN cells has been utilized in previous studies. The effect of the exposure has then been quantified by the reduction of TEER followed by assessment of ZO-1 integrity and rearrangement of F-actin characterized by fluorescence microscopy (Buret et al., 2002; Teoh et al., 2000).

In the present study, no effect of exposure to recombinant EcCDT was seen on cells grown on transwell inserts, while cells grown on plastic plates showed a loss of viable cells and cytotoxicity were detected by the CellTox™ Green assay. The use of cells cultured *in vitro* onto tissue culture plastic is limiting as an alternative to animal model due to the failure of development of normal tissue architecture, resulting in a poor level of differentiating and loss of tissue-specific functions like the polarized morphology of epithelial cells (Ramaiahgari et al., 2014). Nevertheless, the model system verified that the SCBN cells were susceptible of

CDT and identified differences in toxicity assessed by the CellTox™ Green assay due to exposure of different concentrations of the toxin.

Results indicated the absence of mucins and the brush border enzyme Alkaline Phosphatase in the SCBN cell line grown for 21 days. The toxin solution then contacts the cell surface directly without any anti-bacterial proteins secreted or regulation of surface pH by Alkaline Phosphatase. The observed differences of toxicity in cells grown onto transwell inserts versus plastic plates must then rely on the barrier function of polarized monolayer with functional TJs proteins and cell density alone. The SCBN cells grown on transwell inserts may therefore serve as a good enough model system for characterizing the effects of CDT with focus on TEER as the barrier function.

4.3 Optimalization of culture conditions for increased CDT production

Based on previous studies where the culture conditions have been linked to the concentration of CDT, we attempted to optimize bacterial culture conditions for increased CDT production. Shima et al. demonstrated that filter-sterilized, sonicated lysates of *P. alcalifaciens* strains grown in BHI at 37°C for 16 hours induced cytotoxicity on CHO, Vero and Caco-2 cells seeded onto plastic plates (Shima et al., 2012). Another study determined CDT titres in culture filtrates from which *E. coli* was grown in four different media. It was then shown that CDT concentration in culture filtrates were highest when the bacteria were grown in Evan´s toxin medium, and 8-fold higher compared to cultures grown for 24 hours with shaking (Johnson & Lior, 1988). The yeast-extract concentration in Evan´s toxin medium has been found to increase the vascular permeability factor produced by an enterotoxigenic *E. coli* strain (Evans et al., 1973). In addition, in a study screening for the prevalence of CDT in periodontopathogenic bacteria, *Actinobacillus actinomycetemcomitans* was cultivated for 72 hours in a CO_2-rich atmosphere where most of the strains produced a CDT activity (Yamano et al., 2003).

Further, as the different growth phases affect transcription of genes differently, it would be useful to construct a growth curve and quantify the transcription rate of CDT at different timepoints. During exponential phase of bacterial growth, bacterial cells start to grow and divide exponentially. As the growing bacteria exhaust nutrient sources, cells enter into stationary phase where the cell number remains the same. Many gram-negative bacteria

develop resistance cells in this phase as stress response alter the expression of genes. Genes essential for cell growth are typically replaced by genes essential for survival and damage protection by the alteration of sigma factors. In many gram-negative pathogens, virulence genes are transcribed during stationary phase (Navarro Llorens et al., 2010). There are also gram-negative bacteria such as Shiga toxin-producing E. coli which transcribe the toxin during exponential growth phase, but do not release it into the growth medium before they reach stationary growth phase (Yokoyama et al., 2000).

The results indicated the lowest number of bacterial cells in samples grown for 72 hours in Evan´s toxin medium in an anaerobic milieu. The optical density of these samples can only be comparable to samples grown for 48 hours, but enteric bacteria are probably especially adapted to the approximately 5% CO_2 present in the mammalian gut. There may be an optimum CO_2 concentration for the anaerobic growth resulting in the indicated poor bacterial growth. Further, the physiology and growth rate of facultative anaerobes change in anaerobic conditions. Thus, it may be differences in the optimal conditions for growth and the optimal conditions for toxin production (DeMars et al., 2016; Lacoursiere et al., 1986). Also, bacteria belonging to the family Enterobacteriaceae, which includes *P. alcalifaciens* do not generally tolerate high levels of salt which are found in Evan´s toxin medium (Abdulkarim et al., 2009; DeMars et al., 2016). The highest number of bacterial cells were found in bacteria grown in BHI at 120 rpm. This is most likely due to the fact that aerobic energy metabolism is more efficient than anaerobic metabolism (Iuchi & Weiner, 1996).

One of the main challenges in this study was to extract RNA in high concentrations without contamination, and the removal of gDNA in the RNA samples. This was a crucial step on the way to indirectly measure the amount of CDT produced by the bacteria and to determine which samples from toxin production *in vitro* to apply for exposure on the cells. As troubleshooting of the column-based RNA extraction method would be laborious, an optimized solution-based RNA extraction method was applied for enhancing RNA quality and purity, without luck. If the methods would have yield high RNA concentrations, it would have been possible to dilute the extracted RNA to remove some of the contamination. However, low RNA concentrations were obtained.

The TURBO DNase™Enzyme applied for the removal of gDNA contamination in the samples, did not show any improvement. Existing literature has highlighted the same problem

with gDNA contamination in isolated RNA from *C. jejuni* strains without being able to identify the source of the problem, although one out of eight extraction methods were found to yield DNA-free RNA (Phongsisay et al., 2007).

4.4 The effect of exposure to CDT from *P. alcalifaciens*

The results from cells exposed to samples from toxin production in vitro, experimental design 3, indicates that filter-sterilized sonicated lysates of *P. alcalifaciens* strain 1723 grown under specific conditions induced toxicity on dog intestinal epithelial cells grown onto plastic plates.

This was only observed by microscopy as the CellTox™ Green assay did not detect any cytotoxicity and could not be quantified. A possible reason could be that acute necrotic cell death, with the loss of plasma membrane integrity results in a background noise when analyzing fluorescence by the plate reader.

In experimental design 3, the culture medium together with the cultivated bacteria were sonicated and sterile filtrated. There was no washing step of the cells, to remove residual medium. Instead, the medium together with all its bacterial waste products were not removed prior to sonicating the bacterial cells. However, this only applied for bacteria grown in BHI. The clearly visible changes of the cells after 48 hours of exposure, observed by light microscopy are from samples of bacteria grown in Evan´s toxin medium and at blood agar plates for 72 hours in an anaerobic milieu. The cells were washed in BHI before resuspended in a new volume of BHI, and then sonicated and filtrated. This indicates that bacterial waste products in the medium did not affect the cells. Rather growth in a CO_2-rich atmosphere and salt- and yeast containing medium affected the bacteria, thereby the composition of the sonicated lysates. CDT proteins produced by *C. jejuni* have been shown to remain tightly associated to the bacterial envelope, and it has been suggested that the amount of toxin present in culture supernatants is too low for meaningful experiments (Lara-Tejero & Galán, 2001). Nevertheless, the supernatant from Evan´s toxin medium was not tested so the suggestion is hard to discuss.

CDT was not quantified in the samples, which is clearly needed. Quantification of CDT from *P. alcalifaciens* is, however, difficult as there is no Enzyme-linked immunosorbent assay (ELISA) or pure CDT from *P. alcalifaciens* for use as analytical standard available.

4.5 Cloning and transfection of genetic variants of subunit cdtB

We were not able to detect the constructs in the cells after electroporation. From the obtained results it is not clear whether it was due to failure of transfection, if the proteins could not be expressed, or if the epitope tags were inaccessible for the antibodies.

Plasmid size and DNA construct size is known to affect transfection efficiency (Campeau et al., 2001; Yin et al., 2005). The cells were clearly transfected by the pmaxGFP plasmid. The pmaxGFP plasmid is approximately 4.7 kb, and do not differ that much in size from the pcDNA3.1 plasmid. Also, the different constructs, ranging from 304 bp – 851 bp is not considered to be large in size (Venken et al., 2006).

The correct inserts were verified by Sanger sequencing. If there had been an error in the construct, it would probably not account for all of the four different constructs. Also, the method applied for purification of the plasmids is considered good enough for mammalian cell transfection as described in section 2.6.3.6. The lack of codon optimization of the gene sequences might explain why the proteins were not expressed. Different use of codons varies significantly between different organisms and may have a great impact on the expression of heterologous proteins (Gustafsson et al., 2004). Codon optimization was omitted due to a previous study where recombinant plasmid pcDNA3.1/cdtB was constructed, and cdtB from *A. actinomycetemcomitans* was successfully expressed in the A549 human lung adenocarcinoma cell line without codon optimization. (Yaghoobi et al., 2016). If time had permitted, it could have been useful to make *E. coli* express the pcDNA3.1 vector as a control of that there was nothing wrong with the constructs (Izadi et al., 2009).

A third explanation could be that the proteins were expressed, but that the epitope tags were inaccessible for the antibodies, making it not possible to detect the proteins by flow cytometry.

Also, the cells were seeded out onto a 96-well plate after electroporation for cytotoxicity assay. No differences in cell viability between cells electroporated with cdtB constructs compared to cells electroporated with an empty pcDNA3.1 vector as a control were detected by the CellTox™ Green assay or by light microscopy, indicating that the proteins were not expressed.

3 Conclusion

The SCBN cell line forms polarized monolayers with a high level of organization of the TJ protein ZO-1. The polarized monolayers have a high TEER, which makes the cell line suitable for studying the effect of CDT with focus on barrier function. No mucin expression was observed, suggesting that the cell model is not well suited for studying mucus-dependent functions.

High cytotoxicity in cells seeded onto plastic plates were observed after 24 hours of exposure to recombinant CDT from E. *coli*, while exposure of recombinant CDT from *E. coli* onto cells forming a confluent monolayer had no effect on TEER and ZO-1 integrity after 24 hours of exposure.

Increased CDT production in bacteria cultured in an anaerobic milieu was indicated. Less viable cells were observed by light microscopy when exposed to sterile-filtrated lysates of bacteria grown under this condition.

6.0 Future perspectives

The toxicity induced by samples from toxin production *in vitro* was only observed on cells seeded onto plastic plates. It is not known whether cells seeded onto transwell inserts would have been affected. It would have been interesting to test the same samples with focus on barrier function. It would also have been interesting to expose cells seeded onto plastic plates with samples from the other strains cultivated under the same conditions to screen for any genetic differences.

Further optimalization of transfection is needed for studying the genetic differences of subunit cdtB. If the constructs are expressed in *E. coli*, codon optimizing is necessary for the expression in the SCBN cells. If they are not expressed in *E. coli*, a re-evaluation of the constructs is needed.

A development of a method for the quantification of CDT is needed, as well as the production of pure CDT from *P. alcalifaciens*.

References

Abdel-Banat, B. M. A., Nonklang, S., Hoshida, H. & Akada, R. (2010). Random and targeted gene integrations through the control of non-homologous end joining in the yeast Kluyveromyces marxianus. *Yeast*, 27 (1): 29-39. doi: https://doi.org/10.1002/yea.1729.

Abdulkarim, S., Fatimah, A. & Anderson, J. (2009). Effect of salt concentrations on the growth of heat-stressed and unstressed Escherichia coli. *Journal of Food Agriculture and Environment*, 7 (3-4): 51-54.

Aibinu, I. E., Pfeifer, Y., Ogunsola, F., Odugbemi, T., Koenig, W. & Ghebremedhin, B. (2011). Emergence of β-lactamases OXA-10, VEB-1 and CMY in Providencia spp. from Nigeria. *Journal of Antimicrobial Chemotherapy*, 66 (8): 1931-1932. doi: 10.1093/jac/dkr197.

Albert, M. J., Alam, K., Ansaruzzaman, M., Islam, M. M., Rahman, A. S., Haider, K., Bhuiyan, N. A., Nahar, S., Ryan, N., Montanaro, J., et al. (1992). Pathogenesis of Providencia alcalifaciens-induced diarrhea. *Infect Immun*, 60 (12): 5017-24. doi: 10.1128/iai.60.12.5017-5024.1992.

Allaire, J. M., Crowley, S. M., Law, H. T., Chang, S.-Y., Ko, H.-J. & Vallance, B. A. (2018). The Intestinal Epithelium: Central Coordinator of Mucosal Immunity. *Trends in Immunology*, 39 (9): 677-696. doi: https://doi.org/10.1016/j.it.2018.04.002.

ANINDYAJATI, ARTARINI, A. A., RIANI, C. & RETNONINGRUM, D. S. (2016). Plasmid Copy Number Determination by Quantitative Polymerase Chain Reaction. *Scientia Pharmaceutica*, 84 (1): 89-101.

Apostolopoulos, V., Stojanovska, L. & Gargosky, S. E. (2015). MUC1 (CD227): a multi-tasked molecule. *Cellular and Molecular Life Sciences*, 72 (23): 4475-4500. doi: 10.1007/s00018-015-2014-z.

Asif, A., Mohsin, H., Tanvir, R. & Rehman, Y. (2017). Revisiting the Mechanisms Involved in Calcium Chloride Induced Bacterial Transformation. *Frontiers in Microbiology*, 8 (2169). doi: 10.3389/fmicb.2017.02169.

Attili, D., McClintock, S. D., Rizvi, A. H., Pandya, S., Rehman, H., Nadeem, D. M., Richter, A., Thomas, D., Dame, M. K. & Turgeon, D. K. (2019). Calcium-induced differentiation in

normal human colonoid cultures: Cell-cell/cell-matrix adhesion, barrier formation and tissue integrity. *PLoS One*, 14 (4): e0215122.

Bandhaya, P., Saraithong, P., Likittanasombat, K., Hengprasith, B. & Torrungruang, K. (2012). Aggregatibacter actinomycetemcomitans serotypes, the JP2 clone and cytolethal distending toxin genes in a Thai population. *Journal of Clinical Periodontology*, 39 (6): 519-525. doi: https://doi.org/10.1111/j.1600-051X.2012.01871.x.

Barbat, A., Pandrea, I., Cambier, D., Zweibaum, A. & Lesuffleur, T. (1998). Resistance of the human colon carcinoma cell line HCT-8 to methotrexate results in selection of cells with features of enterocytic differentiation. *International journal of cancer*, 75 (5): 731-737.

Barril, P. & Nates, S. (2012). Introduction to agarose and polyacrylamide gel electrophoresis matrices with respect to their detection sensitivities. *Gel electrophoresis-Principles and basics*: 3-14.

Basson, M. D., Turowski, G. & Emenaker, N. J. (1996). Regulation of human (Caco-2) intestinal epithelial cell differentiation by extracellular matrix proteins. *Experimental cell research*, 225 (2): 301-305.

Boron, W. F. & Boulpaep, E. L. (2009). Intestinal Fluid and Electrolyte Movement. In *Medical Physiology A Cellular and Molecular Approach, Updated 2nd Ed.*, pp. 933-948. Philadelphia, PA: Saunders/Elsevier.

Budelier, K. & Schorr, J. (1998). Purification of DNA by anion-exchange chromatography. *Current protocols in molecular biology*, 42 (1): 2.1. 11-2.1. 18.

Buret, A., Mitchell, K., Muench, D. & Scott, K. (2002). Giardia lamblia disrupts tight junctional ZO-1 and increases permeability in non-transformed human small intestinal epithelial monolayers: effects of epidermal growth factor. *Parasitology*, 125 (1): 11-19.

Buret, A. & Lin, Y.-C. (2008). Genotypic Characterization of an Epithelial Cell Line for the Study of Parasite–Epithelial Interactions. *Journal of Parasitology*, 94 (2): 545-548, 4.

Busch, K., Suchodolski, J. S., Kühner, K. A., Minamoto, Y., Steiner, J. M., Mueller, R. S., Hartmann, K. & Unterer, S. (2015). Clostridium perfringens enterotoxin and Clostridium difficile toxin A/B do not play a role in acute haemorrhagic diarrhoea syndrome in dogs. *Veterinary Record*, 176 (10): 253-253. doi: https://doi.org/10.1136/vr.102738.

Camilleri, P. (1997). *Capillary electrophoresis: theory and practice*: CRC press.

Campeau, P., Chapdelaine, P., Seigneurin-Venin, S., Massie, B. & Tremblay, J. (2001). Transfection of large plasmids in primary human myoblasts. *Gene Therapy*, 8 (18): 1387-1394.

Cao, H. & Shockey, J. M. (2012). Comparison of TaqMan and SYBR Green qPCR Methods for Quantitative Gene Expression in Tung Tree Tissues. *Journal of Agricultural and Food Chemistry*, 60 (50): 12296-12303. doi: 10.1021/jf304690e.

Capaldo, C. T., Powell, D. N. & Kalman, D. (2017). Layered defense: how mucus and tight junctions seal the intestinal barrier. *Journal of Molecular Medicine*, 95 (9): 927-934.

Carrillo-Casas, E. M., Hernández-Castro, R., Suárez-Güemes, F. & de la Pena-Moctezuma, A. (2008). Selection of the internal control gene for real-time quantitative RT-PCR assays in temperature treated Leptospira. *Current microbiology*, 56 (6): 539-546.

Chang, A. Y., Chau, V., Landas, J. A. & Pang, Y. (2017). Preparation of calcium competent Escherichia coli and heat-shock transformation. *JEMI methods*, 1: 22-25.

Chen, S., Einspanier, R. & Schoen, J. (2015). Transepithelial electrical resistance (TEER): a functional parameter to monitor the quality of oviduct epithelial cells cultured on filter supports. *Histochemistry and cell biology*, 144 (5): 509-515.

Chlibek, R., Jirous, J. & Beran, J. (2002). Diarrhea outbreak among Czech Army Field Hospital personnel caused by Providencia alcalifaciens. *Journal of travel medicine*, 9 (3): 151-152.

Costanzo, L. S. (2013). Gastrointestinal Physiology. In *Physiology*, pp. 329-382: Saunders/Elsevier.

DeMars, Z., Biswas, S., Amachawadi, R. G., Renter, D. G. & Volkova, V. V. (2016). Antimicrobial susceptibility of enteric gram negative facultative anaerobe bacilli in aerobic versus anaerobic conditions. *PLoS One*, 11 (5): e0155599.

Depping, R. & Seeger, K. (2019). 1H-NMR spectroscopy shows cellular uptake of HEPES buffer by human cell lines—an effect to be considered in cell culture experiments. *Analytical and Bioanalytical Chemistry*, 411 (4): 797-802. doi: 10.1007/s00216-018-1518-4.

Desjardins, P. & Conklin, D. (2010). NanoDrop microvolume quantitation of nucleic acids. *JoVE (Journal of Visualized Experiments)* (45): e2565.

Ding, L.-W., Sun, Q.-Y., Wang, Z.-Y., Sun, Y.-B. & Xu, Z.-F. (2008). Using silica particles to isolate total RNA from plant tissues recalcitrant to extraction in guanidine thiocyanate. *Analytical Biochemistry*, 374 (2): 426-428. doi: https://doi.org/10.1016/j.ab.2007.11.030.

DiRienzo, J. M. (2014). - Cytolethal Distending Toxin: A Unique Variation on the AB Toxin Paradigm. - 2014.

Esch, M. B., Mahler, G. J., Stokol, T. & Shuler, M. L. (2014). Body-on-a-chip simulation with gastrointestinal tract and liver tissues suggests that ingested nanoparticles have the potential to cause liver injury. *Lab on a Chip*, 14 (16): 3081-3092.

Evans, D. J., Jr., Evans, D. G. & Gorbach, S. L. (1973). Production of vascular permeability factor by enterotoxigenic Escherichia coli isolated from man. *Infect Immun*, 8 (5): 725-30. doi: 10.1128/iai.8.5.725-730.1973.

Fauske, A. K. & Hirsch, M. N. (2006). *Kan Providencia alcalifaciens være en primærpatogen bakterie ved diaré hos hund? («Providencia alcalifaciens as a possible primarily pathogen in dogs with diarrhea»)*. Bachelor thesis. Oslo: Norwegian School of Veterinary Science. Available at: https://nmbu.brage.unit.no/nmbu-xmlui/bitstream/handle/11250/2619607/Kan%20Providencia%20alcalifaciens%20være%20en%20primærpatogen%20bakterie%20ved%20diaré%20hos%20hund.pdf?sequence=1&isAllowed=y (accessed: 05.05.2021).

Gendler, S. J. (2001). MUC1, the renaissance molecule. *Journal of mammary gland biology and neoplasia*, 6 (3): 339-353.

Gomes, A. É. I., Stuchi, L. P., Siqueira, N. M. G., Henrique, J. B., Vicentini, R., Ribeiro, M. L., Darrieux, M. & Ferraz, L. F. C. (2018). Selection and validation of reference genes for gene expression studies in Klebsiella pneumoniae using Reverse Transcription Quantitative real-time PCR. *Scientific Reports*, 8 (1): 9001. doi: 10.1038/s41598-018-27420-2.

Gottwald, E., Müller, O. & Polten, A. (2001). Semiquantitative reverse transcription-polymerase chain reaction with the Agilent 2100 Bioanalyzer. *Electrophoresis*, 22 (18): 4016-4022.

Groschwitz, K. R. & Hogan, S. P. (2009). Intestinal barrier function: Molecular regulation and disease pathogenesis. *Journal of Allergy and Clinical Immunology*, 124 (1): 3-20. doi: https://doi.org/10.1016/j.jaci.2009.05.038.

Guerra, L., Cortes-Bratti, X., Guidi, R. & Frisan, T. (2011). The Biology of the Cytolethal Distending Toxins. *Toxins*, 3 (3): 172-190.

Gurtovenko, A. A. & Anwar, J. (2007). Modulating the Structure and Properties of Cell Membranes: The Molecular Mechanism of Action of Dimethyl Sulfoxide. *The Journal of Physical Chemistry B*, 111 (35): 10453-10460. doi: 10.1021/jp073113e.

Gustafsson, C., Govindarajan, S. & Minshull, J. (2004). Codon bias and heterologous protein expression. *Trends in biotechnology*, 22 (7): 346-353.

Günzel, D. (2017). Claudins: vital partners in transcellular and paracellular transport coupling. *Pflügers Archiv - European Journal of Physiology*, 469 (1): 35-44. doi: 10.1007/s00424-016-1909-3.

Hall, J., Hazlewood, G., Surani, M., Hirst, B. & Gilbert, H. J. (1990). Eukaryotic and prokaryotic signal peptides direct secretion of a bacterial endoglucanase by mammalian cells. *Journal of Biological Chemistry*, 265 (32): 19996-19999.

Haynes, J. & Hawkey, P. M. (1989). Providencia alcalifaciens and travellers' diarrhoea. *BMJ: British Medical Journal*, 299 (6691): 94.

Huang, B. Q. & Yeung, E. C. (2015). Chemical and physical fixation of cells and tissues: an overview. *Plant microtechniques and protocols*: 23-43.

Hughes, P., Marshall, D., Reid, Y., Parkes, H. & Gelber, C. (2007). The costs of using unauthenticated, over-passaged cell lines: how much more data do we need? *BioTechniques*, 43 (5): 575-586. doi: 10.2144/000112598.

Interaminense, J. A., Nascimento, D. C. O., Ventura, R. F., Batista, J. E. C., Souza, M. M. C., Hazin, F. H. V., Pontes-Filho, N. T. & Lima-Filho, J. V. (2010). Recovery and screening for antibiotic susceptibility of potential bacterial pathogens from the oral cavity of shark species involved in attacks on humans in Recife, Brazil. *Journal of Medical Microbiology*, 59 (8): 941-947. doi: https://doi.org/10.1099/jmm.0.020453-0.

Iuchi, S. & Weiner, L. (1996). Cellular and molecular physiology of Escherichia coli in the adaptation to aerobic environments. *The Journal of Biochemistry*, 120 (6): 1055-1063.

Izadi, M., Abiri, M. & Keramatipour, M. (2009). Producing a Mammalian GFP Expression Vector Containing Neomycin Resistance Gene. *Avicenna journal of medical biotechnology*, 1 (1): 33-36.

Jaroszeski, M. J. & Radcliff, G. (1999). Fundamentals of flow cytometry. *Molecular biotechnology*, 11 (1): 37-53.

Jinadasa, R. N., Bloom, S. E., Weiss, R. S. & Duhamel, G. E. (2011). Cytolethal distending toxin: a conserved bacterial genotoxin that blocks cell cycle progression, leading to apoptosis of a broad range of mammalian cell lineages. *Microbiology (Reading)*, 157 (Pt 7): 1851-1875. doi: 10.1099/mic.0.049536-0.

Johansson, C., Nilsson, A., Kaden, R. & Rautelin, H. (2019). Differences in virulence gene expression between human blood and stool Campylobacter coli clade 1 ST828CC isolates. *Gut Pathogens*, 11 (1): 42. doi: 10.1186/s13099-019-0322-9.

Johnson, W. M. & Lior, H. (1988). A new heat-labile cytolethal distending toxin (CLDT) produced by Escherichia coli isolates from clinical material. *Microbial Pathogenesis*, 4 (2): 103-113. doi: https://doi.org/10.1016/0882-4010(88)90052-6.

Jørgensen, H. J., Wisløff H., Sekse C., Bergsjø B. A., Valheim M., Skancke E., Haaland A. H., Nørstebø S. F., Lagesen K., Hofshagen M., et al. (unpublished). *Providencia*

alcalifaciens possible cause of an outbreak of acute haemorrhagic diarrhoea syndrome in Norway. Unpublished manuscript.
Kendall, M. M., Gruber, C. C., Parker, C. T. & Sperandio, V. (2012). Ethanolamine Controls Expression of Genes Encoding Components Involved in Interkingdom Signaling and Virulence in Enterohemorrhagic Escherichia coli O157:H7. *mBio*, 3 (3): e00050-12. doi: 10.1128/mBio.00050-12.
Kim, G.-Y., Moon, J.-M., Han, J.-H., Kim, K.-H. & Rhim, H. (2011). The sCMV IE enhancer/promoter system for high-level expression and efficient functional studies of target genes in mammalian cells and zebrafish. *Biotechnology letters*, 33 (7): 1319-1326.
Kim, T. K. & Eberwine, J. H. (2010). Mammalian cell transfection: the present and the future. *Analytical and Bioanalytical Chemistry*, 397 (8): 3173-3178. doi: 10.1007/s00216-010-3821-6.
Koynova, R. & Tenchov, B. (2011). Recent patents in cationic lipid carriers for delivery of nucleic acids. *Recent Patents on DNA & Gene Sequences (Discontinued)*, 5 (1): 8-27.
Król, J., Janeczek, M., Pliszczak-Król, A., Janeczek, W. & Florek, M. (2007). Providencia alcalifaciens as the presumptive cause of diarrhoea in dog. *Polish journal of veterinary sciences*, 10 (4): 285-287.
Kumar, P., Nagarajan, A. & Uchil, P. D. (2019). Electroporation. *Cold Spring Harb Protoc*, 2019 (7). doi: 10.1101/pdb.top096271.
Lacoursiere, A., Thompson, B. G., Kole, M. M., Ward, D. & Gerson, D. F. (1986). Effects of carbon dioxide concentration on anaerobic fermentations of Escherichia coli. *Applied Microbiology and Biotechnology*, 23 (5): 404-406. doi: 10.1007/BF00257042.
Lallès, J.-P. (2019). Recent advances in intestinal alkaline phosphatase, inflammation, and nutrition. *Nutrition Reviews*, 77 (10): 710-724. doi: 10.1093/nutrit/nuz015.
Lamb-Rosteski, J. M., Kalischuk, L. D., Inglis, G. D. & Buret, A. G. (2008). Epidermal Growth Factor Inhibits Campylobacter jejuni-Induced Claudin-4 Disruption, Loss of Epithelial Barrier Function, and Escherichia coli Translocation. *Infection and Immunity*, 76 (8): 3390-3398. doi: 10.1128/iai.01698-07.
Lara-Tejero, M. a. & Galán, J. E. (2001). CdtA, CdtB, and CdtC Form a Tripartite Complex That Is Required for Cytolethal Distending Toxin Activity. *Infection and Immunity*, 69 (7): 4358-4365. doi: 10.1128/iai.69.7.4358-4365.2001.
Lauková, A. (2000). In vitro treatment of different isolates from cattle dung and pig slurry by nisin. *Acta Veterinaria Brno*, 69 (2): 147-151.
Lazarevic, V., Gaïa, N., Girard, M. & Schrenzel, J. (2016). Decontamination of 16S rRNA gene amplicon sequence datasets based on bacterial load assessment by qPCR. *BMC Microbiology*, 16 (1): 73. doi: 10.1186/s12866-016-0689-4.
Lee, B., Moon, K. M. & Kim, C. Y. (2018). Tight Junction in the Intestinal Epithelium: Its Association with Diseases and Regulation by Phytochemicals. *Journal of Immunology Research*, 2018: 2645465. doi: 10.1155/2018/2645465.
Linz, G., Djeljadini, S., Steinbeck, L., Köse, G., Kiessling, F. & Wessling, M. (2020). Cell barrier characterization in transwell inserts by electrical impedance spectroscopy. *Biosensors and Bioelectronics*, 165: 112345. doi: https://doi.org/10.1016/j.bios.2020.112345.
Manos, J. & Belas, R. (2006). The Genera Proteus , Providencia , and Morganella. In vol. 6, pp. 245-269.

Mao, X. & DiRienzo, J. M. (2002). Functional studies of the recombinant subunits of a cytolethal distending holotoxin. *Cellular Microbiology*, 4 (4): 245-255. doi: https://doi.org/10.1046/j.1462-5822.2002.00186.x.

Massey-Harroche, D. (2000). Epithelial cell polarity as reflected in enterocytes. *Microscopy Research and Technique*, 49 (4): 353-362. doi: https://doi.org/10.1002/(SICI)1097-0029(20000515)49:4<353::AID-JEMT4>3.0.CO;2-8.

Mazloom-Farsibaf, H., Farzam, F., Fazel, M., Wester, M. J., Meddens, M. B. & Lidke, K. A. (2021). Comparing lifeact and phalloidin for super-resolution imaging of actin in fixed cells. *Plos one*, 16 (1): e0246138.

McAuley, J. L., Linden, S. K., Png, C. W., King, R. M., Pennington, H. L., Gendler, S. J., Florin, T. H., Hill, G. R., Korolik, V. & McGuckin, M. A. (2007). MUC1 cell surface mucin is a critical element of the mucosal barrier to infection. *The Journal of clinical investigation*, 117 (8): 2313-2324.

McConnell, R. E., Benesh, A. E., Mao, S., Tabb, D. L. & Tyska, M. J. (2011). Proteomic analysis of the enterocyte brush border. *American Journal of Physiology-Gastrointestinal and Liver Physiology*, 300 (5): G914-G926. doi: 10.1152/ajpgi.00005.2011.

McKinnon, K. M. (2018). Flow Cytometry: An Overview. *Curr Protoc Immunol*, 120: 5.1.1-5.1.11. doi: 10.1002/cpim.40.

Monro, R. L., Bornstein, J. C. & Bertrand, P. P. (2008). Synaptic transmission from the submucosal plexus to the myenteric plexus in Guinea-pig ileum. *Neurogastroenterology & Motility*, 20 (10): 1165-1173. doi: https://doi.org/10.1111/j.1365-2982.2008.01157.x.

Mortier, F., Strohmeyer, K., Hartmann, K. & Unterer, S. (2015). Acute haemorrhagic diarrhoea syndrome in dogs: 108 cases. *Veterinary Record*, 176 (24): 627-627. doi: https://doi.org/10.1136/vr.103090.

Mukherjee, T., Squillantea, E., Gillespieb, M. & Shao, J. (2004). Transepithelial electrical resistance is not a reliable measurement of the Caco-2 monolayer integrity in Transwell. *Drug delivery*, 11 (1): 11-18.

Murata, T., Iida, T., Shiomi, Y., Tagomori, K., Akeda, Y., Yanagihara, I., Mushiake, S., Ishiguro, F. & Honda, T. (2001). A large outbreak of foodborne infection attributed to Providencia alcalifaciens. *J Infect Dis*, 184: 1050-1055.

Möhr, A. J., van der Merwe, L. L., van der Lugt, J. J., Josling, D. & Picard, J. (2002). Primary bacterial enteritis caused by Providencia alcalifaciens in three dogs. *Veterinary Record*, 150 (2): 52-53. doi: https://doi.org/10.1136/vr.150.2.52.

Nachamkin, I., Panaro, N. J., Li, M., Ung, H., Yuen, P. K., Kricka, L. J. & Wilding, P. (2001). Agilent 2100 bioanalyzer for restriction fragment length polymorphism analysis of the Campylobacter jejuni flagellin gene. *Journal of clinical microbiology*, 39 (2): 754-757.

Naser, S. M., Thompson, F. L., Hoste, B., Gevers, D., Dawyndt, P., Vancanneyt, M. & Swings, J. (2005). Application of multilocus sequence analysis (MLSA) for rapid identification of Enterococcus species based on rpoA and pheS genes. *Microbiology*, 151 (7): 2141-2150. doi: https://doi.org/10.1099/mic.0.27840-0.

Natoli, M., Leoni, B. D., D'Agnano, I., D'Onofrio, M., Brandi, R., Arisi, I., Zucco, F. & Felsani, A. (2011). Cell growing density affects the structural and functional properties of Caco-2 differentiated monolayer. *Journal of Cellular Physiology*, 226 (6): 1531-1543. doi: https://doi.org/10.1002/jcp.22487.

Navarro Llorens, J. M., Tormo, A. & Martínez-García, E. (2010). Stationary phase in gram-negative bacteria. *FEMS Microbiology Reviews*, 34 (4): 476-495. doi: 10.1111/j.1574-6976.2010.00213.x.

Neuzil, P., Zhang, C., Pipper, J., Oh, S. & Zhuo, L. (2006). Ultra fast miniaturized real-time PCR: 40 cycles in less than six minutes. *Nucleic Acids Research*, 34 (11): e77-e77. doi: 10.1093/nar/gkl416.

Nolan, T., Hands, R. E. & Bustin, S. A. (2006). Quantification of mRNA using real-time RT-PCR. *Nature protocols*, 1 (3): 1559-1582.

Oliveira, M. G. d., Rizzi, C., Galli, V., Lopes, G. V., Haubert, L., Dellagostin, O. A. & Silva, W. P. d. (2019). Presence of genes associated with adhesion, invasion, and toxin production in Campylobacter jejuni isolates and effect of temperature on their expression. *Canadian Journal of Microbiology*, 65 (4): 253-260. doi: 10.1139/cjm-2018-0539 %M 30532987.

Padhi, B. K., Singh, M., Huang, N. & Pelletier, G. (2016). A PCR-based approach to assess genomic DNA contamination in RNA: Application to rat RNA samples. *Analytical Biochemistry*, 494: 49-51. doi: https://doi.org/10.1016/j.ab.2015.10.012.

Pan, J.-Z., Fang, P., Fang, X.-X., Hu, T.-T., Fang, J. & Fang, Q. (2018). A Low-Cost Palmtop High-Speed Capillary Electrophoresis Bioanalyzer with Laser Induced Fluorescence Detection. *Scientific Reports*, 8 (1): 1791. doi: 10.1038/s41598-018-20058-0.

Panaro, N. J., Yuen, P. K. i., Sakazume, T., Fortina, P., Kricka, L. J. & Wilding, P. (2000). Evaluation of DNA Fragment Sizing and Quantification by the Agilent 2100 Bioanalyzer. *Clinical Chemistry*, 46 (11): 1851-1853. doi: 10.1093/clinchem/46.11.1851.

Pang, G., Buret, A., O'loughlin, E., Smith, A., Batey, R. & Clancy, R. (1996). Immunologic, functional, and morphological characterization of three new human small intestinal epithelial cell lines. *Gastroenterology*, 111 (1): 8-18.

Pfaffl, M. W. (2007). Relative quantification. In *Real-time PCR*, pp. 89-108: Taylor & Francis.

Phongsisay, V., Perera, V. N. & Fry, B. N. (2007). Evaluation of eight RNA isolation methods for transcriptional analysis in Campylobacter jejuni. *Journal of Microbiological Methods*, 68 (2): 427-429. doi: https://doi.org/10.1016/j.mimet.2006.09.002.

Puliafito, A., Hufnagel, L., Neveu, P., Streichan, S., Sigal, A., Fygenson, D. K. & Shraiman, B. I. (2012). Collective and single cell behavior in epithelial contact inhibition. *Proceedings of the National Academy of Sciences*, 109 (3): 739-744. doi: 10.1073/pnas.1007809109.

Qiagen. (2009). *QuantiTect Reverse Transcription Handbook*. Available at: https://www.qiagen.com/us/products/discovery-and-translational-research/pcr-qpcr-dpcr/real-time-pcr-enzymes-and-kits/reverse-transcription-cdna-synthesis-qpcr/quantitect-reverse-transcription-kit/ (accessed: 10.05.21).

Rai, M. & Padh, H. (2001). Expression systems for production of heterologous proteins. *Current science*: 1121-1128.

Ramaiahgari, S. C., Den Braver, M. W., Herpers, B., Terpstra, V., Commandeur, J. N., van de Water, B. & Price, L. S. (2014). A 3D in vitro model of differentiated HepG2 cell spheroids with improved liver-like properties for repeated dose high-throughput toxicity studies. *Archives of toxicology*, 88 (5): 1083-1095.

Reis, L. A. & Rocha, M. S. (2017). DNA interaction with DAPI fluorescent dye: Force spectroscopy decouples two different binding modes. *Biopolymers*, 107 (5): e23015. doi: https://doi.org/10.1002/bip.23015.

Riss, T., Niles, A., Moravec, R., Karassina, N. & Vidugiriene, J. (2019). Cytotoxicity assays: In vitro methods to measure dead cells. *Assay Guidance Manual [Internet]*.

Rocha, D. J. P., Santos, C. S. & Pacheco, L. G. C. (2015). Bacterial reference genes for gene expression studies by RT-qPCR: survey and analysis. *Antonie van Leeuwenhoek*, 108 (3): 685-693. doi: 10.1007/s10482-015-0524-1.

Salehi, Z. & Najafi, M. (2014). RNA preservation and stabilization. *Biochem Physiol*, 3 (126): 2.

Sánchez, C., Villacreses, J., Blanc, N., Espinoza, L., Martinez, C., Pastor, G., Manque, P., Undurraga, S. F. & Polanco, V. (2016). High quality RNA extraction from Maqui berry for its application in next-generation sequencing. *SpringerPlus*, 5 (1): 1243-1243. doi: 10.1186/s40064-016-2906-x.

Saper, C. B. (2009). A guide to the perplexed on the specificity of antibodies. *The journal of histochemistry and cytochemistry : official journal of the Histochemistry Society*, 57 (1): 1-5. doi: 10.1369/jhc.2008.952770.

Schierack, P., Nordhoff, M., Pollmann, M., Weyrauch, K. D., Amasheh, S., Lodemann, U., Jores, J., Tachu, B., Kleta, S. & Blikslager, A. (2006). Characterization of a porcine intestinal epithelial cell line for in vitro studies of microbial pathogenesis in swine. *Histochemistry and cell biology*, 125 (3): 293-305.

Schroeder, B. O. (2019). Fight them or feed them: how the intestinal mucus layer manages the gut microbiota. *Gastroenterology report*, 7 (1): 3-12. doi: 10.1093/gastro/goy052.

Scuron, M. D., Boesze-Battaglia, K., Dlakić, M. & Shenker, B. J. (2016). The Cytolethal Distending Toxin Contributes to Microbial Virulence and Disease Pathogenesis by Acting As a Tri-Perditious Toxin. *Frontiers in Cellular and Infection Microbiology*, 6 (168). doi: 10.3389/fcimb.2016.00168.

Shah, M. M., Odoyo, E., Larson, P. S., Apondi, E., Kathiiko, C., Miringu, G., Nakashima, M. & Ichinose, Y. (2015). First report of a foodborne Providencia alcalifaciens outbreak in Kenya. *The American journal of tropical medicine and hygiene*, 93 (3): 497-500.

Shah, M. M., Odoyo, E. & Ichinose, Y. (2019). Epidemiology and Pathogenesis of Providencia alcalifaciens Infections. *Am J Trop Med Hyg*, 101 (2): 290-293. doi: 10.4269/ajtmh.18-0376.

Shima, A., Hinenoya, A., Asakura, M., Sugimoto, N., Tsukamoto, T., Ito, H., Nagita, A., Faruque, S. M. & Yamasaki, S. (2012). Molecular characterizations of cytolethal distending toxin produced by Providencia alcalifaciens strains isolated from patients with diarrhea. *Infection and immunity*, 80 (4): 1323-1332. doi: 10.1128/IAI.05831-11.

Siqueira, J. F. & Rôças, I. N. (2003). PCR methodology as a valuable tool for identification of endodontic pathogens. *Journal of Dentistry*, 31 (5): 333-339. doi: https://doi.org/10.1016/S0300-5712(03)00051-4.

Sivaganesan, M., Haugland, R. A., Chern, E. C. & Shanks, O. C. (2010). Improved strategies and optimization of calibration models for real-time PCR absolute quantification. *Water Research*, 44 (16): 4726-4735. doi: https://doi.org/10.1016/j.watres.2010.07.066.

Srinivasan, B., Kolli, A. R., Esch, M. B., Abaci, H. E., Shuler, M. L. & Hickman, J. J. (2015). TEER measurement techniques for in vitro barrier model systems. *Journal of laboratory automation*, 20 (2): 107-126.

Tan, S. C. & Yiap, B. C. (2009). DNA, RNA, and protein extraction: the past and the present. *Journal of biomedicine & biotechnology*, 2009: 574398-574398. doi: 10.1155/2009/574398.

Teoh, D. A., Kamieniecki, D., Pang, G. & Buret, A. G. (2000). Giardia lamblia rearranges F-actin and α-actinin in human colonic and duodenal monolayers and reduces transepithelial electrical resistance. *Journal of Parasitology*, 86 (4): 800-806.
ThermoFisher. (2018). TURBO DNA-free Kit.
Thornley, D. J. (1997). *Analysis of trace data from fluorescence based Sanger sequencing*: Citeseer.
Thornton, B. & Basu, C. (2011). Real-time PCR (qPCR) primer design using free online software. *Biochemistry and Molecular Biology Education*, 39 (2): 145-154. doi: https://doi.org/10.1002/bmb.20461.
Toni, L. S., Garcia, A. M., Jeffrey, D. A., Jiang, X., Stauffer, B. L., Miyamoto, S. D. & Sucharov, C. C. (2018). Optimization of phenol-chloroform RNA extraction. *MethodsX*, 5: 599-608.
Torres-Morquecho, A., Giono-Cerezo, S., Camorlinga-Ponce, M., Vargas-Mendoza, C. F. & Torres, J. (2010). Evolution of bacterial genes: Evidences of positive Darwinian selection and fixation of base substitutions in virulence genes of Helicobacter pylori. *Infection, Genetics and Evolution*, 10 (6): 764-776. doi: https://doi.org/10.1016/j.meegid.2010.04.005.
Ulluwishewa, D., Anderson, R. C., McNabb, W. C., Moughan, P. J., Wells, J. M. & Roy, N. C. (2011). Regulation of Tight Junction Permeability by Intestinal Bacteria and Dietary Components. *The Journal of Nutrition*, 141 (5): 769-776. doi: 10.3945/jn.110.135657.
Unterer, S., Busch, K., Leipig, M., Hermanns, W., Wolf, G., Straubinger, R., Mueller, R. & Hartmann, K. (2014). Endoscopically visualized lesions, histologic findings, and bacterial invasion in the gastrointestinal mucosa of dogs with acute hemorrhagic diarrhea syndrome. *Journal of Veterinary Internal Medicine*, 28 (1): 52-58.
Venken, K. J., He, Y., Hoskins, R. A. & Bellen, H. J. (2006). P [acman]: a BAC transgenic platform for targeted insertion of large DNA fragments in D. melanogaster. *Science*, 314 (5806): 1747-1751.
Vincze, T., Posfai, J. & Roberts, R. J. (2003). NEBcutter: a program to cleave DNA with restriction enzymes. *Nucleic acids research*, 31 (13): 3688-3691.
Yaghoobi, H., Bandehpour, M. & Kazemi, B. (2016). Apoptotic effects of the B subunit of bacterial cytolethal distending toxin on the A549 lung cancer cell line. *Asian Pacific journal of cancer prevention: APJCP*, 17.
Yamano, R., Ohara, M., Nishikubo, S., Fujiwara, T., Kawamoto, T., Ueno, Y., Komatsuzawa, H., Okuda, K., Kurihara, H., Suginaka, H., et al. (2003). Prevalence of cytolethal distending toxin production in periodontopathogenic bacteria. *Journal of clinical microbiology*, 41 (4): 1391-1398. doi: 10.1128/jcm.41.4.1391-1398.2003.
Ye, J., Coulouris, G., Zaretskaya, I., Cutcutache, I., Rozen, S. & Madden, T. L. (2012). Primer-BLAST: a tool to design target-specific primers for polymerase chain reaction. *BMC Bioinformatics*, 13: 134. doi: 10.1186/1471-2105-13-134.
Yin, W., Xiang, P. & Li, Q. (2005). Investigations of the effect of DNA size in transient transfection assay using dual luciferase system. *Analytical Biochemistry*, 346 (2): 289-294. doi: https://doi.org/10.1016/j.ab.2005.08.029.
Yoh, M., Matsuyama, J., Ohnishi, M., Takagi, K., Miyagi, H., Mori, K., Park, K.-S., Ono, T. & Honda, T. (2005). Importance of Providencia species as a major cause of travellers' diarrhoea. *Journal of medical microbiology*, 54 (11): 1077-1082.
Yokoyama, K., Horii, T., Yamashino, T., Hashikawa, S., Barua, S., Hasegawa, T., Watanabe, H. & Ohta, M. (2000). Production of Shiga toxin by Escherichia coli measured with

reference to the membrane vesicle-associated toxins. *FEMS microbiology letters*, 192 (1): 139-144.

Zhao, X., Li, G. & Liang, S. (2013). Several affinity tags commonly used in chromatographic purification. *Journal of analytical methods in chemistry*, 2013: 581093-581093. doi: 10.1155/2013/581093.

Zhu, B., Cai, G., Hall, E. O. & Freeman, G. J. (2007). In-Fusion™ assembly: seamless engineering of multidomain fusion proteins, modular vectors, and mutations. *Biotechniques*, 43 (3): 354-359.

Appendix

Colony-PCR primers:

Table 1: T7 and BGH primers used for colony-PCR

Colony-PCR primers		
Name	Target	Sequence
T7 promoter primer (F)	Vector	5´-TAATACGACTCACTATAGGG-3’
BGH Reverse primer (R)	Vector	5’-TAGAAGGCACAGTCGAGG-3’

Norges miljø- og biovitenskapelige universitet
Noregs miljø- og biovitskapelege universitet
Norwegian University of Life Sciences

Postboks 5003
NO-1432 Ås
Norway